2-6-2017

From the Science of Nanorod Growth to Low Temperature Metallic Attachment

Paul R. Elliott
University of Connecticut - Storrs, paul.elliott@uconn.edu

From the Science of Nanorod Growth to Low Temperature Metallic Attachment

Paul Robert Elliott, PhD

University of Connecticut, 2017

To move nanotechnology out of the lab and into common use requires understanding and experience of the structures and processes involved. The technological maturity allowing the widespread use of nanotechnology is practically nonexistent outside of the integrated circuit industry. This work provides a synergy of the science of nanorod growth and the technology of metallic glue in ambient. Starting from the science, this thesis presents the design and control of the structure and morphology of nanorods grown by physical vapor deposition. We demonstrate the use of deposited seeds as a method to control the diameter and spacing of surface grown nanorods. These seeds are made of low melting temperature metals that form nonwetting clusters on a substrate. Materials In, Sn, and Ga are used and demonstrated to be effective. The diameter and spacing of nanorods made of the materials Ag and Cu are controlled by use of these seeds. We also demonstrate the capping of nanorods produced by physical vapor deposition with a second step also conducted with PVD. The caps demonstrated are made of metals and metal oxides. The primary application of the metal oxide shells is longer survivability of sensing substrates in Surface Enhanced Raman Spectroscopy. Metal shells on metal nanorods offer improvements in room temperature metallic sealing. Additionally, we introduce our developing technology of metallic sealing using non-vacuum processes. The advance of metallic glue offers enhancements in computing as it can be used to allow processors to run cooler, and provides a room temperature alternative to soldering, among many others. Through this work we build and expand upon the understanding of nanorod growth to produce a technology that may have a widespread impact.

From the Science of Nanorod Growth to Low Temperature Metallic Attachment

Paul Robert Elliott

B.S., Harding University, **2009**

M.S., University of Dayton, **2011**

A Dissertation
Submitted in Partial Fulfillment of the
Requirements for the Degree of

Doctor of Philosophy
at the
University of Connecticut

2017

APPROVAL PAGE

Doctor of Philosophy Dissertation

From the Science of Nanorod Growth to Low Temperature Metallic Attachment

Presented by

Paul Robert Elliott, B.S., M.S.

Major Advisor _____
Dr. Hanchen Huang

Associate Advisor _____
Dr. Stephen Stagon

Associate Advisor _____
Dr. Tai-Hsi Fan

Associate Advisor _____
Dr. Michael Pettes

University of Connecticut

2017

Table of Contents

Table of Figures

Abbreviations and Symbols

°C – degrees Celsius

3-D- Three dimensional

A- Area of contact

Ag- Silver

Au- Gold

Bi- Bismuth

BLT- Bond line thickness

CCD- Charge-coupled device

cm- Centimeter

CPU- Central processing unit

Cr- Chromium

CTE- Coefficient of thermal expansion

Cu- Copper

EBPVD- Electron beam physical vapor deposition

EDS- Energy dispersive X-ray spectroscopy

ES- Ehrlich-Schwoebel

eV- Electron volt

FIB- Focused ion beam

Ga- Gallium

GaN- Gallium nitride

GPa- Giga Pascal

GLAD- Glancing angle deposition

Hg- Mercury

hr- Hours

In- Indium

k - thermal conductivity

KV- Kilovolt

Ls- Separation of nanorods

Lmin- Diameter of nanorods

μΩ·m- Micro ohm meter

μm- Micrometer

mM- Millimolar

min- Minutes

MPa- Mega Pascal

N719 dye- Di-tetrabutylammonium cis-bis(isothiocyanato)bis(2,2′-bipyridyl-4,4′-dicarboxylato)ruthenium(II)

nm- Nanometer

O- Oxygen

Pa- Pascal

PCB- Printed circuit board

Pt- Platinum

PVD- Physical vapor deposition

RA- Thermal resistance

R_c – Contact resistance

R_{eff} – Thermal resistance of an interface

SEM- Scanning electron microscope

SERS- Surface-enhanced Raman spectroscopy

Si- Silicon

SiC- Silicon carbide

SiO_2- Silicon dioxide

Sn- Tin

STEM- Scanning transmission electron microscope

TEM- Transmission electron microscope

Ti- Titanium

TIM- Thermal interface material

TiO_2- Titanium dioxide

TSK- Terrace Step Kink

Tm- Melting Temperature

V- Volt

X_{CuDisk} – Thickness of Cu disk

W/m-K- Watts per meter Kelvin

Zn- Zinc

I. Introduction

This dissertation describes developments that lead to the process of metallically gluing two solids together at low temperature, in air, and under a small pressure. It includes two elements – the science of nanorod growth and the technology of metallic glue. In this chapter, we will first introduce technologies of gluing, and then continue with the introduction of the science of nanorod growth. In Section I.1, we will present existing technologies of attachment in terms of their advantages and disadvantages; these primarily include polymer glues, soldering, brazing, and welding. Through the introduction in this section, we define the need of metallic glue in ambient, after which we explore some of the more recent attempts to meet the needs of a low temperature metallic glue. We will see the steps these take to get us closer to the goal, but ultimately discover how nothing yet meets all the desired criteria for this technology.

In Section I.2, we will present the current state of nanorod growth in terms of both theory and experiment. Through the introduction in this section, we define the need of scientific advancement in nanorod growth. We will then look at the specific technology required for metallic glue, electron beam physical vapor deposition, and overview how the science that reveals how these nanostructures grow allows us the understanding to produce the necessary nanostructures involved.

The introduction ends with section I.3 where we discuss the specific challenges that must be overcome to allow for a low temperature metallic glue. We begin with the scientific understanding in two areas that must be developed. First is the control of nanorod size and spacing and second is the production and application of core-shell nanorods. After this we delve into the technological side of things and explore the necessary mechanical and thermal properties of the metallic glue. To end the introduction, the goal and benefits of using non-vacuum processes are discussed.

To overcome these challenges this work investigates the control of morphology of nanorods. In Section II the methods and equipment used to produce the nanostructures is described. This includes the materials and the electron beam physical vapor deposition system. Characterization of the nanostructures is also described, including imaging techniques like scanning electron microscopy (SEM) and transmission electron microscopy (TEM), as well as the mechanical and thermal testing conducted.

Section III contains the results of the study. In III.1, a method of controlling the separation and diameter of nanorods is discussed. Here, silver (Ag) and copper (Cu) nanorods are used with nucleation sites or "seeds" made of materials such as indium (In). The production of core-shell nanorods is discussed in section III.2. We demonstrate protective coatings for thermal stability, as well as coatings that form an alloy upon contact with other nanorods, to allow for the bonding of room temperature metallic glue. Section III.3 demonstrates the use of the coatings of III.2 to produce a room temperature metallic bond and explores mechanical and thermal properties. Section III.4 contains methods to accomplish bonding without using vacuum equipment.

The conclusions and discussion follow in section 4. This will tie the pieces of this work together and define what has been accomplished. It will also explore the limitations of this study and outline the path forward with the metallic glue technology.

I.1 Background of Low Temperature Metallic Attachment

It is a common practice to join two solids together using a third substance in gluing or soldering. Gluing usually refers to the joining process that is made in ambient – at room temperature, in air, and without pressure, or with a small pressure [1]. Sealing an envelope with polymer glue is a good example. Accompanying this inexpensive and easy process are properties that are undesirable for challenging high-tech environments. For example, polymer glue, as compared to metallic solder, is permeable to air and moisture, degrades fast in ambient, has low mechanical strength, does not effectively conduct electricity or heat, and does not retain its function at high temperatures [2, 3]. In contrast, soldering usually refers to the joining process that uses added molten metal at higher temperatures, generally much above room temperature (~180-300 ^{o}C) [1]. Similarly, welding and brazing also involve high temperature melting, where brazing is joining through added molten metal at even higher temperatures than soldering (~425-1000 ^{o}C), and welding involves melting or fusing of the members to be joined, often under an inert environment (~650-1800 ^{o}C) [1]. The joining from such high temperature processes, as compared to polymer glue, is mechanically strong, effectively conducts electricity and heat, degrades slowly, if at all, in ambient, and its leak resistance to air and moisture goes from good to better with time due to oxidation [1].

Here, metallic gluing refers to the process of joining two solids with metal as the connecting material, which occurs at room temperature, in air, and under low pressure. Metallic glues have the combined advantages of (1) the ambient condition of gluing, and (2) the superior properties of the joint by using metal as the interface material similar to high-temperature soldering (or welding and brazing) making them beneficial to many advanced technologies.

The possibility of a metal glue was realized in the successful attempt to create airtight metal seals using low temperature and pressure [4]. Physical vapor deposition is used to produce nanorods, which are structures with diameters of less than ~100 nm and an aspect ratio of around ~10:1. In this case Ag nanorods are produced on two surfaces. When these surfaces coated with nanorods are brought together, the nanorods coalesce to form a metal film that bonds the surfaces together. The bonded interface shows low porosity,

indicated by the very low diffusion of air and water vapor through the interface, and can be seen in cross sectional images. These results lead us to the realization that high heat transfer should be possible through this thin, pure metal interface [5].

The Importance of Metallic Glue

Desktop and laptop computers are one form of advanced technologies that are common household commodities. The core of computing is the central processing unit (CPU). Removing heat from electronic components is vital to their continued operation. As power densities of components increase, this becomes an ever more challenging task. A current bottleneck in transferring heat out of power generating components is the material used to connect the device to a heat sink, or to connect it to some intermediary structure like a heat spreader. In 2004 this problem forced Intel to switch from focusing on making faster processors to putting more processors on a single chip [6]. This is why the clock speed of computers has not significantly increased in 10 years, but most systems contain at least 4 processors.

Connecting a CPU to external components for heat dissipation is usually necessary, as forced or natural air convection over the device alone provides insufficient cooling. It is possible to merely bolt or clamp the surface of a CPU to a heat sink to improve heat transfer out of a hot device, and this is done in many devices with lower power density. For more power dense devices, this still does not provide enough cooling. The innate surface roughness leads to a relatively low amount of surface area that actually comes into contact between the two surfaces [7], Figure 1 (a). This leads to a high resistance to heat transfer at the interface that slows down the removal of heat from a device [8]. Often thermal grease is used as an interface material, filling the gaps between the heat sink and CPU, but other materials are used such as thermal epoxy, elastomeric pads, and phase change materials Figure 1 (b). Thermal grease is generally made up of a silicone paste, used for its wetting characteristics, low modulus of elasticity, and good thermal stability which is often mixed with a high percentage of high thermal conductivity metal, metal oxide, or

nitride microparticles to help improve thermal conductivity [9]. However, the thermal conductivity of these greases are quite low, a mere 1-2% of copper [10,11]. Greases offer significant advantages of being very easy to apply and remove, are inexpensive, and they overcome the problem of a difference in the coefficient of thermal expansion (CTE) between materials. However, the low thermal conductivity of the grease limits the amount of heat that can be dissipated away from the CPU. This is a significant barrier to further miniaturization and reliability of these devices, such as tablets and computers as the thermal interface material (TIM) layer makes up most of the total thermal resistance of the system [12]. Cooler operating devices are advantageous as keeping the CPU 10-15 ºC cooler can double the lifespan [13]. Additionally, if more heat can be removed from a CPU, then less expensive CPUs can be run faster without damage. Thermal greases also suffer from other problems such as pump out, where the grease is forced out of the interface during thermal cycling, and dry out, where the filler material separates from the paste over time [13]. Both of these conditions result in reduced heat transfer through the interface.

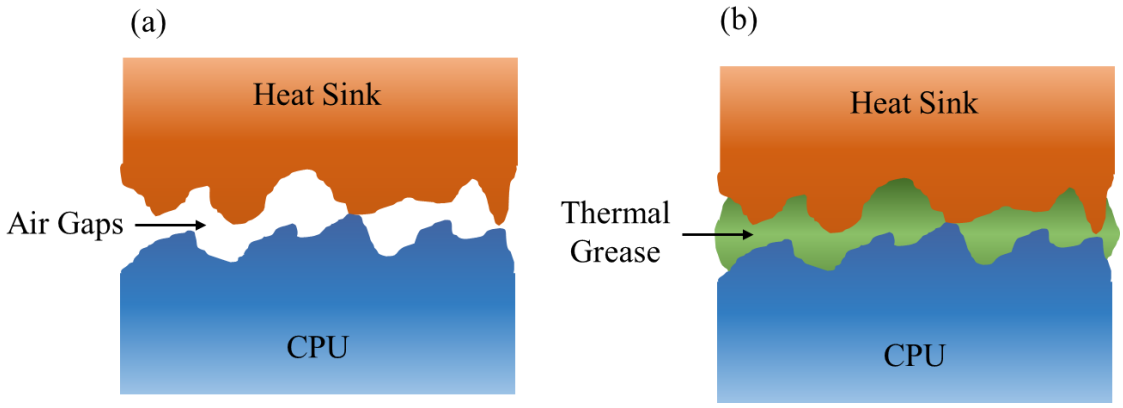

Figure 1. Schematic showing the interface between a heat sink and a CPU. (a) The innate microscale surface roughness leads to airgaps between the surfaces and very little surface contact. (b) Thermal grease fills in these airgaps and provides an easier path for heat through the interface.

For the best heat dissipation the ideal connection conducts heat efficiently. Metals tend to perform very well due to their relatively high thermal conductivity and are common and inexpensive compared to

some of the best performers like diamond and carbon nanotubes [13]. However, if solder is used, the temperatures necessary to create a good bond can damage the CPU by exceeding the "thermal budget" [14]. Also, solder bonds can be relatively thick, which results in reduced heat transfer, and the thermal conductivity of most solders is relatively low, only conducting about 5-20% as effectively as a pure metal like copper [15,10]. Solder can also inconvenient to remove, making repairs difficult [18]. Lower melting temperature metals and alloys, such as those containing gallium, indium, and tin have been used as an interface material in the place of solder [21]. These provide a relatively high thermal conductivity with an all metal interface, but must be liquid at the operational temperature of the device and so suffer from a possibly of dripping out of the interface which can cause electrical shorts, and forming intermetallics that gradually decrease performance [19, 20].

Figure 2 (a) shows the configuration of a CPU with a heat sink in a laptop computer with Figure 2 (b) showing a typical setup in a desktop computer. Desktop computers often contain a heat spreader, which is a plate between CPU and heat sink that is used to spread the heat to a larger area heatsink and acts as a protective covering for the processor. It contains, however, two separate interfaces which require thermal grease or solder, effectively doubling the thermal resistance of a TIM problem. In Figure 2, these are labeled as TIM1 for the CPU to heatspreader interface, and TIM2 for the heatspreader to heatsink interface. As the area of TIM2 is larger than TIM1, a high thermal conductivity in TIM2 interface is not as critical as in TIM1 [22]. It is desirable to find a method to improve the heat transfer through the interface, while eliminating other problems associated with greases and solders. A pure metal glue that sets at or near room temperature would accomplish these objectives.

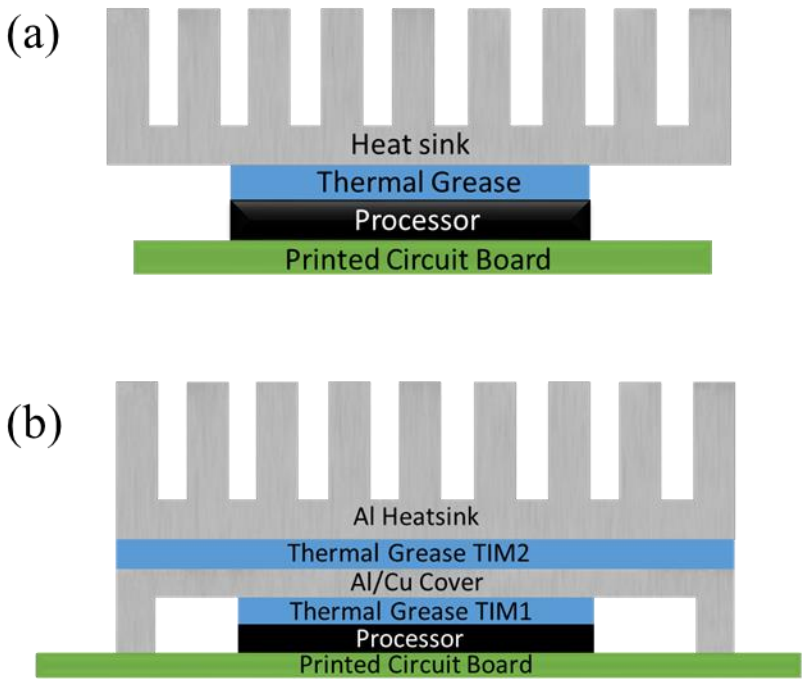

Figure 2. Schematic of a CPU processor attached to a heatsink. (a) Attachment of processor directly to heatsink with thermal grease used in laptop computers. (b) The addition of heat spreader layer acts as a protective cover for the processor but adds additional material interfaces, often used in desktop computers.

In CPUs, and also in many through-hole and surface-mount devices, the electrical connection of the component to other components, generally through a printed circuit board (PCB), is a necessity. The components experience heating when they are soldered to a PCB or require very precise wire bonding or flip chip equipment, which often require a thermosonic bonding method. In some cases, temporary heat sinks must be attached to the component during soldering to prevent damage [16]. Also, as component sizes decrease, soldering or wire bonding become more challenging and voids can lead to joint failure [17]. Additionally, surface mount components must be individually placed onto a circuit board by a robot called a pick and place machine after solder paste is spread onto the solder pads. This then must pass through an oven on a conveyor belt to melt the solder. A metallic glue bond would eliminate the possibility of heat damage during attachment, reduce the cost by eliminating the solder melting oven, and simplify the soldering process by allowing the component to be attached during the pick and place step; Figure 3 (b).

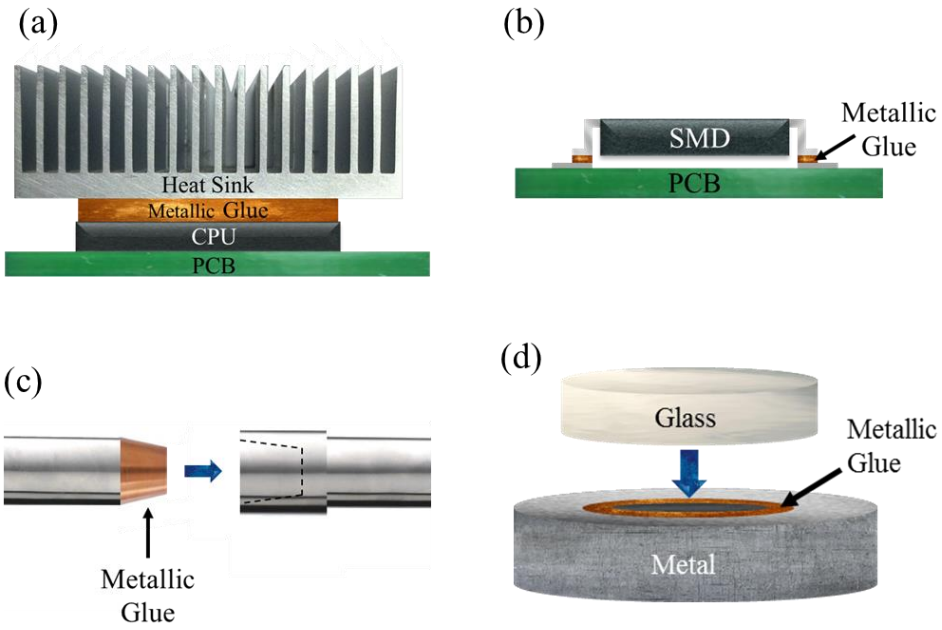

Figure 3. A schematic detailing various applications of metallic glue. (a) A CPU on a printed circuit board connected to a heat sink. (b) A surface mount device being attached to a printed circuit board. (c) A press-fit pipe fitting for environments where welding is dangerous or impossible. (d) A glass plate being attached to metal with a different coefficient of thermal expansion to cover a cavity with a hermetic seal.

A third example is for use in connecting pipes or construction members together and highlights the benefits of the strength of the metal bond; Figure 3 (c). With metallic glue, no gases, electricity, or heat is necessary to form the bond. This leads to a process that has no risk of asphyxiation, electric shock, or burns, and is safe in environments where welding may not be possible, such as hot work in confined spaces. Additionally, no welding skill would be required.

As a forth example, the hermetic sealing of materials with much different coefficients of thermal expansion (CTE) benefits greatly from a room temperature bonding method, Figure 3 (d) . Generally, when sealing metal to ceramic or glass the materials have to be carefully selected to have a similar CTE. If the CTE difference is too large the parts may separate due to geometric mismatch when cooled. When the selection of similar CTE materials is not possible, the geometry of the part has to be carefully designed so that thermally induced stresses to not become too large to cause warpage or material failure. Specific

applications can include, compact fluorescent light bulbs, glass encapsulated diodes, and pressure tight windows for inspection in industrial processes and vacuum chambers.

Metallic Joining

Metallic joining is a common joining process that usually takes the form of soldering and welding. Sealing with metal has many advantages with some of the most notable being, it tends to be very mechanically strong, conducts electricity and heat very well, the bond degrades slowly in ambient if made correctly, and it has a low leak rate to air and moisture. These are very useful in many cases, but it has one significant disadvantage of the high temperatures that must be used to melt the metal to form the bond.

The use of solder is commonplace in joining of electronics. This process generally takes place above 180 ^{o}C and has typically been made up of a large percentage of the toxic metal, lead [23]. To avoid lead, solder materials are making a shift to other materials such as silver and indium. These materials are much more expensive and rare, and most combinations have a higher melting temperature than the lead containing mixtures [25]. Phasing out the use of lead tends to require solders with higher melting temperatures, typically in the range of 260-300 ^{o}C. Compared to certain pure metals (Ag, Au, Cu, etc.), these solder connections have low thermal and electrical conductivity and experience fatigue failure due to low yield strength [26].

Additionally, lead free solders tend to form whiskers, especially those that contain tin. These whiskers can grow quickly under certain conditions and can bridge connections in electronics leading to shorts and failures [27]. Notable failures from such whiskering include the failure of a number of satellites, failures in pacemakers, and the complete shutdown of the Millstone nuclear power station; Figure 4 [28].

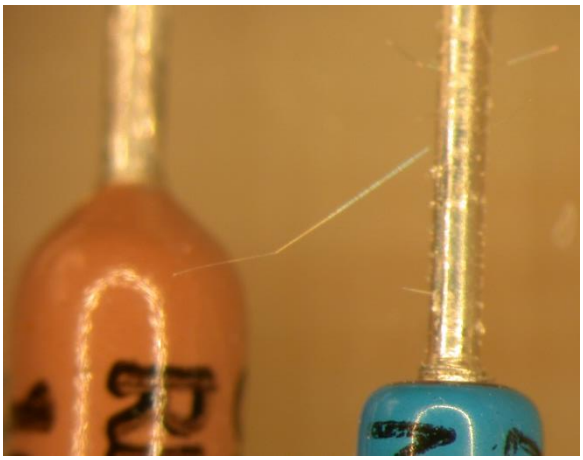

Figure 4. Example of tin whiskers growing from exposed component at Millstone power station. [**31**]

In some high power applications such as automotive hybrid and electric vehicles, aircraft, nuclear environments, radar, or down hole oil environments the current solders cannot meet the temperature requirements experienced by the devices, which can operate at above 350 ^{o}C [24]. Devices based on wide-bandgap semiconductor materials such as silicon carbide (SiC) and Gallium nitride (GaN) are being developed to survive in these environments, and have many additional advantages over silicon based devices, such as improved switching characteristics.

Low Temperature Metallic Sealing

In many cases, it is desirable to form metallic bonds below the melting temperature of the metals involved. To reduce the processing temperature, cold welding of metals at room temperature is possible. This on bulk metals however, requires very high pressures to accomplish, often on the order of 1 GPa [29]. This process happens well with clean, oxide free metals, with Ag and Au being among the best. It is possible to cold weld more reactive metals that form oxide layers, but the pressure must be sufficient to crack the oxide layer and then force the deformation of the metals underneath into contact to from the weld [30].

To reduce the pressure required to form a cold weld, nanostructured metals can be used. Very small particles or films, on the order of less than 10nm, are shown to have different properties than bulk materials,

such as reduced melting temperature [36, 40]. There is some uncertainty to the mechanism, but the most supported causes are high surface diffusion and surface relaxation [35, 41]. In nanostructures the surface area to volume ratio becomes large, as does surface curvature. This leads to movement of a large amount of adatoms on the surface of the structure that can lead to changes in shape [32]. The shape tends to favor the lowering of the overall surface energy of the structures causing structures to work toward becoming spherical in shape for the minimum surface to volume ratio. Factors that affect the lowering of the coarsening temperature can include size [33], morphology [34], and defects [53].

Early work included the investigation of using SiO_2 nanoparticles to form bulk coesite at temperatures less than the melting temp of SiO_2. Temperatures of 450 ^oC we used under the high pressure of 5 GPa for ~30min [37]. Later work included metals with this process. The sintering of Ag and Au nanoparticles of 20nm in diameter was investigated, with findings of sintering occurring at room temperature for Au and at 60 ^oC for Ag, with no pressure applied, under high vacuum, Figure 5. It was seen that the sintering was slowed by exposure to air before heating indicating that the formation of an oxide layer on the surface likely hinders the process [38]. At room temperature, while under high vacuum, nanoparticles deposited onto glass of Au, Ag, Al, and Cu all showed decreases in resistivity over time caused by necks forming and growing between nanoparticles [39]. When oxygen, wet air, or dry air was added an immediate jump in resistivity occurred and preventing further neck growth in Ag, Al, Cu. Au was less effected by the gases and showed only a slowing of the resistivity decrease. Ni and Ar gas did not affect the neck growth.

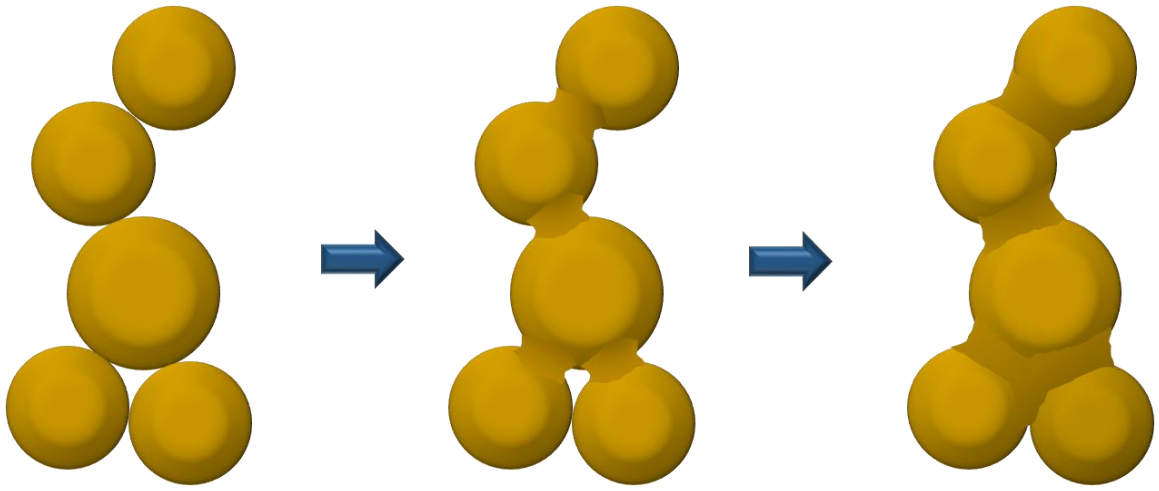

Figure 5. The sintering of Au particles at room temperature under high vacuum. Necks between nanoparticle form and grow.

In a more recent case, Au nanowires are welded together at close to room temperature under a pressure of ~4.7 MPa, under high vacuum [35]. The process occurs very quickly and results in single crystal welds with no defects. The electrical and mechanical properties of a welded wire are the same as in a whole, non-welded wire. This welding was observed using insitu TEM when very small wires (~3-10nm in diameter) are brought into contact, if the crystal orientation of both are aligned.

Silver Sintering

A field of interest has developed around the process called Silver Sintering, especially in the electronics industry as it offers advantages over soldering, such as much higher operating temperatures, up to around 0.8 Tm of Ag (~715 ^{o}C), and the potential to require lower temperatures during manufacturing. Here, in the attempt to move away from the expensive vacuum processes, Ag nanoparticles are dispersed in a paste or liquid and then forced to combine by various means at temperatures and pressures low enough that they can be used on computer chips and components. A few companies have begun offering sintered Ag paste such as, Henkel, Heraeus, and Namics. Users of these pastes include Hitachi and ON Semiconductor, and they are present in some Ford and Nissan vehicles [42]. Disadvantages include the fact

that Ag paste is generally 4-5 times more expensive than the more common solder and epoxy solutions and that significant applied pressure can be required [42].

There are two main areas being investigated to perform nanoscale sintering more effectively. The first method utilizes raised temperature to activate the nanoparticles. This consists of decomposing an organic shell to expose the pure Ag metal underneath, allowing it to sinter with other particles. The second method uses chemical instead of heat to strip away the protective coating, Figure 6.

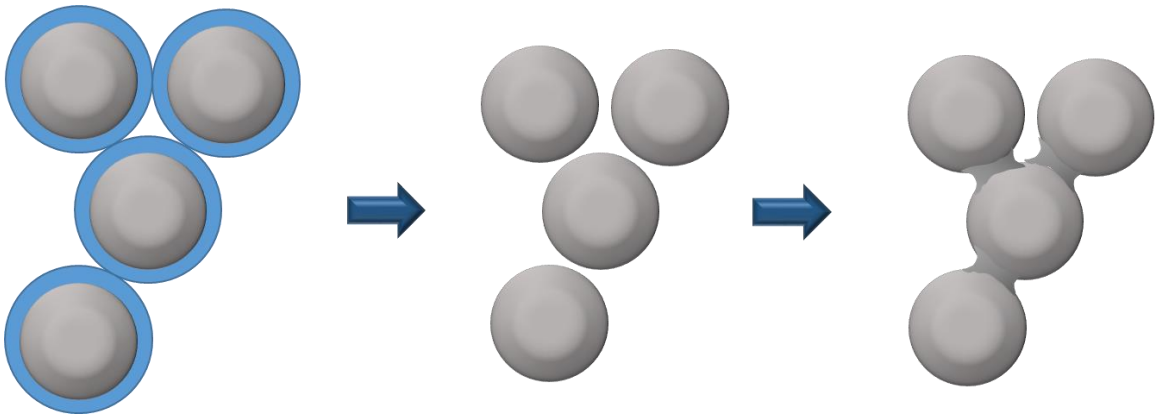

Figure 6. The sintering of Ag particles at room temperature after removal of organic shell by temperature or chemical means.

Temperature Activation

Ag nanoparticles of ~11nm in size that are produced using a solution synthesis method have been used to attach Cu disks together [43]. The nanoparticles have an organic coating layer derived from myristyl alcohol during the manufacturing process that help to keep the particles from clumping or sintering before the desired time. This protective layer is an important aspect to make the process work, but it can prove difficult to remove so that the metal beneath is exposed sufficiently to allowing bonding. In this case, a raised temperature of 300 ºC is used to oxidize the organic layer. The pressure applied during bonding is either 1 or 5MPa. The shear strength of the bond once made in the 1 MPa case is greater than 25 MPa.

Ag nanoparticles have also been used to attach Cu foil to Cu wire (~50 μm in diameter). In this example, the organic layer is largely destroyed at 160 ºC allowing for the nanoparticle sintering to take place [44]. At this temperature the bond is sufficiently strong for the wire to break before the bond in shear tests while using an applied pressure of 5 MPa during bonding. Shear tests showed failure at 2.8 MPa when 160 ºC was used and 21.9 MPa when 300 ºC was used.

Various sintering solutions exist commercially through companies such as Henkel. One embodiment is Ag sintering paste [45]. This is generally applied to PCBs the same as solder paste by using a stencil and squeegee. The layer is then dried in an oven for 20 minutes at a temperature of 120 ºC. Components are then put in place with a pick and place machine that uses raised temperature to temporarily stick the component in place. The paste is then sintered at 250 ºC using a pressure of 10 MPa for 2 minutes. This provides good adhesion with good electrical and thermal conductivity, with better thermal and power cycling performance than lead-free solder, but there is a risk of components cracking from the pressure applied during the sintering.

Chemical Activation

It is also possible to remove the protective capping layers on nanoparticles by using solvents instead of raised temperatures. A dodecyclamine coating on Ag nanoparticles can be removed by dipping them in methanol [46]. The coating was sufficiently removed for coalescence to begin after ~30s. The resistivity was shown to continue to decrease with dip time, reaching 0.73 μΩ·m with the longest dip of 7200s. For comparison, the electrical resistivity of the common tin lead (Sn60Pb40) solder is around 0.153 μΩ·m. In another case by the same group, Ag nanoparticles are coated by Alkylamine, in a toluene solution [47]. When the toluene evaporates, the organic coating is destroyed, leaving the exposed Ag and allowing sintering. The resistivity in this case reached 4.9 μΩ·m.

In an applied case, a solution containing Ag nanoparticles with polyacrylic acid sodium salts coating is printed with a desktop injet printer onto an area of photo paper [48]. Drops of poly(diallyldimethylammonium chloride) (PDAC) are placed onto the layer causing small areas to sinter

at room temperature. This allows for very good control over the areas where sintering occurs on a surface allowing for the printing of circuit components. In a similar case, Ag nanoparticles with a polymer coating are dispersed in a solution. Here, Cl- ions in the solution that act as destabilizing agents. When the paste dries, the Cl- ions come into contact with the polymer shells on the Ag nanoparticles which causes the shells to detach. This allows the Ag particles to contact and sinter at room temperature [49].

It is worth noting that the solution methods do allow for sintering of Ag at room temperatures, however, it is difficult to use these processes to bond surfaces together, and none of the reviewed literature report accomplishing this. This is likely due to the difficulty in getting the activating chemicals to the nanoparticles when they are covered, or with the difficulty of the solvent evaporating.

Solid-State Bonding

Another method of bonding involves making a layer of Ag nanoparticles on a film by using a solution process and then pre-sintering the particles to form a film. In this method the preformed film can be cut to a particular size and then placed between the two surfaces that are to be attached. This makes it convenient to use in a pick and place machine, as parts or areas on a board can be precoated with the film layer. When bonded at 200 ^{o}C and at 3 MPa, a thermal conductivity of 250 W/m-k can be achieved. The shear strength of the attached die is around 15 MPa, increasing to about 30 MPa when pressing is used at 35 MPa [50]. Additionally, thin Ag foils can be used to perform a similar process in place of the nanoparticle film. These are generally in the range of 10-20 um thick and are attached at 150-250 ^{o}C, but they require a much higher force for bonding, >50 MPa [51].

Reactive Metals Bonding

Using more reactive metals that tend to form oxide shells, such as Cu, to perform low temperature attachment is more challenging due to the protective nature of the shell. Cu is an important area of investigation as it has similar thermal and electrical conductivity to Ag, while being much less expensive.

In one study, Cu nanorods were grown on a surface by using the glancing angle physical vapor deposition technique [52]. These nanostructures were observed to begin coarsening under high vacuum at 400 ºC, which is well below the melting temperature of 1083 ºC. At 550 ºC the nanorods formed a continuous film. Similar results are seen in individual nanorods of Cu that are not attached to a substrate [53].

More practically, a Cu nanorod coated surface has been used to bond two Si wafers together [54]. After deposition of the Cu, the samples are quickly transferred to a vacuum environment or a reducing atmosphere to reduce the effects of the oxide layer that quickly forms on the outside of Cu nanorods in air. Bonding temperatures of 200ºC to 400ºC are used under an pressure of 0.32MPa for one hour. Cross sectional images of the bonds show many pits and voids at temperatures below 400ºC as described in Figure 7. While being significantly less than the bulk melting temperature of Cu, this processing temperature is still quite high for use in most electronics.

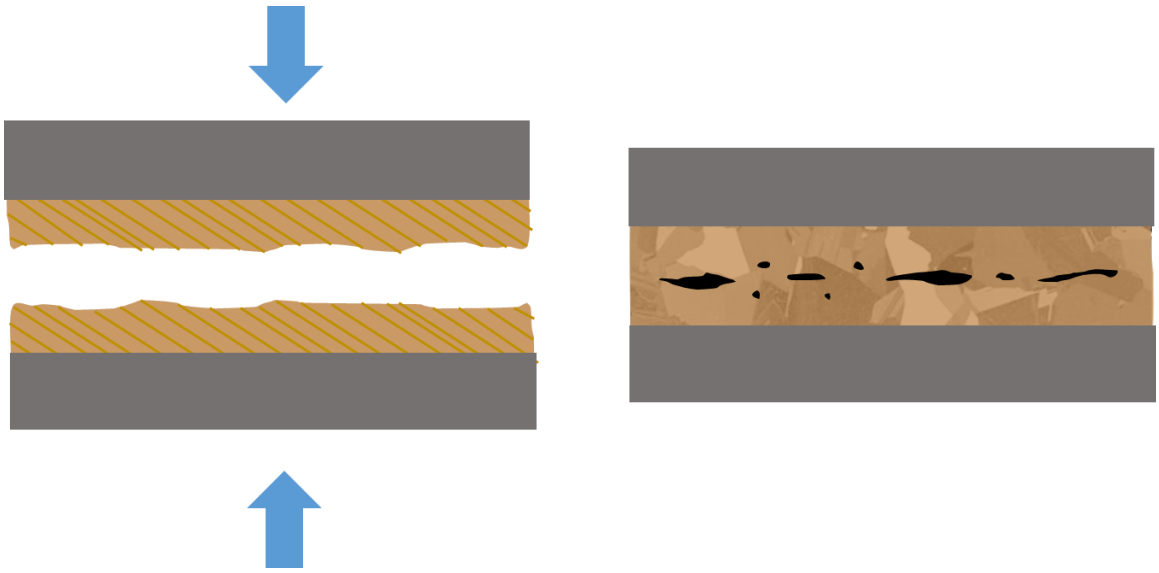

Figure 7. Si wafer bonding process using Cu nanorods. Cu nanorods are spaced very close together essentially making and oriented porous film on a Si wafer (left). After pressing and heating in a reducing environment a bond is produced with voids (right).

Transient Liquid Phase Bonding

The Transient Liquid Phase Bonding attachment method is a way to attach surfaces together at a relatively low temperature to produce a bond that is stable to a much higher temperature. This uses a thin layer of a low melting temperature material that is spread between two layers of a different material with a higher melting temperature. The lower melting temperature material is generally deposited onto one side of the high temperature material, or is placed as a foil [55]. The sandwich is pressed together and heated to just above the melting temperature of the low Tm material, Figure 8. The low Tm material then diffuses into the high Tm material to form an alloy with a resulting Tm between the high and low material. Advantages of this process include void free bonds, low bonding temp with high temperature stability after bonding, and a flux free process as fluxed are corrosive and can leave residues that must be cleaned [56].

Common transient liquid phase bonding systems include Sn-Ag, Cu-Ag, Au-Sn, Au-In with the lower temperature metal acting as the middle layer. Processes using Au have been used to mount SiC diodes [57] and Cu-Sn systems have been used to mount solar cells [58]. In one example the Sn-Ag system is used to bond SiC Schottky diodes where the tin (Sn) is placed between the two sides of Ag as a thin foil [55]. Under a pressure of 5 MPa the layers are heated to 240 ^{o}C for 30 min in an atmosphere of 0.02 Pa. For reference, the melting temperature of Sn is 232 ^{o}C and Ag is 962 ^{o}C. Initially, the Sn is consumed to form Ag3Sn with a melting temperature of 480 ^{o}C. After annealing at 48 hr at 200 ^{o}C the Ag3Sn has largely been converted to Ag85Sn15 with a melting temp of 600-724 ^{o}C.

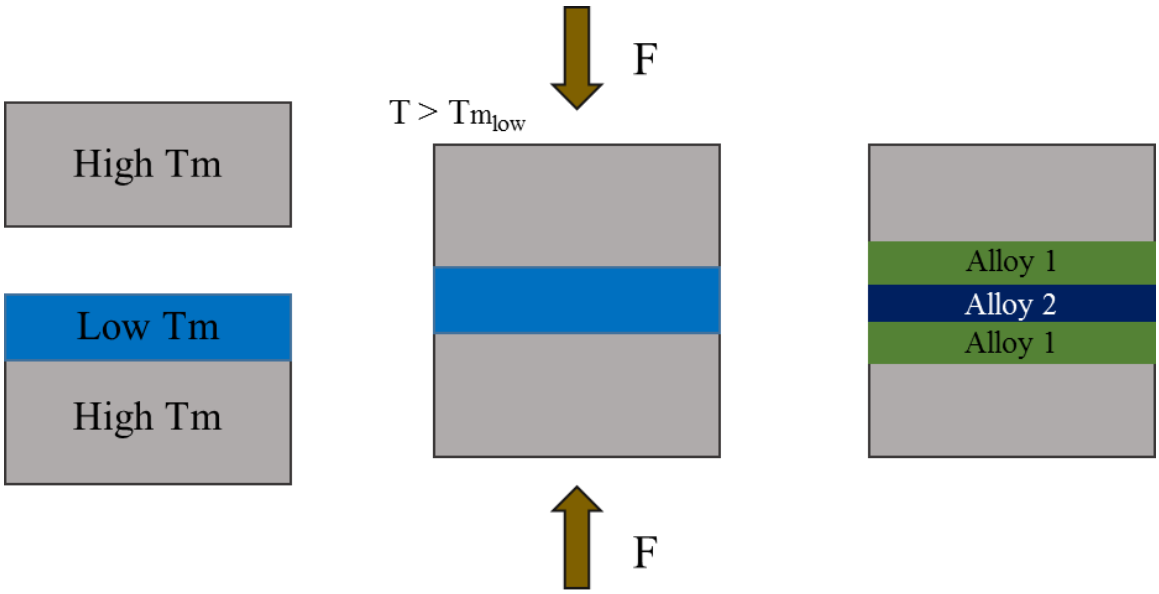

Figure 8. Process of Transient Liquid Phase Bonding. A low Tm material is sandwiched and pressed at raised temperature between a high Tm material. Over time various alloys are formed with a higher Tm than the low Tm material.

Metal Amalgams

Metal amalgams are alloys made up of different elements that begin as a liquid metal and solid powder mixture which solidifies over time. These are typically used in dentistry to fill cavities that form in teeth from tooth decay. The first record of the use of an amalgam is from China in 659 [59]. The liquid mixture is placed into the tooth cavity and compacted and shaped. Over a few minutes the different elements combine to form alloys, and the amalgam hardens and expands to fill in the hole and to lock into place.

Figure 9. Dental amalgam filling a cavity in a molar.

Modern Amalgams contain about one part liquid mercury (Hg) that is mixed with one part of a solid powder consisting of a mixture typically of Ag, Sn, Cu, Zn, and Hg [61]. Often, both components are prepackaged into a small capsule in separate compartments. Before mixing, a separating membrane is broken, which allows the components to mix. The capsule in then placed into an amalgamator or triturator, which shakes the capsule at high speed for around 20 s.

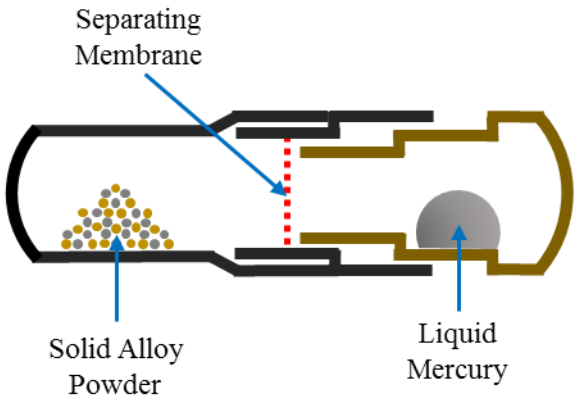

Figure 10. Capsule of dental amalgam containing solid powder and liquid mercury in different compartments separated by a membrane. The capsule is compressed lengthwise to rupture the membrane.

The two primary mixtures of solid particles fall into the categories of low copper alloys (<6% Cu) and high copper alloys (6-30% Cu) [62]. High copper alloys are used most often as they have better physical properties such as better corrosion resistance due to a reduction of Sn7Hg, and lower creep. A typical composition of high copper alloy is Ag 40–70%, Sn 12–30% and Cu 12–24%, with the possibility of In 0–4%, Pd 0.5% and Sb <1% [61].

The solid powder can be a mixture of individual particles of the specific elements used, or can be alloy particles that contain all of the materials. They are produced by lathe-cutting or milling a bulk part of the element or alloy, which produces irregularly shaped particles, or they can be produced in a roughly spherical form by atomizing the material. The atomization process occurs by spraying the liquid metal into a chamber filled with an inert gas which causes the material to cool and solidify into a round shape before reaching the bottom. Both kinds of particles are then heat treated to remove stress in the material and then washed in acid to remove oxide from the surface. The average particle size is ~15-35 µm [61].

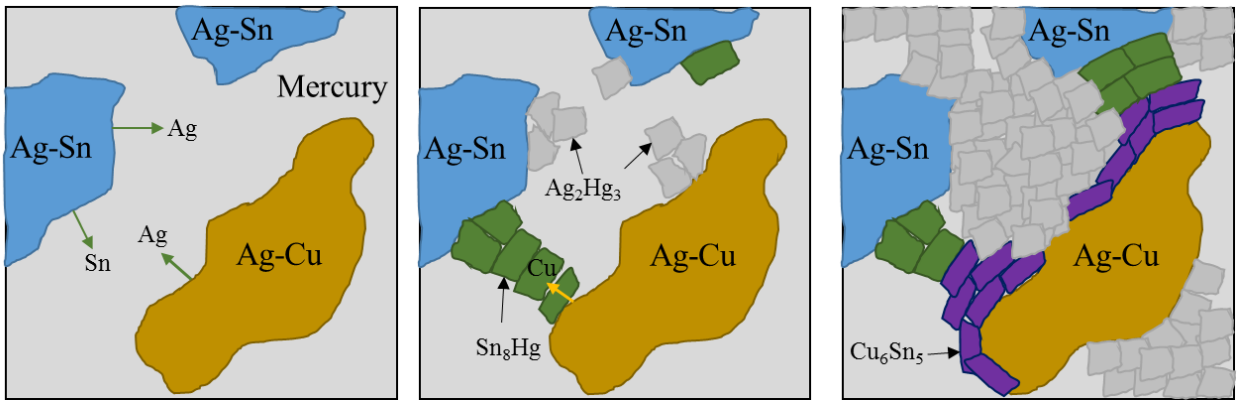

Figure 11. The mixing process in a high copper amalgam.

A significant disadvantage to the use of conventional amalgams in the presence of mercury. Mercury is a heavy metal that is known to have significant negative impacts on human health [64]. While the negative impacts of dental amalgams remains controversial, a non-mercury option is preferred to put patient's minds at ease, and to eliminate the need for extra precautions such as waste water mercury treatment systems in dental offices [63].

One possible all metal alternative uses the element Gallium (Ga), in place of Hg. Ga has a low melting temperature (30 ^{o}C), similar to Hg, and can be mixed with In and Sn to form a liquid eutectic alloy at room temperature [60]. One gallium based product that received FDA approval in 1995 is called Galloy. The composition for the liquid portion consists of Ga (62%), In (25%), Sn (13%) and Bi (0.05%), with the solid portion of spherical particles of Ag (60.1%), Sn (28.05%), Cu (11.8%) and Pt (0.05%) [65]. Gallium alloys have not gained widespread use due to difficulty in handling as they adhere more strongly to mixing capsules and placement tools than traditional amalgams, as well as having poor corrosion resistance usually lasting less than 2 years in a tooth [60]. Additionally, gallium based amalgams show more expansion than those with Hg, especially when contaminated with moisture, seen in one study to cause teeth to rupture in when larger cavities are filled [66].

Bonding Using Silver Nanorods

The first realization of bonding at less than 100 ^{o}C while not using chemicals, high pressure, or a vacuum environment during bonding occurred in 2013 by our group [4]. In this case, the goal was to produce hermetic seals that could be fabricated at low temperature and pressure. The application in mind was to seal dye sensitized solar cells to reduce the cell's fast degradation due to the penetration of oxygen and water through the typically used polymer seal. The seal needs to be fabricated at low temperature so as not to damage the cells. This was successfully accomplished and the leak rate of the metallic seal was shown to be three orders of magnitude lower than that of polymer seal, allowing the organic solar cells to survive long term.

This was accomplished by the process shown in Figure 12. In Figure 12 (a) two surfaces, which are to be bonded together, are shown facing one another. Each surface is covered with silver nanorods that stand off the surface at a high angle relative to the surface normal. When the mating surfaces are brought together, the large spacing of the nanorods allows them to slide between those on the opposing surface and to interpenetrate, Figure 12 (b). Further, due to the small normal diameter a mechanism of surface diffusion

becomes active, so diffusion on the nanorod surface is much faster than on flat surfaces [35]. The contact of the sides of the nanorods through interpenetration provides high surface area contact, maximizing the effects of the fast surface diffusion, causing the sides to bond together, Figure 12 (c).

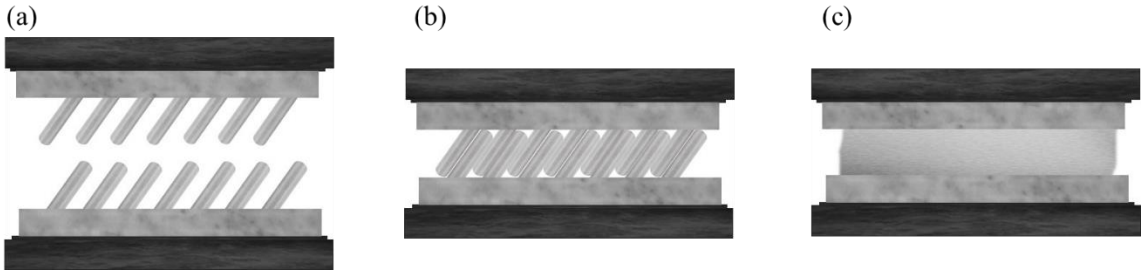

Figure 12. A schematic of metallic gluing enabled by well-separated metallic nanorods: (a) two sets of well-separated nanorods of Ag are brought together; (b) they interpenetrate; (c) under pressure the fast surface diffusion allows for the joining of the two sides.

The SEM images in Figure 13 show a cross section of the metal glue after two surfaces have been bonded following the processes in Figure 12 (a-c). When pressed together at room temperature at 9MPa some voids occur – Figure 13 (a) [4]. To reduce the void concentration a higher processing temperature is needed. As shown in Figure 13 (b), performing the gluing process at 100^{o}C will largely eliminate the voids.

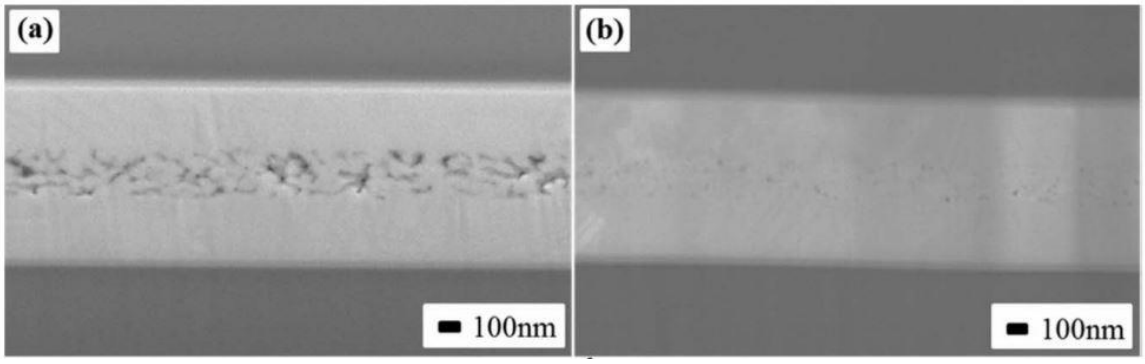

Figure 13. A metallic glue formed in air, and under a small pressure of 9 MPa (a) at room temperature, and (b) at 100 ^{o}C. Reprinted with permission from [**4**].

Even with voids, the metallic glue shown in Figure 13 (a) has superior thermal conductivity and leak resistance. In tests running a simulated CPU at moderate load with forced air cooling the metallic glue has been shown to reduce the CPU temperature by 8 ^{o}C ±3 ^{o}C as compared to the widely used thermal grease, Arctic Silver® 5, when operating at 61 ^{o}C. This is significant as keeping the CPU 10-15 ^{o}C cooler can double the lifespan [13]. The leak rate of the metallic glue shown in Figure 13 (a) is three orders of magnitude lower than that of polymeric glue. This leak resistance meets the standard for organic solar cell and organic light emitting diode technologies [4] allowing them to survive long term. These cells have been too costly thus far and this sealing technique may help launch a new generation of inexpensive solar and lighting technology.

The first material of interest in nanorod bonding is Ag. This has high thermal conductivity and has been shown to produce low temperature seals in previous work [4]. The noble metal nature of Ag makes it a good candidate as it is resistant to the formation of oxide layers which impedes the bonding process. Other noble metals are also likely to form bonds in a similar matter, such as Au and Pt, but these are more expensive and have lower thermal conductivities. It is also desirable to use Cu as the nanorod material as a method to reduce the cost which still achieving a comparable thermal conductivity to Ag.

I.2 Overview of Nanostructures

Physical vapor deposition (PVD) allows for the growth of both continuous thin films and small (<100 nm in diameter) nanorods of metals. Well-separated metallic nanorods have many technological applications. Metal nanorods are the fundamental component in making metal glue a reality. They are also fundamental in the production of many surface-enhanced Raman spectroscopy (SERS) substrates. Nanorods are produced in our research by the physical vapor deposition process [67]. An electron beam is directed onto a source material in a vacuum chamber, causing the source material to vaporize. The vapor moves away from the source in a straight line, eventually striking the walls and top of the vacuum chamber. When a substrate is placed in a normal orientation in the path of the vapor, atoms of the source material

strike it and stick, forming a film. When the substrate is tilted to a high angle, due to the wetting condition of the vapor material on the substrate material and a geometrical shadowing process, nanorods form instead of a film.

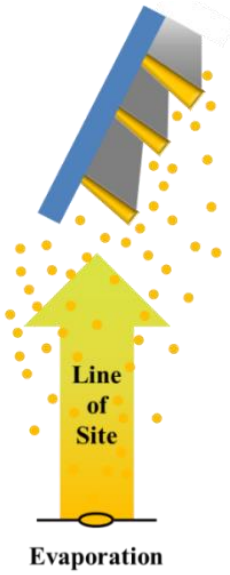

Figure 14. Schematic of the PVD growth of metallic nanorods under GLAD using evaporation.

The physical vapor deposition method of growing nanorods offers important advantages to make the metallic gluing process possible. The first advantage is the cleanliness of the system. As the process occurs in a vacuum, there is little interaction with air that can cause oxidation or other chemical reactions with the metals being used. Most importantly, nanorods grown in vacuum have a pure metal structure with no contamination as a coating. In solution processes especially, nanorods nearly always have a contamination coating. By using high purity source materials in the vacuum process, high purity nanorods can be produced, and contamination can be largely avoided.

Physical Vapor Deposition

Physical Vapor Deposition is a process that adds energy to a material, causing it to vaporize and then deposit on some other surface. It is performed in a vacuum environment and is capable of depositing many different kinds of atoms and molecules including metals, metal oxides, and polymers [68, 69]. PVD is used in a variety of applications such as coating cutting tools to improve abrasion resistance [70], coatings on optics to change the reflectivity [71] or make them conductive [72], and producing thin film solar panels [71], among many others [73, 74, 75]. Many methods exist to provide the energy necessary for the evaporation of the source materials. A few examples include: evaporative deposition which adds energy by resistive heating, pulsed laser deposition which adds energy by a pulsed laser, electron beam deposition adds with an electron beam, and sputter deposition where a source material is bombarded with atoms or ions causing the source material to be ejected.

Typically, thin films are formed when producing coatings by PVD. Other structures are also possible, however. To form nanorods by physical vapor deposition a number of variables must be correct. This section will describe this process and the important contributions that lay the foundation for metallic glue on which this work will be built.

The method used to produce nanorods by physical vapor deposition is known as glancing angle deposition or GLAD [78]. A similar process is used to produce thin films on a surface, but in the case of GLAD, the surface normal of the substrate is highly angled as compared to the incoming deposition. This process can result in a number of different nanorod morphologies. The standard shape is a basic column at a low angle relative to the substrate surface. Figure 15 demonstrates standard Ag nanorods produced by GLAD. By rotating and angling the substrate in various ways during deposition, other shapes are possible such as nanorods perpendicular to the substrate, fans, zigzags and helices [67]. Figure 16 demonstrates nanorods produced close to substrate normal by rotating the substrate during deposition, and in a zig-zag shape by rotating 180 degrees quickly multiple times.

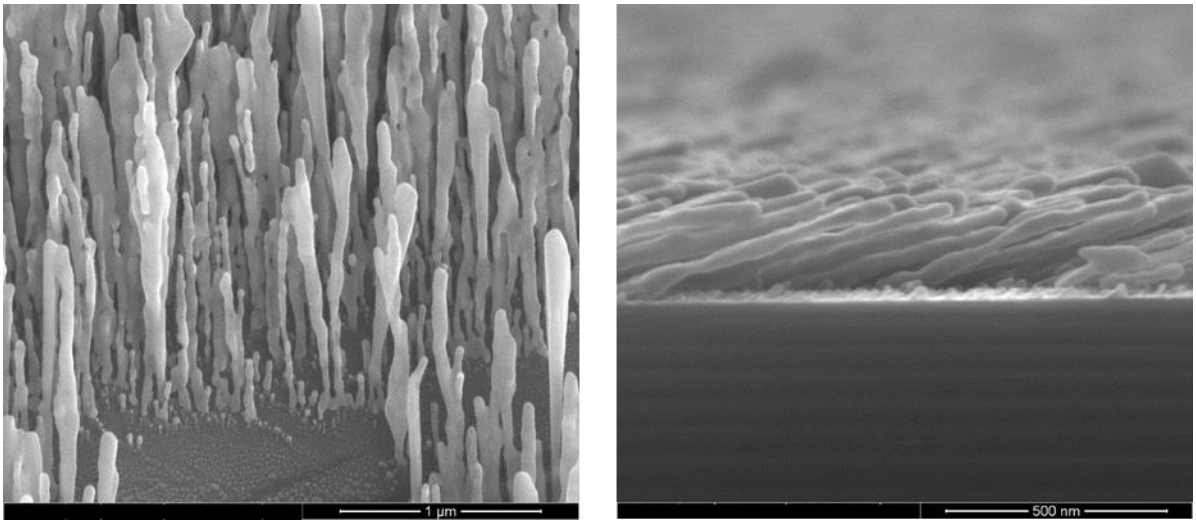

Figure 15. SEM images of Ag nanorods. The left image in viewed normal to the substrate. The right is a cross sectional image showing the low angle of nanorods from parallel to the substrate.

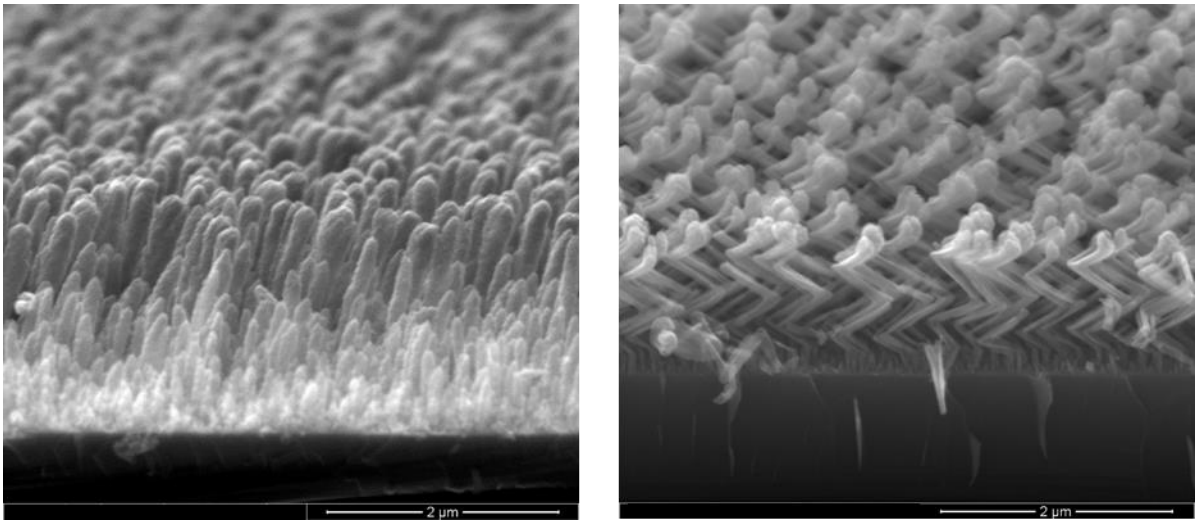

Figure 16. SEM images of TiO2 nanorods formed into shapes using substrate rotation. Nanorods with an angle close to substrate normal (left), and nanorods with a zig-zag shape (right).

The process of physical vapor deposition occurs under high vacuum which allows for a very clean environment that eliminates many variables that normally occur in nanorod production, such as other species in a solution, and many kinds of contamination [79]. The small amount of air and contamination that is present in the vacuum chamber is still a factor and is considered in some cases [80]. The diagram in Figure 17 shows the deposition process. A very pure source material is heated inside of the chamber using

a directed electron beam. This becomes a vapor in the low pressure environment and travels away from the source ballistically. As these atoms of source material hit the walls of the chamber or a substrate placed inside they tend to stick due to the very high supersaturation environment and surface energy. This sticking or adsorption usually begins with physisorption, which is a weakly bonded precursor state, caused by van der Waals force. From here atoms either desorb and leave the surface to go back into free space, or form a stronger chemical bond with the surface atoms; chemisorption. These stronger bonds are usually metallic, but can also be covalent or ionic, depending on substrate and deposition material. A sticking coefficient describes the fraction that remains on the surface [81].

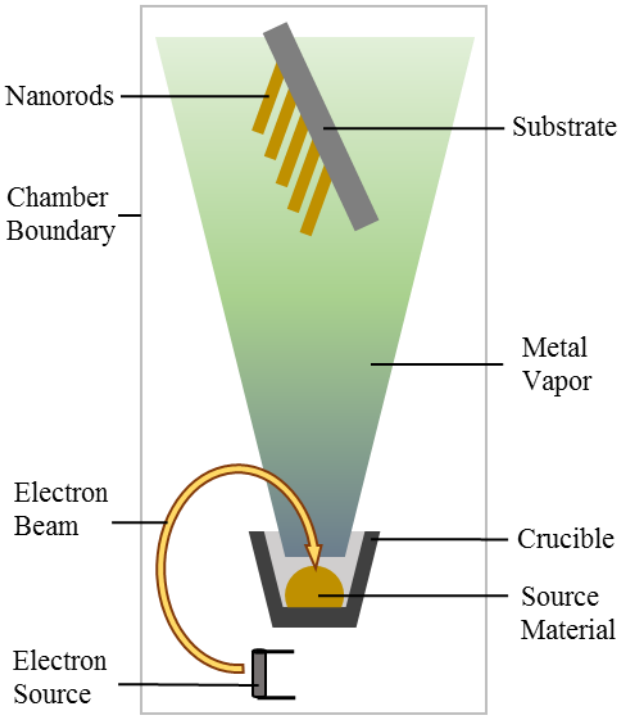

Figure 17. Schematic of vapor deposition process, with nanorods growing on a substrate near the top.

Once chemisorbed on a surface, the atoms are still able to move about in a process called surface diffusion [82]. This involves the partial breaking of bonds between the new atom and the surface atoms, allowing the new atom to move to a new site and form bonds there. The adatom sits in a potential energy

well when it is in a bonded location. To change location it has to move up out of this saddle point, where it will then resettle into a neighboring well. This process of random walk of atoms on a surface is described by the Arrhenius equation and atoms tend to spread out in a Gaussian pattern [81].

Nucleation occurs when an adatom on a flat surface meets another adatom. They tend to stick together due to the overall lowering of surface energy, forming a dimer. Once a dimer or larger, the nucleus tends to stop moving on the surface. As other atoms move about and hit the cluster, they tend to stick together. The process of adatoms moving about and sticking in low energy locations is described by the Terrace Step Kink (TSK) model; Figure 18 [76, 77, 83]. An adatom on a surface desires to have as many of its bonds filled as possible. When and adatom moving along a terrace meets a step it prefers that location to the terrace, as its free energy is lowered. If it enters a kink, it is even more preferred.

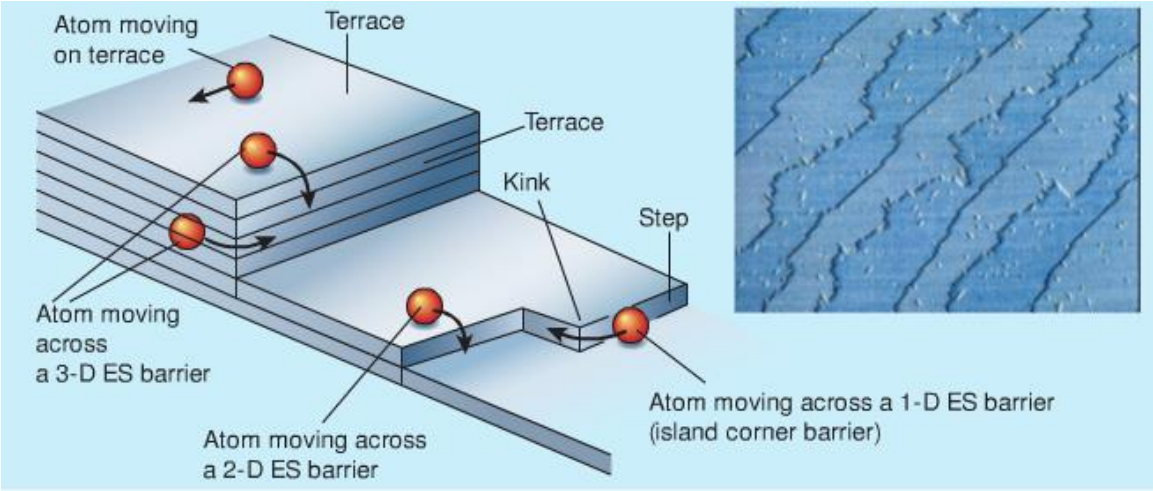

Figure 18. The terrace-step-kink (TSK) model of a thin-film surface. The surface consists of terraces separated by steps; a kink is a step on a step. Atoms travelling over steps that are one-atomic-layer high must cross an energetic barrier, the two-dimensional Ehrlich–Schwoebel (ES) barrier. At kinks, atoms experience the 'corner-crossing' barrier, a one-dimensional version of the ES barrier. Liu et al. [**85**] have identified a three-dimensional ES barrier for atoms travelling over steps that are four or more atomic layers high, or over the edges between two facets. The validity of the TSK model for thin films has been confirmed by the detailed imaging made possible by the scanning tunneling microscope. The inset image shows the surface of a thin film of silicon (100 nm x 80 nm). Terraces separated by single-atom-high steps with many kinks can be seen, stepping down across the image from upper left to lower right. The white spots are atomic vacancies in the terraces. [**84**]

To better understand the process, atoms were placed on terraces and observed. They were seen to reflect back at the edge of terraces [86]. As an atom on a terrace has more nearest neighbors than it does at an edge it was understood that the decrease in binding energy at the edge acts like a diffusion barrier. Other work explained that atoms are captured on steps at different probabilities, depending on whether they are moving up or moving down [87]. This barrier or edge has come to be known as the Elrich-Schwoebel (ES) barrier where moving along step edges is considered 1-D and moving over step edges is 2-D. The difficulty is that it predicts that multiple layer surface steps would not be kinetically stable as adatoms would tend to move away from step edges. This would indicate that the formation of nanorods is not possible.

In additional to the 1-D and 2-D ES barriers, more recent work has shown the existence of an additional 3-D ES barrier. This is the barrier of movement over multiple layer steps. This barrier is able to be quite large even when the 2-D barrier is small and can be thought of as diffusion between surface facets [88]. In 3 dimensional models the 3-D ES barrier is reached at ~4 surface steps [85] and that the large 3-D barrier causes steps to bunch and cluster thus allowing the production of nanorods [89].

Controlling the growth of nanorods from PVD relies on two primary factors. The first is the control of the process variables, and the second is depends on the nucleation on the substrate. Some of the variables that can be controlled during growth include (1) incidence angle of the substrate relative to the vapor flux, (2) the deposition rate of metal atoms, and (3) the substrate temperature. Deposition rate and substrate temperature – coupled control of kinetics. The nucleation can be heterogeneous on a flat substrate, with nuclei forming randomly on the surface, or nucleation can be forced at locations by various means.

The strength of interaction between atoms of the substrate and atoms of the deposition material effect what sort of structure is formed. If the interaction is very strong, or the deposition wets the substrate, the substrate material has a strong desire to be covered by the other material energetically. This results in flat films being formed and is called the Frank-van der Merwe (or layer-by-layer) growth. When the interaction is not very strong, or non-wetting, the deposition atoms prefer to form 3D islands, as a spherical shape is preferred. This is called Volmer-weber (island formation) growth. An intermediate phase is also

possible, where the exposed substrate first is covered by layer-by-layer growth to a critical thickness, then as the surface becomes effectively a different material, the condition changes to energetically prefer island formation. This is Stanski-Krasanov (or layer plus island) growth.

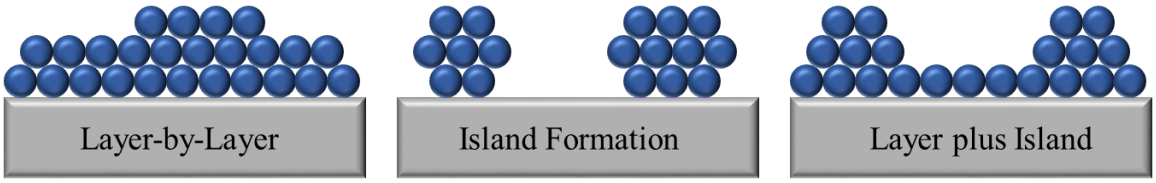

Figure 19. The primary modes of film formation. The grey rectangle represents the substrate with the blue balls representing adatoms on the surface.

When vapor hits a flat surface and is adsorbed, either on a plain substrate or the top of a nanorod, it is still very free to move about as a single atom due to surface energy interactions. The atom will move about on the surface until it meets another atom. When these atoms meet they tend to stick together as this causes the total free energy to be lowered. As more atoms on the surface are encountered they are captured and the group grows and has a higher chance of remaining where it is on the surface as it gets larger. The higher the deposition rate, the more atoms there are moving about on the surface at one time, this will increase the probability of them meeting and sticking. This tends to keep rod diameter small. The higher the temperature, the more likely it is that an atom will have enough energy to move off the top surface of a growing rod to the side. This causes rods to grow in diameter until a certain point where the diameter stabilizes.

The separation of the nanorods (Ls) relies primarily upon the material deposition rate the substrate angle and the substrate temperature and the wettability of the substrate [90, 91]. When the substrate is nonwetting to the nanorod material a type of growth occurs, called type II, where nanorods resemble cylinders or inverted towers. Here, the spacing of the clusters as the cluster density approaches its maximum determines the spacing of the nanorods. Higher deposition rates increase the adatom

concentration on the surface, increasing the probability of single adatoms meeting, and therefore decreasing the size of clusters. High substrate temperatures increase adatom mobility on the surface and increase the likelihood of clusters joining, resulting in fewer larger clusters. The angle of the substrate doesn't directly affect the formation of cluster on the surface, aside from higher angles resulting in lower deposition rates, but higher angles increase geometric shadowing, which causes rods to grow only on farther apart clusters.

To bring the various parts of the process together, the growth of nanorods is shown in Figure 20. Metal vapor atoms from the electron beam heated source land on the substrate at a high angle relative to substrate normal. These adatoms then move about until nuclei or mounds are formed. The height of the growing nuclei then block atoms from landing in the shadowed region behind the nuclei, landing on the top instead. The 3-D ES barrier tends to trap adatoms on the top of the nuclei, leading to the growth of nanorods.

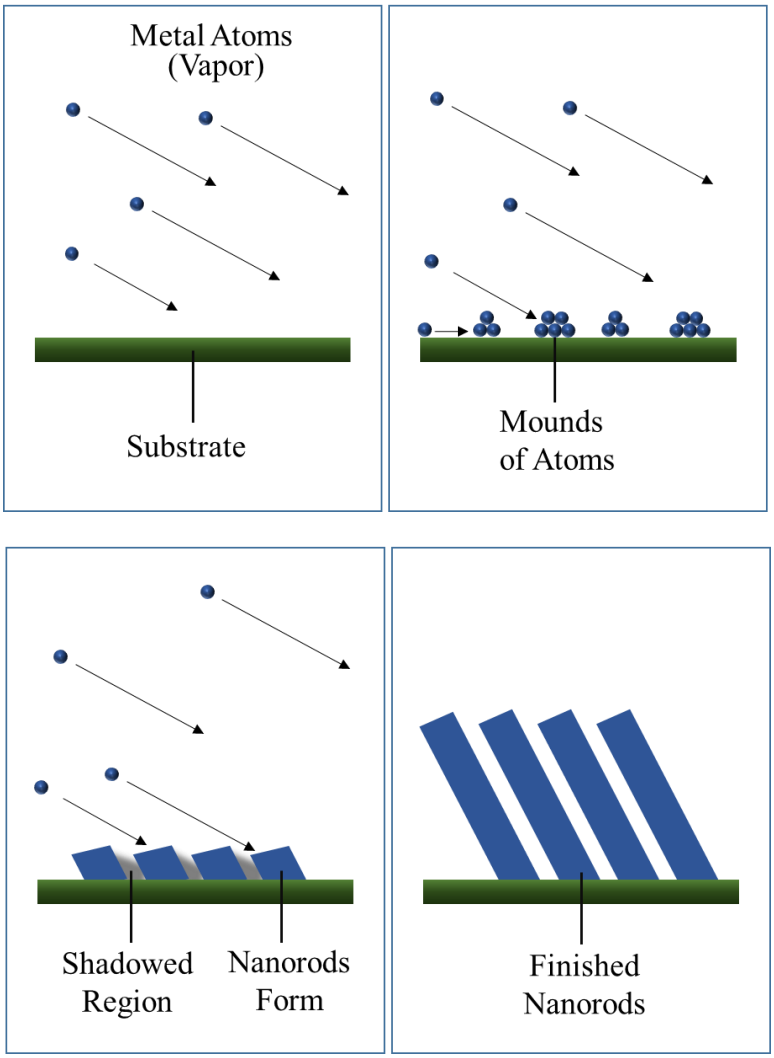

Figure 20. A schematic showing the growth process of nanorods by PVD. Atoms landing on an angled substrate form mounds. The mounds shadow areas behind from further deposition leading to the growth of the mounds into nanorods.

A significant problem exists in that Lmin and Ls are both controlled by the same variables [92]. For example to decrease rod diameter deposition rate can be increased. As the deposition rate increases, however, the rod spacing (Ls) decreases, bringing the rods closer together. Rod spacing (Ls) decreases faster than rod diameter (Lmin) decreases and this causes the rods to coalesce into film. Therefore, it is only possible to grow nanorods within a small range of diameters and spacings based on these conditions. It is

desirable to have the capacity to produce both well separated and small nanorods. This can be accomplished by creating small nuclei, well-spaced through seeding.

Beside from the heterogeneous nucleation on a flat substrate there are methods to control the size of seed nuclei. One method is lithography. This technology is quite mature due to the electronics industry and is able to produce precise well-spaced rods [93]. This process requires a cleanroom environment and expensive equipment. A second method is FIB milling. This also can produce well-spaced and separated rods, but the process is very time consuming and requires the use of an expensive FIB [94]. Chemical vapor deposition is able to produce well-spaced rods, but the chemistry of the deposition process can be complicated and the substrate generally must be exposed to very high temperatures [95]. Additionally, anodized aluminum oxide has been used as a template and filled by electroplating to produce nanorods, after which the template is removed, requiring chemicals and multiple steps [96]. A solution to these problems is to use PVD while using a substrate that is patterned. This pattern creates a random or ordered grid of raised areas on the substrate which act as nucleation sites for nanorods. This can be done using self-assembled monolayer of nano or microspheres, often of polystyrene [97, 98]. This process is delicate and requires the substrate to be dipped into a liquid bath with a single layer of the sphere floating on the surface. Additionally, substrate patterns can be made for later use in PVD, by lithography [99, 100], FIB [94], and templates [102] but with the same problems as above.

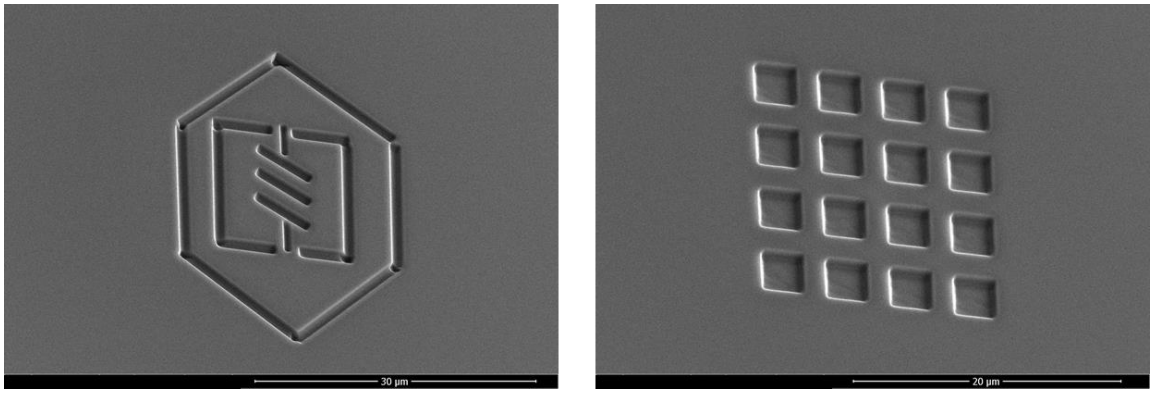

Figure 21. Simple patterns created on a Si surface using FIB milling.

A possible additional method to control nanorod spacing is the use of a material to modify the preferential nucleation of the nanorods. A material could be selected with a drastically different wetting condition from that of the substrate and would be deposited first. The nanorod growth on top of this layer would be determined by the wetting interaction of this "nucleation layer" material and nanorod material. Additionally, the nucleation layer material could be selected so that it is non-wetting on the substrate, thus producing 3-D clusters that would enhance geometrical shadowing and be sized in accordance with the critical diffusion distance of the nanorod material on the nucleation layer material.

The PVD growth of thin films is mature in both fabrication knowledge and scientific understanding, due in part to wide spread industrial use of PVD for integrated circuits [103]. Alternatively, the PVD growth of small and separated nanorods is immature; only recently has a scientific understanding of nanorod growth been realized [91]. Further, fabrication know-how is still lacking, and as such, large scale industrial application has not yet occurred.

I.3 Scientific and Technological Challenges

To make the desired metallic glue a reality a few challenges must be overcome. We first investigate the control of morphology for nanorods. To move forward with the technology we accomplish two things. (1) For the first time we demonstrate the use of seeds deposited immediately before nanorods as a method to control the diameter and spacing of surface grown nanorods. (2) We also demonstrate the capping of nanorods with physical vapor deposition. The applications for these discoveries include improved signal to noise ratio and longer survivability of sensing substrates in Surface Enhanced Raman Spectroscopy and improvements in room temperature metallic sealing. These methods are then used to produce metallic bonds. These processes are then extended to tackle the challenge of removing the vacuum chamber from the process and thereby reducing the cost and complexity.

Control of Nanorod Size and Spacing

Developing the ability to produce well-separated nanorods is an important step in the realization of this technology, due to the necessity of the interpenetration of the nanorods. If they are not sufficiently well-separated, the rods will primarily hit each other head-on and act like a porous film. Consequently, bonding will not be successful at a low temperature [4]. At this small scale, if the separation is sufficient, a small shear stress will align nanorods for inter-digitation, even if they are not well aligned upon initial contact. A closed-form theory is used to set the conditions during deposition to tailor the nanorods to the desired properties [91]. Methods, such as substrate seeding can further enhance the ability to control nanorod diameter and spacing [104]. This control allows for the improvement of the bonds being formed as a part of this technology, as the interpenetration of nanorods can be better controlled.

Recognizing the advantages of small diameter and sufficiently large separation for metallic nanorods, one naturally asks how to achieve them in a controllable manner. Therefore, here we will focus on PVD processes in designing mechanisms to control the diameter and the separation of metallic nanorods. Recently developed theories on both the diameter [90] and the separation [105] of metallic nanorods serve as the starting point of this design.

According to the theories, [90, 105] the diameter and the separation of nanorods both, in a coupled fashion, decrease with the increase of deposition rate and/or the decrease of substrate temperature, although following different scaling laws. As a result, it is desirable to decouple the variation of the diameter with that of the separation. For this purpose, we propose a new mechanism to decouple the variations by introducing self-organized seeds before the growth of the nanorods. The separation of nanorods derives from that of the seeds and therefore depends on the diffusion kinetics of the seed atoms, instead of that of the nanorod atoms. In contrast, the diameter of the nanorods still depends on the diffusion kinetics of the nanorod atoms.

Small and well-separated metallic nanorods have unique properties that are advantageous for various applications, such as surface-enhanced Raman scattering (SERS) [106, 107] and metallic bonding [4]. For SERS applications, structures with close proximity yet good separation produce the highest signal enhancement [108]. For metallic bonding, densely packed metallic nanorods require about 300 ^{o}C to successfully form bonds [54]. Alternatively, when the nanorods have adequate separation the interpenetration of nanorods on opposing substrates is possible. Once in contact, fast diffusion on the metallic nanorod surfaces drives the interpenetrated nanorods to coarsen into a continuous film, or metallic glue. It is through small and well-separated metallic nanorods that the first room temperature and low-pressure metallic glue technologies have been enabled [4].

In this work we will demonstrate a new mechanism of control using PVD deposition with no interruption of vacuum, as shown in Figure 22. At the initial stage, In is deposited onto a Si substrate and forms islands instead of a continuous film due to the non-wetting interaction; Figure 22 (a). Subsequently, Ag is deposited and Ag atoms preferentially bind to the In islands; Figure 22 (b). This occurs for two reasons. First, thermodynamically, Ag atoms bond more strongly to In than to the native oxide layer of Si [109, 110]. Second, Ag atoms are more likely to land on the taller In islands than the Si substrate due to geometrical shadowing under the glancing angle deposition (GLAD) condition for nanorod growth [67]. As a result, the taller In islands serve as seeds to define the separation of Ag nanorods, and to affect the diameter of Ag nanorods; Figure 22 (c). To achieve large separation of the taller In islands, it is desirable to deposit more In atoms so only fewer In islands survive in the tallest group. The large separation is a result of shadowing from adjacent seeds during the early stages of deposition and from coarsening of small seeds into larger. The seeds that are strongly shadowed receive little or no flux early on and do not grow tall. To achieve small diameter Ag nanorods, it is desirable to deposit fewer In atoms so that the diameters of In islands are sufficiently small to facilitate the Mode II growth according to the theory [91]. As a tradeoff, there is an optimal amount of In deposition.

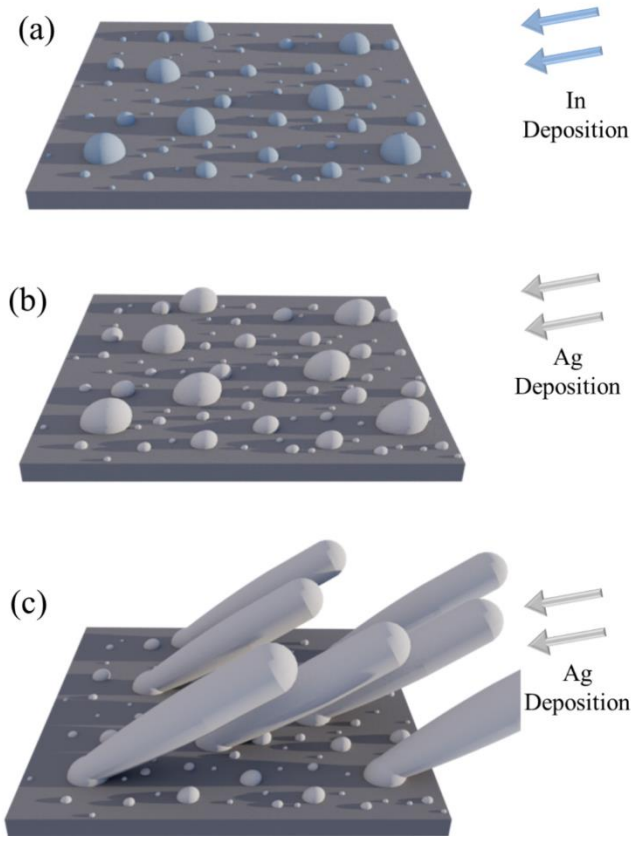

Figure 22. A series of schematics showing Ag nanorod growth on In seeds deposited onto a Si substrate. (a) In (blue) is deposited at high glancing angle onto a Si substrate (dark gray) forming In islands as seeds of various sizes. (b) Ag (light gray) is subsequently deposited at a high glancing angle, causing larger seeds to grow more. (c) Ag nanorods grow with their separation being that of larger In seeds.

Core-Shell Nanorods

A shell produced on Ag nanorods should help improve the durability of the structure if made of a more stable material. Conceptually, we reason that Ag nanorods coarsen through mass transport from the ends to the sides of each nanorod via surface diffusion. By capping the free end(s) of a Ag nanorod with high melting-temperature oxide, mass transport from the ends to the sides is slowed down. Since Ag nanorods from PVD do not have very large aspect ratios, Rayleigh instability, or the tendency of long columns to break up into smaller spheres, is not operational; therefore, the capped Ag nanorods should not coarsen or disintegrate [111, 112].

In metallic sealing, our focus changes slightly to different desirable properties in a capping material. Here we do want the nanorods to coarsen, but not before the right time. A metal oxide shell would provide protection, but in this case the protection would be too great and it would likely block the bond formation from happening at all. It is desirable to use Cu as the nanorod material as it has a low cost but can still achieve a comparable thermal conductivity to Ag. The difficulty with Cu is the oxide shell it quickly forms in ambient conditions. This can be avoided by coating the Cu nanorods with other metals. Additionally, if the coating metals form a low melting temperature eutectic, certain benefits can be obtained. First, the use of eutectic alloys through the core-shell nanorods will reduce or completely eliminate the voids. As a result, the leak resistance will further increase, and the heat conduction will become even more effective. Second, the presence of liquid alloys instead of solids will likely reduce the processing pressure from a few megapascals to a fraction of a megapascal, to allow for room temperature, low pressure metal bonding.

Figure 23 outlines our process utilizing nanostructures and eutectic alloys to produce a room temperature metallic glue. In Figure 23 (a) two surfaces, which are to be bonded together, are shown facing one another. Each surface is covered with core-shell nanorods. When the mating surfaces are brought together, the large spacing of the nanorods allows them to slide between those on the opposing surface and to interpenetrate, Figure 23 (b). When the shell materials from opposing sides, which together form an alloy with a eutectic temperature at or below room temperature, come into contact a liquid alloy is quickly formed, Figure 23 (c). Solidification occurs as the composition deviates from that of the pure eutectic alloy to a ternary alloy as the nanorod material diffuses into the liquid; Figure 23 (d).

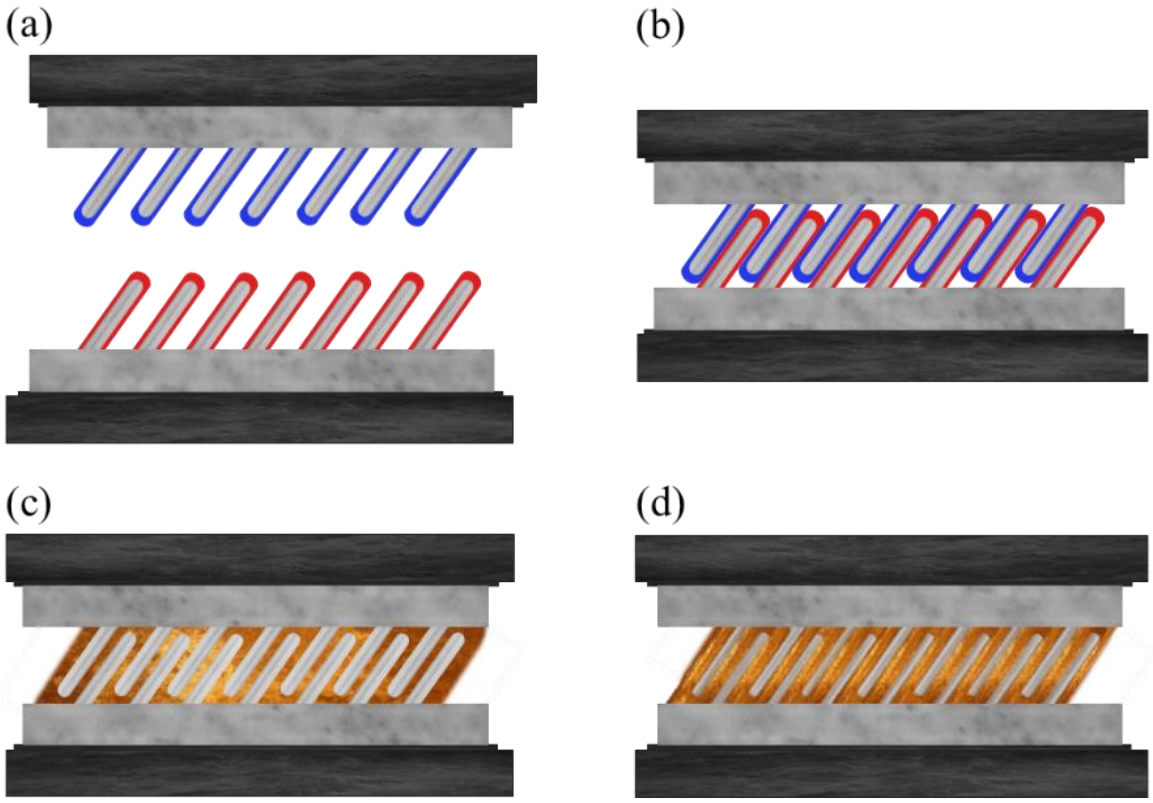

Figure 23. A schematic of low temperature metallic gluing enabled by well-separated metallic nanorods: (a) two sets of well-separated nanorods – which have metallic cores and shell elements that form a eutectic alloy – are brought together; (b) they interpenetrate under finger-tip pressure; (c) shell elements meet and form a eutectic alloy which is liquid at room temperature; and (d) mixing of the eutectic liquid with metallic core leads to the formation of three-component alloys that are solid at room temperature.

Mechanical Properties of the Bond

Determining the mechanical properties of metallic glue bonds are of high importance to determine if the glue will meet the requirements of specific needs. When used as a thermal interface material, the mechanical strength isn't as critical of a factor, as high applied loads generally are not experienced, though in many cases the shocks during shipping can be a significant problem [113]. In some cases however, stresses caused by thermal expansion of materials can be a significant issue. These stresses tend to separate interfaces layers and the adhesion of the layers must be sufficient to prevent this. This is one problem that is faced by using solder as a TIM. As solder cools and solidifies it will shrink and puts a stress on substrate

with a lower CTE [113]. This CTE mismatch between materials can cause the bond interface to delaminate due to poor thermal fatigue resistance [18]. This is a problem that Intel has experienced in the certain small CPU dies. Soldering small dies to the heatspreader can lead to cracks that grown over time, so thermal grease is used, but on larger size dies soldering has been used but is no longer in standard computers [114]. Another significant issue is the attachment of the solder to the silicon die. Tin based solder, such as the common Sn60Pb40 does not wet silicon [117]. The much more expensive In does wet both Si and heat sink materials, such as Cu, but In tends to diffuse into silicon and copper, so a barrier layer, such as nickel or titanium, is typically used. Indium does not bond strongly to these metals, so an adhesion layer of gold or silver is used between. The In layer is relatively thick at 1mm to prevent cracking [114]. All these layers and costly materials make for an expensive and difficult interface to produce.

Strong attachment is preferred to provide a lasting connection between device and heat sink. In addition, good adhesion should provide good contact and better heat transfer, and bonds of higher strength are also likely to indicate the presence of fewer voids which results in improved heat transfer. In another example, in the current attachment methods GaN and heat sink materials, such as copper have significant coefficient of thermal expansion (CTE) mismatch. Stresses induced during heating can cause the interface to separate. Materials that have a CTE closer to GaN have been used such as CuW, but these only provide about half the thermal conductivity as pure copper, at a higher price.

To test the mechanical strength of the metallic glue bonds lap shear tests using a tensile testing machine are conducted of the joints to failure. This will reveal the strength in any particular case, and help guide the path the produce stronger bonds. In addition, pull-off tests will also be performed to determine the adhesion in the surface normal direction of the bonds. The shear and pull-off tests are shown in Figure 24. Failure of these tests can occur in four different locations. These are: (1) the mated nanorods interface can fail, (2) the nanorods can separate from the bond layer, (3) the bond layer and adhesion layer can separate, (4) the adhesion layer can separate from the substrate, and (5) the substrate itself can break first, or some combination of these modes. SEM will be used to analyze the failure mode after the test.

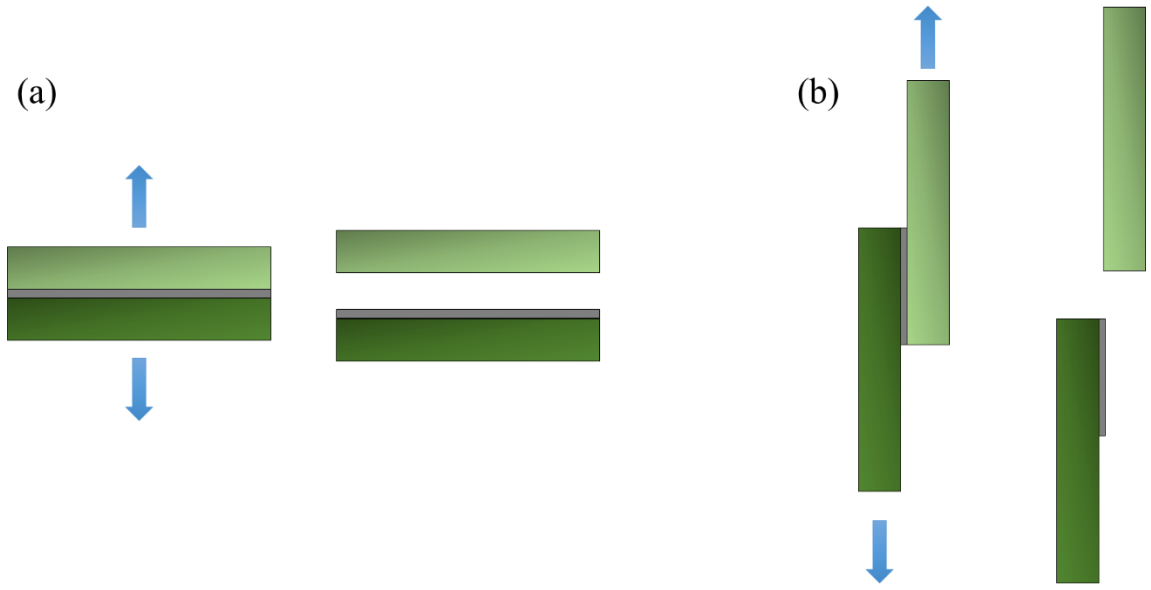

Figure 24. A schematic showing the (a) pull-off and (b) shear strength tests used on the metallic glue bonds.

A number of different factors have been determined to be likely influencers of the properties of the bond that is formed. These can be explored to seek the best quality bond and include: adhesion layer materials, thickness of bond film layers, nanorod length and diameter, nanorod spacing, temperature of the substrates during bonding, pressure applied during bonding, length of time of bonding.

Thermal Conductivity of the Bond

Heat dissipation is of high interest in the study of this technology. It is speculated that a metallic glue layer attaching a heat producing electronic device to the heat spreader or heat sink will act as an excellent conduit for heat, far surpassing that of thermal grease, solder or thermal epoxy that is commonly used. The materials that make up metallic glue are primarily Ag or Cu and have a thermal conductivity of around 400 W/m-k. This is 13X greater than silver epoxy (29 W/m-K) and 7x greater than AuSn eutectic

solder (57 W/m-K) [118] and at least 100x better than most thermal grease [15]. While the resistivity of thermal grease is relatively low (~0.5-5 W/m-K) it is still much better the pockets air that it fills in (0.0257 W/m-K) [119].

The ability of heat to move from one surface to another has to do primarily with the surface flatness, the surface roughness, and the type and thickness of the filler material in between the surfaces. If the interface is completely filled with a TIM, leaving no air gaps, then the flatness and roughness dictate the minimum thickness of the interface. In heatsinks of extruded aluminum the flatness of less than 4 milli-inches per inch is considered satisfactory [119]. For roughness, 50-60 microinches is considered acceptable, with a better finish being expensive [119]. For example, one study shows that there is less than a 2.5% difference in resistance through an interface filled with thermal grease when finishes of 16 and 63 microinches are compared [120]. A surface finish that is milled is usually sufficient when using thermal greases [119].

The resistance of an interface, R_{eff}, is comprised of the bulk resistance of the interface material and the contact resistance of the TIM to each surface. Figure 25 represents the interface schematically. It is desirable to reduce R_{eff} to the maximum extent possible. This can be accomplished by minimizing the bulk resistance, by reducing the bond line thickness (BLT) or by improving the thermal conductivity of the TIM. Contact resistance can also be reduced by decreasing surface roughness, increasing surface flatness, or increasing the clamping pressure between the surfaces [18].

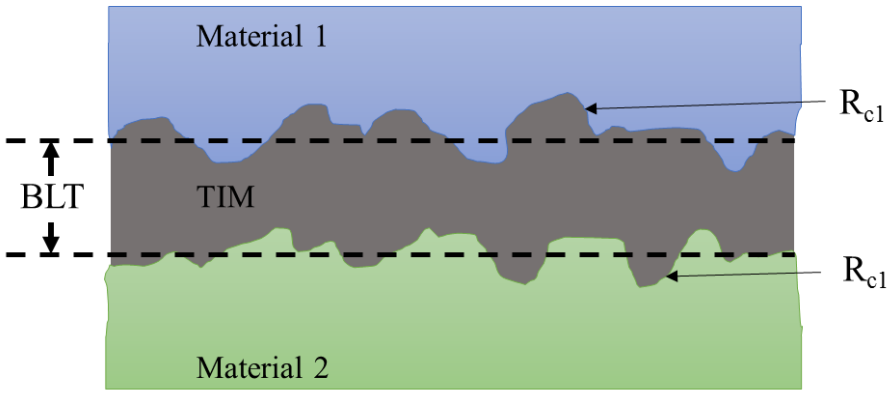

Figure 25. Schematic of an interface between two surfaces filled with a TIM. The bond line thickness BLT, and contact resistances, R_{c1} and R_{c2}, are shown.

The effective resistance through an interface is described by Equation 1 [122]. Here, R_{c1} and R_{c2} are the contact resistances between the TIM and the first and second surface, respectively. The bulk resistance is represented by the first term in the equation and is comprised of the bond line thickness, BLT, the thermal conductivity of the TIM, k_{TIM}, and the area of contact, A.

$$\boldsymbol{R_{eff} = \frac{BLT}{k_{TIM}A} + R_{c1} + R_{c2}} \quad \textbf{(1)}$$

The thinness of the proposed metallic glue attachment will offer a significant heat transfer advantage as it can be an order of magnitude thinner than other solutions. Figure 26 shows a typically attachment of a GaN chip to a coldplate compared to a metallic glue attachment with much thinner interface. While, it is possible that a thicker interface layer may offer an advantage of heat spreading ability, it is generally preferable to move the heat into the cu carrier in as short a distance as possible.

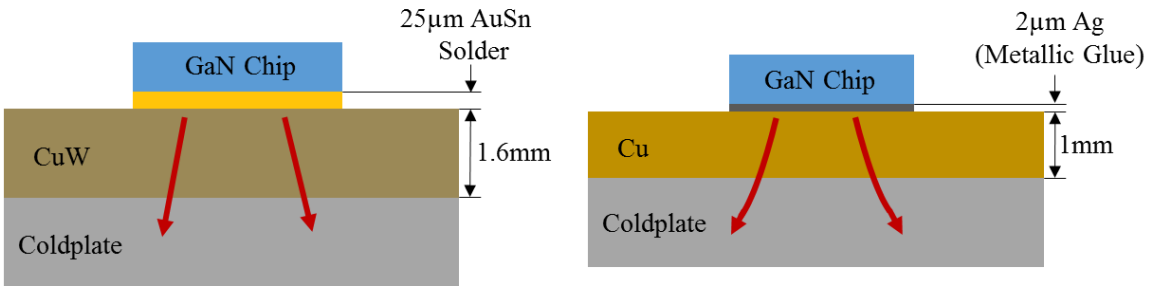

Figure 26. Schematic of a GaN chip attached to a carrier material on a coldplate. The left shows a typical use of AuSn solder and CuW carrier for CTE matching with 25um interface layer. The right shows an Ag metallic glue attachment to a Cu carrier with 2um interface layer.

When dealing with thin thermal interface materials using a material with higher thermal conductivity is only part of the problem. The resistance of the interfaces themselves because much more significant on this scale. The longevity of interface materials is also of concern to ensure that a material will meet the cooling requirements of a device throughout its useful life [8]. The useful life of computer CPU is generally expected to be around 7-10 years [123]. For example with thermal grease it has been found that higher operating temperatures can cause degradation of thermal grease. When temperature cycling tests were performed on one thermal grease from 0-100°C for 7500 cycles, a 4-6 times increase in thermal resistance was observed [13].

To investigate the thermal conductivity of a thin interface a testing apparatus is generally used to perform measurements of the heat transfer coefficient of the tested materials. This is designed according to the ASTM D-5470 Standard Test Method for Thermal Transmission Properties of Thermally Conductive Electrical Insulation Materials, and is described in Figure 27. Typically two copper rods are used with the sample material pressed in-between at a particular force. One end of one rod is heated while the other end of the opposing rod is cooled. Thermocouples embedded in the rods between the hot and cold sources allow for the temperature gradient to be measured, from which the thermal conductivity of the specimen can be determined.

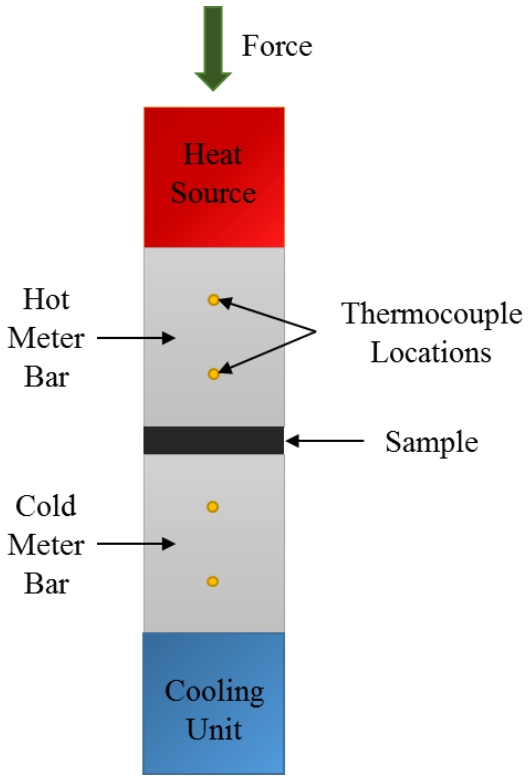

Figure 27. Schematic of the device used in the standard test method ASTM D-5470 used to test the thermal conductivity of metallic bonds.

Moving Beyond the Vacuum Chamber

The process of bonding using a vacuum chamber has certain advantages such as a very clean and high quality bond, and a very thin bond line thickness. These factors can be crucial in high performance situations such as in military use where the best performance is required or in high performance computing. A significant disadvantage, however, in a process requiring the use of a PVD chamber is high cost and relatively slow processing time. This may not be a significant issue in many applications, where higher cost is often acceptable for the higher performance provided. Largely, in industry and especially with consumer products, however, lowest cost and ease of use is very high importance.

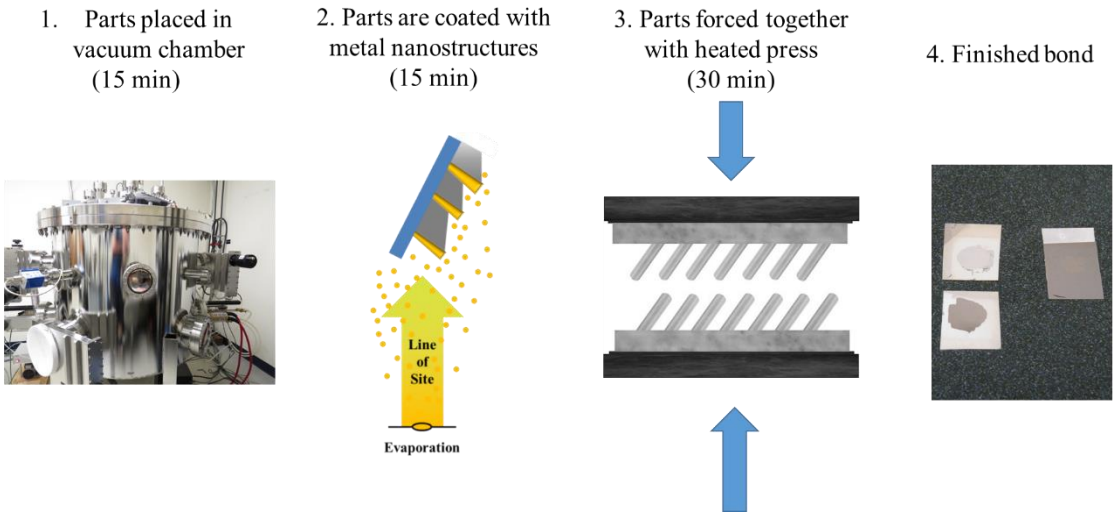

Figure 28. Major steps of process of forming a bond using the expensive PVD process.

To better understand the needs of industry and consumers, 100 interviews were conducted of experts in various industries, as a part of the NSF I-Corps program. The various areas of industry that was explored included soldering, thermal interface materials, glass to metal connections, jewelry manufacture and repair, and general mechanical joining. The main issue that was identified with the bonding process was the high cost of equipment and difficulty in using. Additionally, the use of the formula required a license from the university, which is a lengthy and difficult process to achieve. To become a viable product on a larger scale than high performance military applications, the technology has to be taken out of the vacuum chamber for the user.

Many of the methods described in the Low Temperature Metallic Sealing section seek to perform bonding by using lower cost processes. For example, silver sintering, and amalgams use nanoparticles or microparticles that are produced by chemical synthesis, my mechanical machining, or by atomization. These process tend to be cheaper than a vacuum process, but also are less clean, which can lead to significant challenges in causing the particles to combine to form a bonded interface. The largest challenge is surface contamination. On the one hand, the contamination coats the particles and keeps them from immediately coarsening together. When the particles are in a powder from or when they are in a

solution this coating is necessary to keep particles from clumping and forming one large mass. On the other hand, however, the coating makes it very difficult to get the particles to coarsen when it is desired that they do so, which impedes the formation of a bulk or a bond between surfaces. Previous Figure 6 shows how particles stay separate when surrounded by a coating layer, but begin to coarsen together when the layer is removed.

To move our technology out of the vacuum chamber we utilize the principles of the core-shell nanorod technique that is described in section III.2. To make this less expensive we utilize less expensive solution synthesis methods for the production of nanoparticles and purchase particles from a manufacturer instead of making them ourselves. Processes similar to amalgam mixing and cold spray are used to apply the liquid metal and will be described in more detail in section III.4.

II. Methodology of Nanofabrication

This section describes the processes and equipment used to perform this research. Nanorods are grown in a high vacuum chamber using a physical vapor deposition process. Once the nanorods are produced, they are examined using electron microscopes, such as scanning electron microscope (SEM) and transmission electron microscope (TEM), and with Raman spectroscopy. Specimens are also tested for mechanical strength by tensile testing and for thermal conductivity.

II.1 Experimental Methods

Substrates

For the deposition process to form nanorods there must be a surface present on which the metal vapor can land. For consistent results over the surface this substrate must be very flat. Additionally, due to the usually small size of the nanorods, a very smooth surface is preferred, as roughness will alter the formation process of the nanorods. Significant roughness can act as nucleation sites, which will determine where the nanorods are likely to grow, and even greater amounts of roughness will act like mountains with nanorods being like trees or grass on top. This can shadow large areas entirely from deposition and cause significant surface effects that make the system more complex and add undesirable variables.

The standard substrate that is used is 3 inch in diameter silicon wafers. The wafers have a surface crystal orientation of {100} and are obtained from Nova Electronic Materials (Flower Mound, TX). They are ultrasonically cleaned in acetone, ethanol, and de-ionized water before use. Other materials of use include clear glass slides, Teflon, polyethylene, and Cu, among others.

Figure 29. A package of 3 inch <100> Si wafers from Nova Wafers used as substrates.

Materials

To reduce the number of variables in the process, the materials that are used to form the metal vapor inside the vacuum chamber are very pure. Small amounts of impurities in the source materials can have impacts on the final nanostructures by forming alloys or acting as surfactants. The source materials generally come as pellets in cylinder form of size 1/8" x 1/8" or ¼" x ¼". The purity is 99.99% or better for all materials used. All source materials are from the Kurt J. Lesker Company (Jefferson Hills, PA), and the most commonly used in this work are Ag, Au, Cu, Cr, In, Ga, TiO2, SiO2.

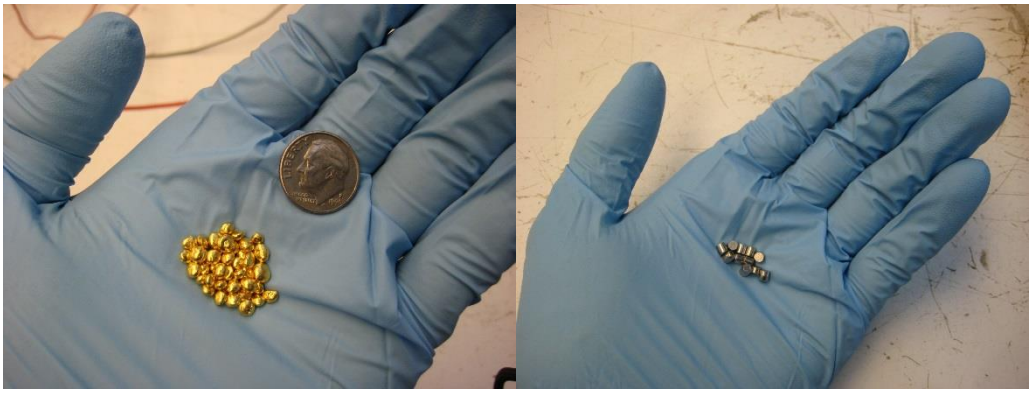

Figure 30. Deposition materials in the form of small pellets. Left image shows Au and right Ag.

Physical Vapor Deposition

To perform the nanorod growth, two electron beam physical vapor deposition (EBPVD) systems were used. They each provide unique capabilities. One is located at University of Connecticut and one at Northeastern University. In both cases an electron beam is directed onto the high purity source materials using a magnetic field. This magnetic field directs the beam in an arc, leaving the electron source below the path of the vapor and free from contamination. The source materials sit in a crucible liner that is stable at high temperatures and is usually made of high purity carbon. Used here is a material called FABMATE which is produced by Kurt J Lesker. These are 99.9995% carbon and are very durable. The electron beam lands on the top of the source material, heating it. The source material begins to vaporize in the high vacuum environment as the vapor pressure overcomes the pressure in the vacuum chamber. The vapor moves away from the source in a straight path and strikes the first surface it lands on and usually sticks there, but in some cases desorbs and again moves off in a straight path.

The rate of deposition is monitored by a quartz crystal microbalance directly adjacent to the substrate. This device primarily consists of a quartz crystal that resonates at a certain frequency due to applied alternating signal. The piezoelectric nature of the crystal causes it to change shape with the applied electric current. As deposition lands on the crystal surface the resonance frequency decreases as the thickness of the film increases. Monitoring of the rate of vibration allows for very precise measurement of the film thickness on the surface or less than a monolayer or about 0.1nm.

University of Connecticut Chamber

The University of Connecticut system consists of a stainless steel vacuum tank approximately 45 cm tall and 25 cm diameter. The source to substrate distance inside is approximately 35 cm. The vacuum level is such that it is statistically very unlikely that an atom leaving the source crucible will strike another particle before hitting the substrate. The chamber is typically evacuated to a base pressure of 1×10^{-6} Torr

prior to deposition. This is provided by a roughing pump and turbomolecular pump combination. While depositing materials the pressure may rise to be in the 1×10^{-5} Torr for metals and 1×10^{-4} Torr for metal oxides. Some metals show an improvement in the vacuum during and after deposition as they tend to act as getters of oxygen inside the chamber, such as Cr, and Ti.

There are a few substrate holder options that are interchangeable on the top of the chamber. One is a precision machined mount that attaches to a feedthrough port in the top center of the chamber. This has 6 machined angle brackets that fit into the tip of 80 degrees, and 85-90 degrees in 1 degree increments. The temperature of the substrate holder can be controlled from the outside of the chamber. The holder can be filled with cold fluids such as ice water or liquid nitrogen to maintain the substrate at the desired temperature, or a cartridge heater can be used to maintain a temperature of 20 C to 400 C. A thermocouple feedthrough allows for monitoring of the substrate on the inside of the chamber.

A second substrate holder consists of a rotary feedthrough in the center position with a large metal disk held perpendicular to the deposition flux on the inside of the chamber. The disk can be covered in multiple samples, usually 4 or less, that are able to be rotated from the outside. A mask below the rotating disk covers all substrates except one, so that only one sample receives deposition at a time. This allows for faster sample processing, as many samples can be performed without the need to break vacuum between each.

Figure 31. Electron beam physical vapor deposition chamber at University of Connecticut. The orange glow in the viewport is the heated source metal during deposition.

Northeastern University Chamber

The Northeastern University chamber is a larger system with multiple electron beam sources. It is a cylinder approximately 100cm wide by 100cm tall with the distance between the source material and the substrate being approximately 40cm. This chamber has base pressure of 1×10^{-9} torr, and a working pressure of 1×10^{-7} torr. This is provided by a roughing pump and turbomolecular pump combination. The temperature of the substrate can be controlled in the range of -196 to 400 ^{o}C by using a custom built liquid feedthrough that acts as a substrate holder. Similar to the University of Connecticut system, cold liquids or a cartridge heater is used to control the temperature. A second double liquid feedthrough with long copper piping attached on the inside acts as a cold finger when liquid nitrogen is forced through the tube. The cold surface inside the chamber captures and helps to remove vapors inside the chamber, most notably water vapor, to eliminate variables and improve the vacuum level.

Programmable substrate rotation allows for advanced control and unique nanorod morphologies. This consists of a rotation feedthrough attached to a stepper motor. The stepper is controlled with an

Arduino that has various programs for different nanorod morphologies, such as constant fast rotation for nanorods perpendicular to the substrate surface, slow constant rotation for spiral nanorods, and stepped rotation at set angles for zig-zags and square helices.

There are twelve source material holders in two separate electron gun assemblies, allowing for deposition of two materials at once or rapid production of multiple layer films. The system has capabilities of depositing several atomic layers to several microns of source material through 10 kW of power available to bombard the sources with electrons.

A load lock and transfer arm allow for fast sample changes. In this system, the sample can be placed into the load lock, which is then pumped down to high vacuum level, and then moved into the main chamber with the transfer arm. This keeps the main chamber at high vacuum level all of the time, except when necessary for maintenance or replacing deposition materials. Keeping the main chamber under vacuum is preferable as it takes a long time to pump down, and it helps maintain the cleanliness of the system.

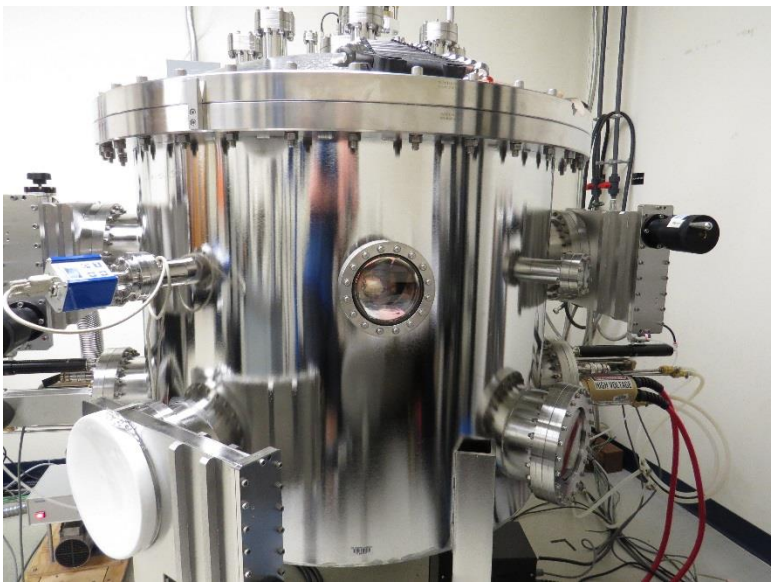

Figure 32. Electron beam physical vapor deposition chamber at Northeastern.

EBPVD Procedures

Nanorods Grown on Seeds

The angle of deposition for the growth of the seeds and nanorods 85 degrees with respect to the source normal. The materials used for seeds are In, Sn and for nanorod growth Ag is used. The power of the electron beam is controlled to maintain a deposition rate of 0.05 nm/s for In, Sn and 1.0 nm/s for Ag and Cu. After the seeds are deposited on the substrate the nanorods are immediately deposited, without breaking vacuum or changing the angle of the substrate. The source materials are placed in separate graphite crucibles at the base of the vacuum chamber. Work is also done to extend the use of the seed method for nanorod control where Cu is the primary nanorod component instead of Ag. In this case In, Sn, and Ga are all used as seed materials.

Core-Shell Nanorods

Nanorods of Ag are deposited on a Si substrate at an angle of 86 degrees. A coating of TiO_2 or SiO_2 is then deposited to form a shell after breaking vacuum at the same angle of deposition. The rate of deposition is 1.0 nm/s for Ag to a thickness of 500nm and 0.01 nm/s for TiO_2 or SiO_2 to a thickness of 5nm.

To produce eutectic nanorods for bonding, Cu nanorods are grown in the range of 500 nm – 2000 nm at various angles and deposition rates. Coatings of In and Ga are then deposited on at various thicknesses.

Bonding Samples

To bond samples together a Carver heated press model 4122 is used. The maximum force the press can operate at is 12 tons. Two PID controllers control the top and bottom hot plate with a max temperature

of 340 ºC with a ramp rate of 5 ºC/min. Various temperatures and pressures are used in bonding. The temperature range is typically from 20 ºC to 200 ºC, and the bonding pressure is typically 5-10 MPa. Two pressure gauges with different scales are used under different circumstances. When 1-4 samples are being bonded a 1 ton gauge, with a resolution of 20 lb is used. When 5 or more samples are being bonded, generally the 2.5 ton gauge is used with a resolution of 50 lb. The bonding time ranges from 15-60min.

II.2 Characterization

The characterization takes place ex situ. After the growth of nanostructures is complete the substrates are removed from the deposition chamber and characterized in various other equipment. This includes a scanning electron microscope (SEM), a transmission electron microscope (TEM), and a Raman Spectrometer.

Scanning Electron Microscopy

Due to the very small size of the nanostructures, electron microscopes must be used for characterization. This is primarily due to the diffraction limit of visible light, which limits the resolution to around 0.2 μm [115], though some techniques such as fluorescence imaging are able to improve on this [116]. As some of the nanorods and seeds have dimensions smaller than 7nm, using an optical microscope would not be sufficient. As the wavelength of electrons is much smaller than photons of visible light (often 100,000 times shorter), this gives a sufficient diffraction limit to image the small structures [124].

The scanning electron microscope forms a tiny beam of electrons and passes the beam in a raster pattern over the surface of the sample [125]. As the electron beam interacts with the sample various kinds of interactions can occur. The different resulting signals can be detected to form images. In this work,

what are called secondary electrons are used to form images. These are fairly low energy electrons (<50 eV) that occur due to inelastic scattering with atoms in the sample and usually occur close to the sample surface. These negatively charged electrons are then attracted to the detector by a positively charged screen. The number of electrons detected in a certain amount of time correspond to the brightness recorded for a pixel on the connected computer screen. An array of pixels of different brightness make up the image.

To examine surface morphology a Quanta 250 SEM (FEI) with Schottky field emission source was used. This offers adjustable accelerating voltage from 200V-30 kV, and useable magnification up to around 300,000x. Using an Everhardt Thornley secondary electron detector the resolution at 30 kV is 1.0nm. The option of energy dispersive X-ray spectroscopy (EDS) is possible to aid in identifying and locating different elements within a sample.

Transmission Electron Microscopy

The TEM offers very high resolution imaging of very thin samples. Instead of detecting electrons that emitted from the top of a surface of interest as in an SEM, electrons are sent through a sample and are measured by a detector below it [126]. Also, unlike in SEM, in standard TEM a focused beam with a raster pattern is not used, however, the TEM can be used in scanning mode (STEM) as well. The electron beam interaction with the sample causes variations in intensity which directly forms the image. This is often viewed by the user on a fluorescent screen inside the microscope column viewed through a window forming a green image. A CCD (Charge-coupled device) camera is often inserted for image acquisition.

The TEM is used to examine nanoparticle seeds. These can be very small and are best viewed with the high resolution and contract that a TEM can provide. The microscope used is a FEI Tecnai T12. This uses a field emission source and runs with an accelerating voltage of 20k-120kV. The point resolution is 0.34 nm and it also offers EDS as an option.

To image seeds TEM grids with silicon dioxide support films of 8 nm in thickness are used. A silicon wafer cannot be used in this case because it is much too thick and would block the electron beam from passing through. These substrate, however, closely mimic the native oxide on a silicon wafer producing equivalent seed sizes. In is deposited onto the TEM grids and the In seeds are then viewed in the microscope.

Nanorods are also imaged by TEM in this work. This is done to observe nanorods shells. These are conducted with TEM grids of lacey carbon support film with and without Ultrathin (3 nm) carbon film.

Raman Spectroscopy

The SERS data were taken with a Renishaw Raman 2000 using a 514.5 nm laser. To analyze the Ag nanorods grown on In seeds verses the control Ag nanorods, The samples were first soaked in 5 mM N719 Ruthenium dye (Di-tetrabutylammonium *cis*-bis(isothiocyanato)bis(2,2′-bipyridyl-4,4′-dicarboxylato)ruthenium(II)) (Sigma) in methanol (Sigma) for 12 hours then rinsed with methanol. To take the data the spectrometer was operated with a 50% power reducing filter with 10s acquisition averaged over 3 runs at 50x magnification. To perform the Ag coated with TiO2 analysis no power reducing filter was used and the sample time was 60 seconds.

Mechanical Testing

Mechanical testing is performed on metallic glue samples to determine the strength of the bonds. This is a helpful indicator to determine the effectiveness of the attachment. There are a number of different locations where the bond can fail. After the bonds are destructively mechanically tested, the failed interface is exposed. This makes it relatively straightforward to examine the layer under optical or electron microscopes to determine where the failure occurred and to help shed light on the reason why.

After two substrates are bonded together using metallic glue they are mechanically tested in one of two ways. The first is a lap shear test and the second is a pull-off test. The Figure 24 in section I.3 shows these test configurations. To perform these measurements an Instron 5582 testing system is used. Hard and brittle samples including silicon wafers and glass are glued with JB Weld to aluminum strips for lap shear tests and are glued to aluminum T's for pull-off testing, Figure 33. Gluing the samples to strips is required as clamping the samples into the grips of the Instron machine generally leads to cracking of the sample. The T's are required to provide the correct orientation for the pull-off test. A hole is drilled into each Al holder strip or T to allow for a hook to hold the sample in between the grips. This keeps torsion from being applied to the sample when it is being clamped or during the test. Ductile materials that have been bonded, such as aluminum, can have a hole drilled directly in the sample for lap shear testing, but still require the attachment of a T for pull-off testing due to the geometry constraints during the bonding process. Soft materials, like polycarbonate can be clamped directly into the grips as the flexibility of the material compensates for any slight rotational movement during attachment or testing.

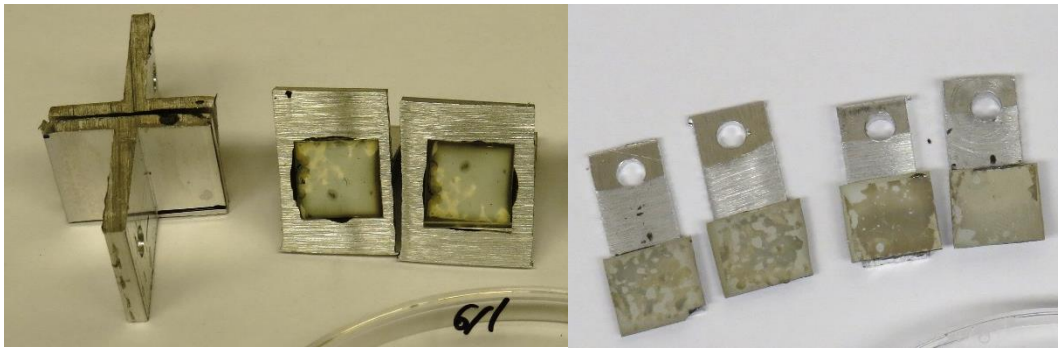

Figure 33. Al T's with used for pull-off testing (left) and Al strips used for lap shear testing (right).

Thermal Conductivity Testing

Thermal conductivity tests are performed according to ASTM D5470 standards using the thermal conductivity tester TIM 1400 from the company AnalysisTech. This equipment was made available for our use by Rogers Corp. Two opposing rods are used to clamp the sample. One rod is heated and the

opposite rod is water cooled. The rods are covered by insulation during testing. Thermocouple probes are used to monitor the temperature profile.

Figure 34. Thermal conductivity tester TIM 1400 by AnalysisTech.

Two OFHC copper disks 1.3” in diameter and 0.12in in thickness are bonded together using metallic glue. The bonded disks are clamped between the upper and lower copper meter blocks. Thermal grease (Super Lube 98003 Silicone Heat Sink) is used as a thermal interface material between the copper disks and the meter blocks to improve thermal conductivity. The heated end is maintained at 50oC and then held at this level for approximately 10min during the test. Measurements are used to determine the thermal resistance through the metallic glue. This includes the bulk and contact resistances. Force is applied to the meter blocks and samples disks with a press screw and is pneumatically maintained at 200 psi.

III. Results

After describing the current state of technology and the benefits of low temperature metallic sealing this dissertation seeks to improve the process in two ways. (1) To improve the control of nanorod diameter and the nanorod spacing by using deposited seeds on the surface. (2) To coat nanorods with other materials for improved oxidation and coarsening protection as well as an improved bonding method by using low melting temperature eutectic metal shells. Based on these advancements, the technology is then extended into the area of processes not requiring a vacuum to produce similar metallic bonds.

III.1 Control of Separation and Diameter of Ag Nanorods through Self-organized Seeds

Control of Indium Seeds

To produce nucleation sites on a substrate, a metal is deposited that forms non-wetting clusters. This acts somewhat like raindrops landing on a waxed car. The surface energy of the water or metal in the case of the seeds is much higher than the surface they land on, the car or silicon substrate. This causes them to have a high tendency to form clusters rather than a flat film. As discussed previously this is called Volmer-Weber (island formation) growth.

Here, we present a new method of controllably growing well-separated nanorods, using PVD through the assistance of In as a cluster material. In is pre-deposited onto Si substrates and acts as preferential nucleation sites for the developing Ag nanorods. By changing the nominal thickness of the In films, the size and density of heterogeneous nucleation sites are controlled, and as such the diameter and spacing of Ag nanorods is controlled. This method has the advantage of occurring entirely in the vacuum chamber and can be performed just prior to the deposition for the growth of the nanorods, without a vacuum

break, in minutes. As an extension, we demonstrate the applicability of a second material, tin (Sn), as an effective nucleation layer material.

Depositing nonwetting In onto Si produces In clusters. By using these clusters it is possible to remove the constraint of the minimum spacing (Ls) of the nanorod material and replace it with the desired Ls. We demonstrate two methods of control of the size of these clusters in Figure 35. The first method is control by the amount of deposition. When a small amount of In is deposited (10 nm), a large number of small, un-touching, In clusters form on the surface, Figure 35 (a). As more In is deposited, the clusters will grow and merge becoming larger and having a greater center to center separation (Ls), Figure 35 (b), (c).

The cluster size can also be controlled by adjusting the angle of the substrate compared to the vapor flux. At high substrate angles (88 degrees), comparatively little In lands on the surface, and small clusters with a small separation are formed, Figure 35 (d). As the angle of the substrate decreases to 45 degrees, Figure 35 (e) and then to 0 degrees, Figure 35 (f) more In is deposited on the surface resulting in larger clusters of greater spacing. The conditions in Figure 35 (c) and (f) are essentially the same.

Higher glancing angle of the substrate results in a lowering of deposition amount on the surface, so the same cluster sizes and spacings can be achieved through either method. Depositing In flat first to form clusters may be preferred if it is desired to use the least amount of material possible for the deposition. The constant angle method may be preferred when the capability to rotate the substrate without breaking vacuum does not exist.

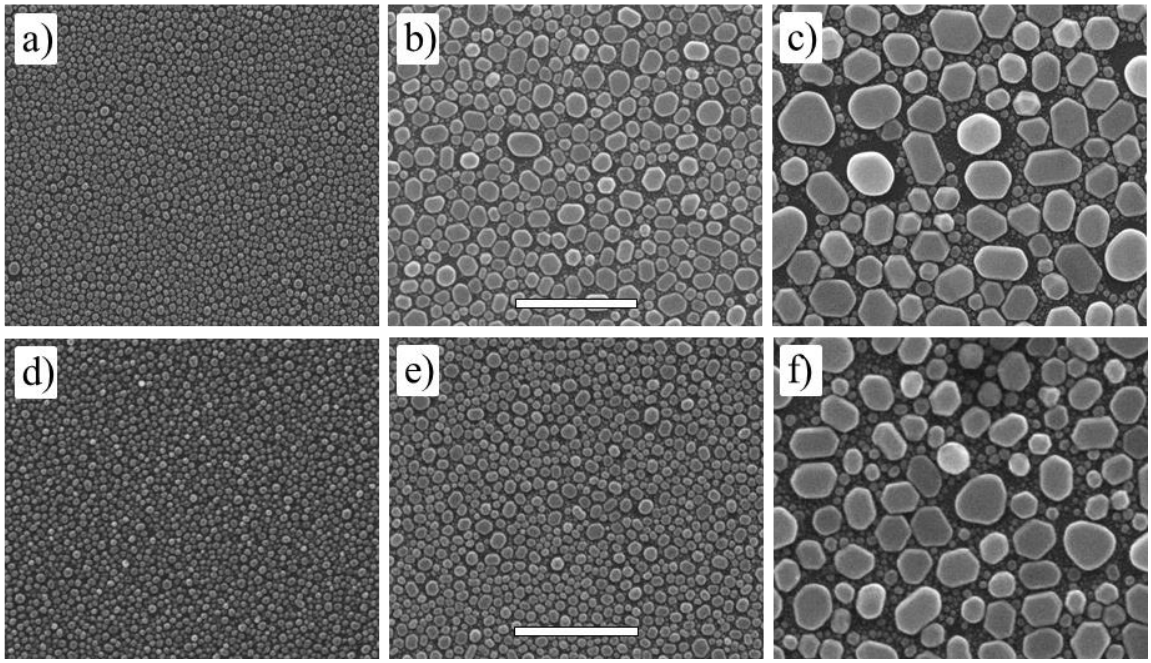

Figure 35. SEM images of In deposited on Si substrates. The top row represent from left to right In deposition of 10nm, 25nm, 50nm on a flat substrate. The second row represents 25nm of In deposited with decreasing GLAD incidence angle on different substrates. From left to right represent an incidence angle of 88 deg, 45 deg, 0 deg. Scale bar is 500nm.

Other Substrates

In addition to Si, this method of pre-seeding a substrate with size and spacing tuned clusters works on a variety of technologically significant materials. We demonstrate this with soda lime glass and polytetrafluoroethylene (Teflon ®). Indium of the amounts 10nm, 25nm, and 50nm are deposited flat onto the surface and the resulting clusters of increasing sizes are seen in Figure 36. These materials were chosen due to the difference in surface energy demonstrated by the observance that glass is wetting to water and Teflon is nonwetting. Both, however are have lower surface energies and are nonwetting to In. Different substrates were also tested using a constant 25nm of In and varying the substrate angle. The results observed were similar to Figure 35 and are not shown.

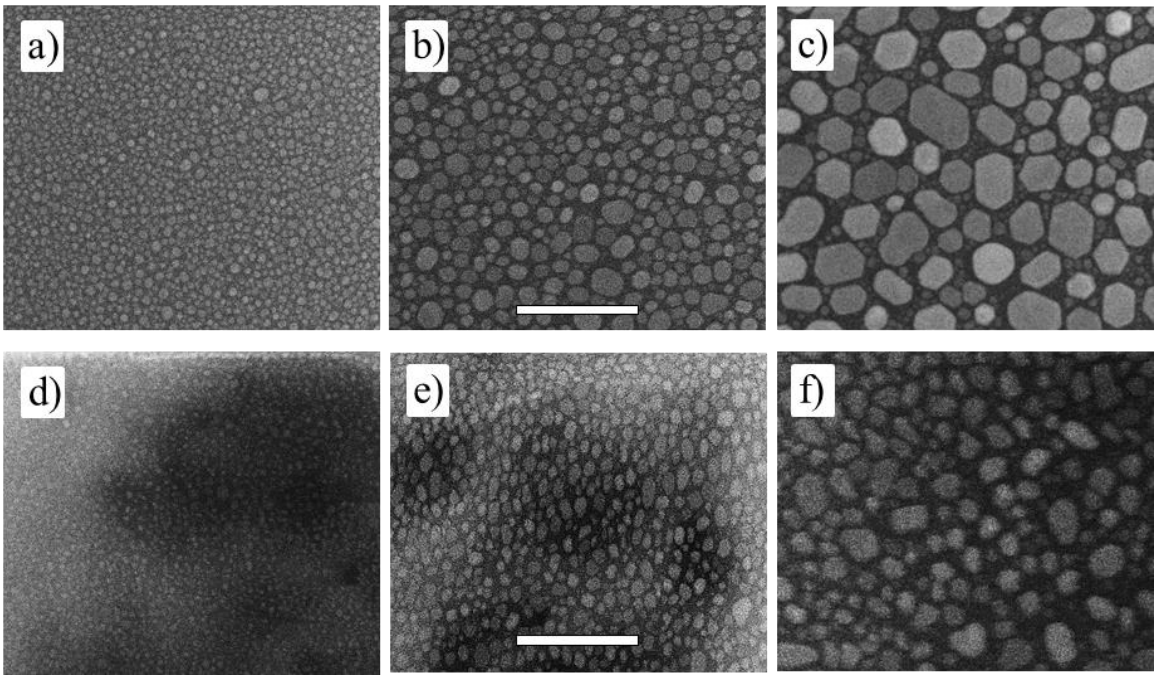

Figure 36. SEM images of Indium deposited flat on different substrates of three different amounts. The columns represent from left to right Indium deposition of 10nm, 25nm, 50nm. The substrate on the top row is glass and the bottom is Teflon. The scale bar is 500nm.

Control of Ag Nanorod Diameter and Spacing

Indium is first deposited onto a Si substrate and forms islands instead of a continuous film due to the non-wetting interaction. When In is used first on the substrate to produce clusters of a certain size, the step of Ag movement and conglomeration on the surface into clusters that would have occurred if Ag nanorods were deposited only, is bypassed. The In now sets the initial size and spacing of the clusters. Once the Ag nanorods growth is started, Ag vapor arrives and lands on the top of the In clusters under the influence of geometric shadowing, and nanorods proceed to grow.

In Figure 37, Ag nanorods are grown on top of In clusters. (a) Shows the substrate with In clusters before deposition, (b) shows an early stage of growth of the Ag nanorods with 200nm of deposition, and (c) shows longer Ag rods at 500nm. The inset image is Ag nanorods of 500nm grown on a bare Si wafer. The nanorods grown with the In are very similar in diameter to the control nanorods. This indicates that the self-selected diameter of the rods (Lmin) is approximately the same with this size In cluster and a bare Si

surface. We do notice that there is a bit more merging of the rods in the case with the In. This indicates that the cluster spacing (Ls) is smaller in the case with In than without. As Lmin is a property of deposition rate and substrate temperature, which are the same in both cases, the diameter that is driven towards will be the same despite the initial close spacing due to In. this will result in the nanorods increasing in diameter during growth. This slight increase in diameter causes merging as they grow until they reach the desired Lmin. So we see in Figure 37 (c) slightly more nanorods closer together, but thickening and merging, compared with the inset.

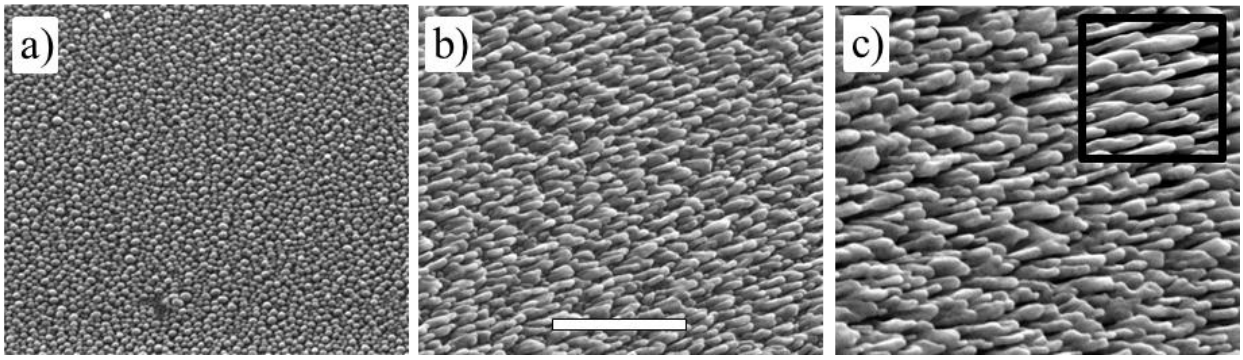

Figure 37. SEM of Ag nanorods grown on In clusters taken at 45 degrees off substrate normal. Images a) through c) contain 25nm In deposited at 88 deg incidence angle on the substrate. For image b) 200nm Ag and c) 500nm Ag was deposited at 88 deg incidence angle. Inset shows Ag nanorods without In. Scale bar is 500nm.

The case where the characteristic size and spacing produced by In is much larger than that which would come about by Ag on Si is also demonstrated. Here larger clusters of In are first created on the substrate; Figure 38 (a). Onto these clusters Ag is deposited to grow nanorods just as they were in the previous example. The nanorods begin with large spacing and large diameter often connected at the base over number of In clusters. Once this base forms the rods grow normally and attempt to approach their desired Lmin for this deposition rate and temperature. As this Lmin is much less than their current diameter they decrease in size as they grow. As growth continues the nanorods will branch as the narrowing rods will allow deposition to land on Ag areas below.

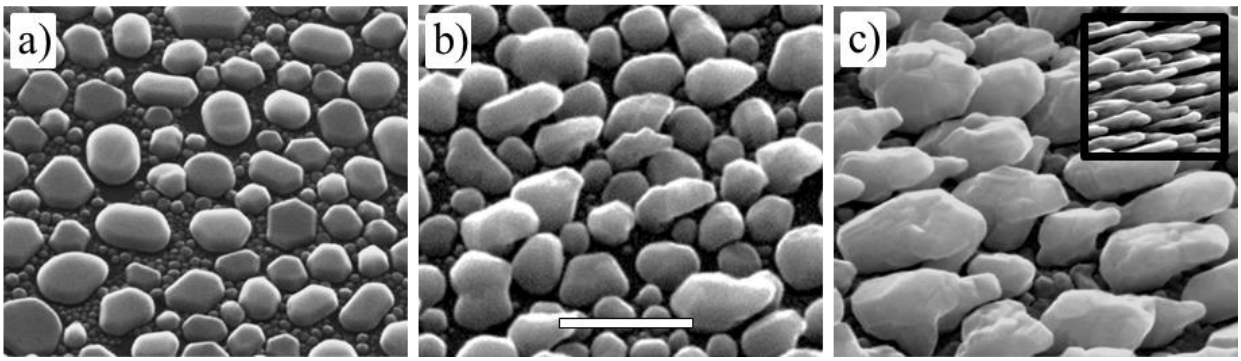

Figure 38. SEM of Ag nanorods grown on In clusters taken at 45 degrees off substrate normal. Images a) through c) contain 25nm In deposited flat on the substrate. For image b) 200nm Ag and c) 500nm Ag was deposited at 88 deg incidence angle. Inset shows Ag nanorods without In. Scale bar is 500nm.

To drive to the smallest diameter nanorods possible, we explore low amounts of In of the substrate for small seeds. Figure 39 shows Ag nanorods when grown with varying amounts of In seed atoms, holding all other variables constant. As proposed, indeed the control of both the separation and the diameter of nanorods is possible through seeding. Further, the In seeds of 5 nm in nominal thickness give rise to the largest separation between adjacent nanorods and the smallest diameter of individual Ag nanorods; Figure 39 (c). When even larger amounts of In, such as 10 nm in nominal thickness, are used as seeds the Ag nanorods have even larger separation, but the diameter also increases.

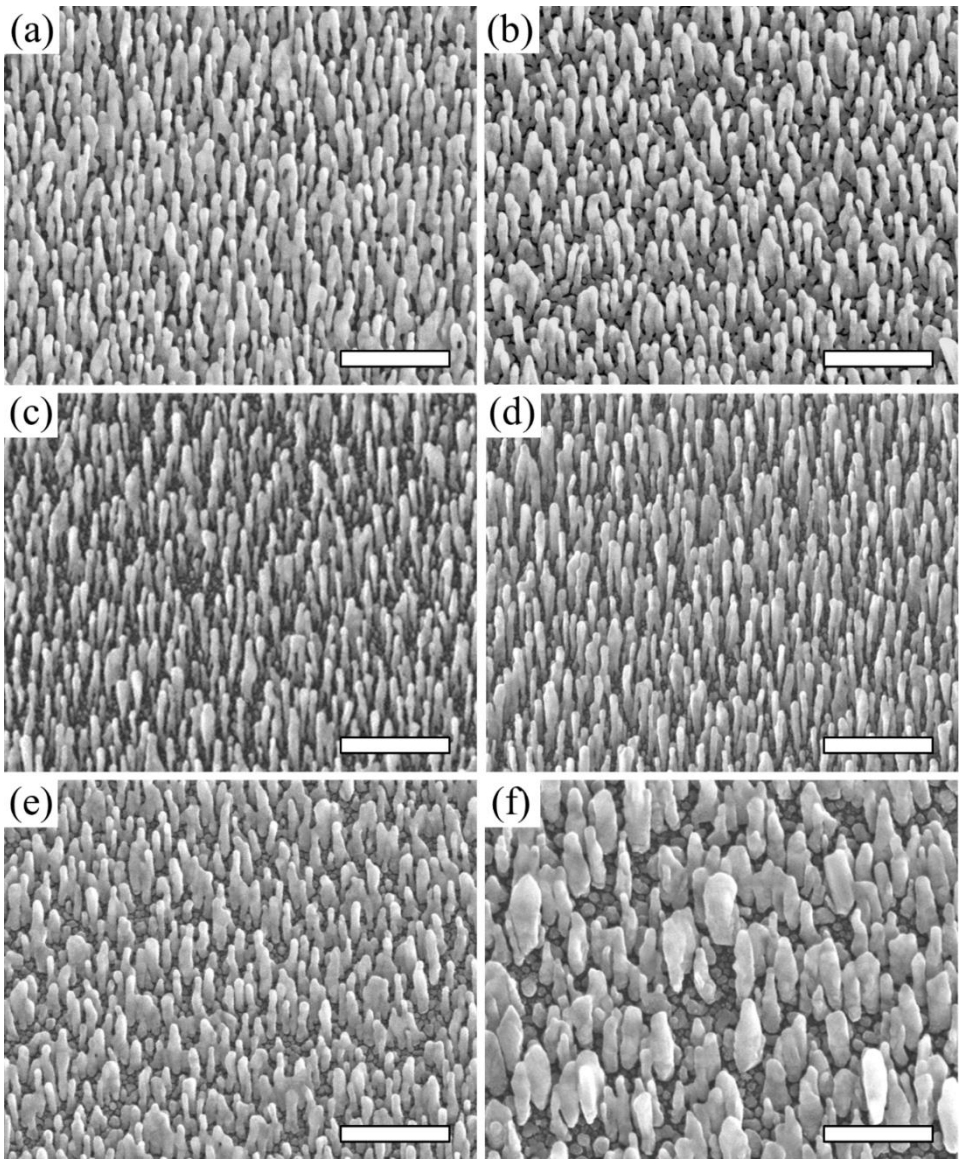

Figure 39. Ag nanorods on In seeds. SEM images, taken normal to the substrate, of Ag nanorods produced by glancing angle PVD on In seeds of various sizes. Indium deposition amounts are (a) 0 nm, (b) 1 nm, (c) 5 nm, (d) 10 nm, (e) 50 nm, and (f) 100 nm; in nominal thickness. The scale bars are 500 nm.

Going one step further, we experimentally analyze the size distribution of the In seeds. The densities of nanorods, from Figure 39, inform us of the density of relevant In seeds on which Ag nanorods successfully develop. From Figure 39 (c), the density of nanorods, or that of relevant In seeds, is ~52/μm^2. The relevant In seeds must be the largest ones. To reach the density of 52/μm^2 for the case of In deposition

of 5 nm in nominal thickness, the diameter of such seeds must be greater than or equal to 7nm; as shown in Figure 40 (a). This value was determined by matching the number of nanorods in a given area to the number of seeds larger than the critical size for the same area. The left insets of Figure 40 show the In seeds of 7 nm in lateral dimension or larger. When an even smaller amount of In is deposited, the In seeds are too small to be effective, as Figure 39 (a) and (b) indicate. As the deposition of In reaches 10 nm in nominal thickness, the relevant In seeds are close together. As a result, the Ag nanorods that develop on the In seeds form bridges; Figure 39 (d). Further increase of In deposition leads to even larger In seeds, which are fewer and thereby more separated; Figure 40 (c) and (d). The increased separation is accompanied by an increased diameter of nanorods; Figure 39 (e) and (f). To strengthen the analyses of size distributions of In seeds, we note that the smallest diameter of relevant In seeds in Figure 39 (a), 7 nm, corresponds to the initial diameter of Ag nanorods; as shown in Figure 41.

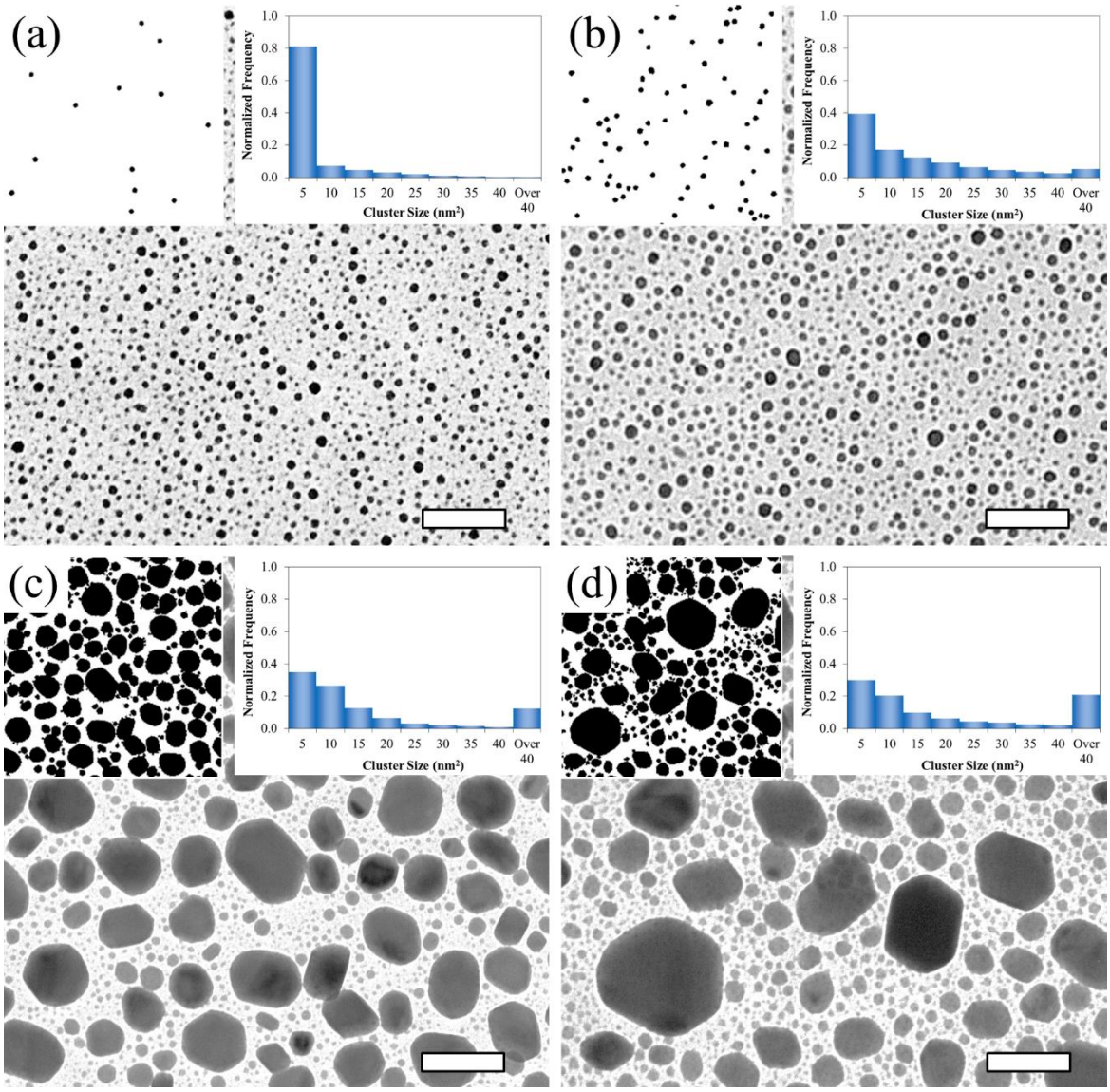

Figure 40. In seeds of various sizes. TEM images of In seeds of (a) 5 nm, (b) 10 nm, (c) 50 nm, and (d) 100 nm on a silicon dioxide substrate; in nominal thickness. Left insets show processed images of In seeds with diameter being 10 nm or larger. Right insets show a histogram of the size distribution of seeds. The scale bars are 50 nm.

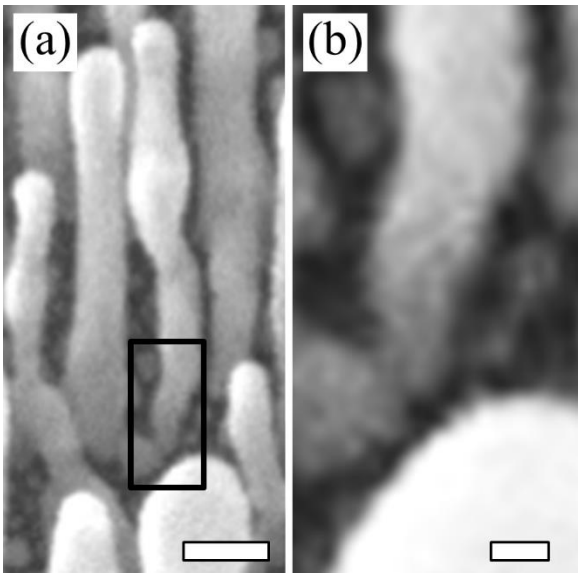

Figure 41. Close view of nanorod diameter growth from seed. (a) Expanded view of **Figure 39** (c), showing the initial diameter of Ag nanorod being ~7nm as highlighted in the black box. Scale bar is 50nm. (b) View of boxed area at higher magnification. Scale bar is 10nm.

SERS Testing

To demonstrate the significance of the change in morphology of Ag nanorods, SERS tests were performed. To test the speculation of performance improvement we compare Ag nanorods grown without seeds to those grown with 5nm In seeds, which are chosen as they have the smallest diameter and best separation. Figure 42 shows the SERS spectra obtained from sensitizing Ag nanorod substrates in low concentrations of N719 dye. With background deleted, the Ag nanorods grown with 5nm of In seed demonstrate a threefold enhancement of the Raman signal over the Ag nanorods grown without seeds.

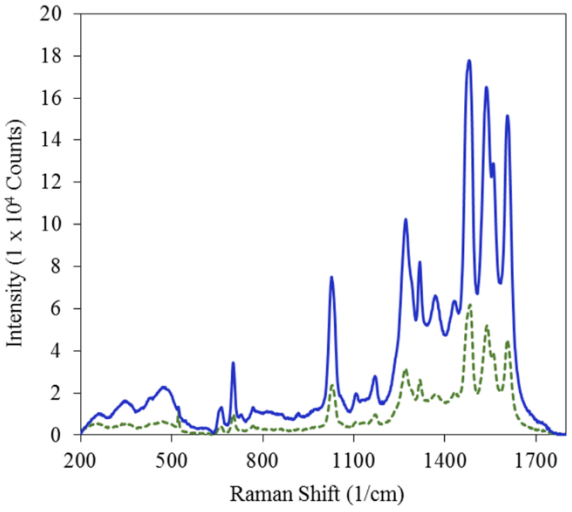

Figure 42. Surface-enhanced Raman spectroscopy. Spectra taken of N719 dye on Ag nanorods with no seed layer (green dotted) and with In 5 nm seed layer (solid blue).

Sn as a Seed Material

To further test the generic nature of our proposed mechanism we replace In by Sn. Post transition metals and metalloids are likely to provide the best cluster forming effects, with examples including tin, antimony, and lead, which have been used as surfactants in metal film growth [101]. Being surfactant, these transition metals and metalloids will not easily mix with Ag, so as to keep the nanorods relatively pure Ag. In addition, these surfactants are also non-wetting on the native oxide layer of a Si substrate and bond strongly with Ag [109, 110]. Like In, Sn is indeed non-wetting on the Si substrate as shown in Figure 43 (a). Figure 43 (b) shows Ag nanorods on the Sn seeds, which are smaller and better separated than those in Figure 39 (a) without seeds. That is, our proposed mechanism is generic in nature, as evidenced by the similarities of seeding effects with In and Sn. While the method is generic, the diffusion and islanding of Sn on the substrate differs from In. As a result, the seeding of 10nm Sn, in contrast to 5nm In, produces the smallest diameter and best separation.

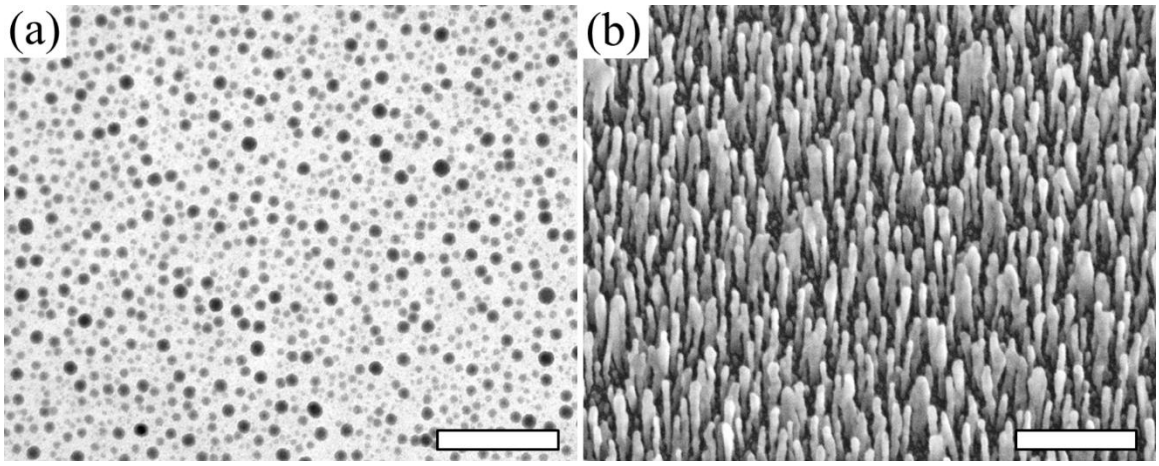

Figure 43. Seeds of Sn and Ag nanorods grown on same. (a) TEM image of Sn seeds of 10 nm nominal thickness. The scale bar is 100 nm. (b) SEM image, taken normal to substrate, of Ag nanorods from glancing angle PVD on Sn seeds; all other conditions are the same as in **Figure 39**. The scale bar is 500 nm.

Control of Copper Nanorods

Here we show that not only is the seed material generic, but nanorods made of other materials can be controlled by seeds as well. The use of seeds on a substrate can also be used to control the size and spacing of copper nanorods. In Figure 44 copper nanorods of 500 nm are deposited on various sizes of Ga seeds. In this case two different scenarios were tested. In one the vacuum level in the deposition chamber was returned to atmospheric pressure between the Ga deposition and the Cu nanorod deposition, and in the other there was no break of the vacuum. This adds an additional factor to the work done previously with the Ag nanorods and In seeds. The reactivity of the metals used as seeds causes them to form quick thin oxide shells on their surface when exposed to atmospheric conditions. Here we investigate if the exposed metal is of importance to the movement of the nanorods material over the substrate and seeds as compared to a metal oxide that will form when exposed to atmosphere, or if the primary importance in determining the final nanorods structure is simply the physical shape and placement of the seeds on a substrate.

The amount of Ga that is deposited as seeds is the same in both the vacuum break and the non-break case. This is 1nm, 5nm, and 10nm, all at the substrate angle 86 degrees relative to substrate normal. In the cases where there was a break between the Ga deposition the Cu deposition not much change is seen

between the control rods, Figure 44 (a) and those deposited on Ga, Figure 44 (b-d). The diameter and the spacing of the nanorods remains largely the same in all cases. When there is no break is a noticeable change between the samples; Figure 45. The case with 1nm Ga, Figure 45 (b) is largely the same as the no Ga case, (a). When 5nm is used the nanorod diameter decreases, Figure 45 (c), leading to better separation between the nanorods. Seeds of Ga 10nm have similar morphology to the 5nm case, Figure 45 (d).

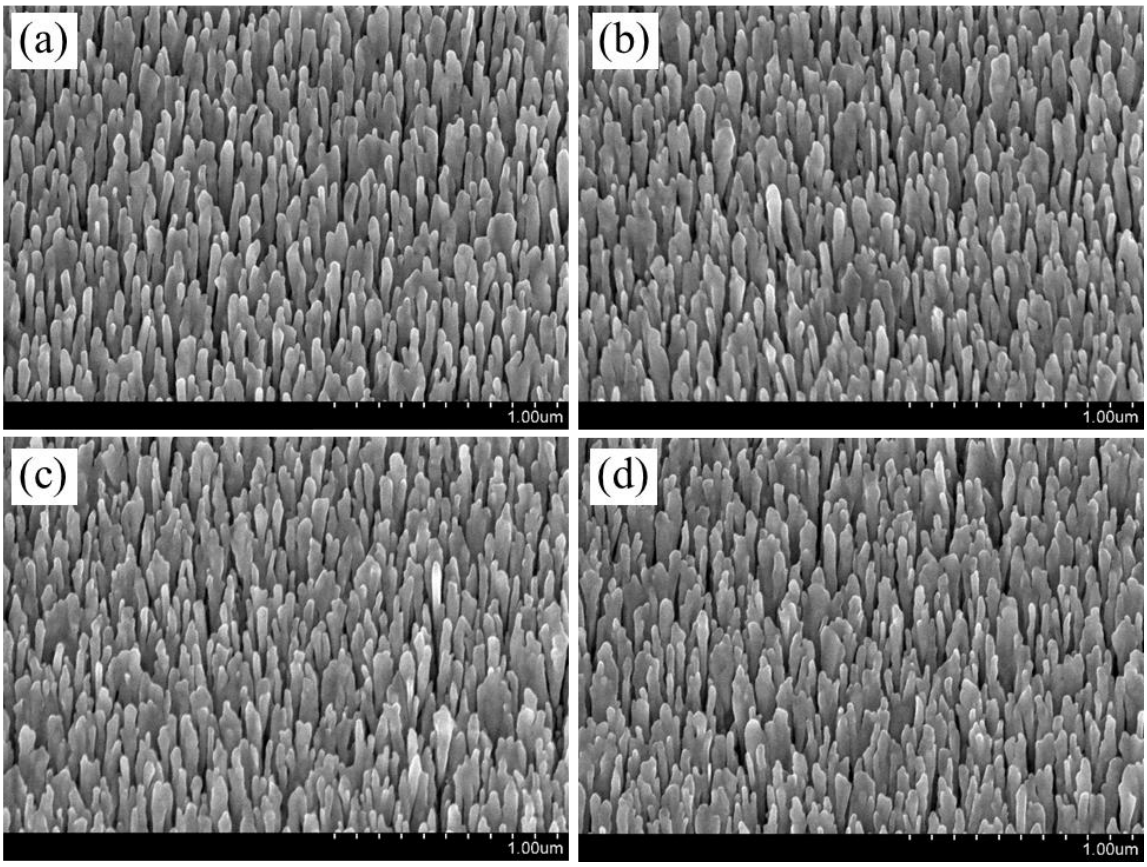

Figure 44. SEM images of Cu nanorods with vacuum break between Ga and Cu deposition. Ga amounts are (a) 0nm, (b) 1nm, (c) 5nm, (d) 10nm.

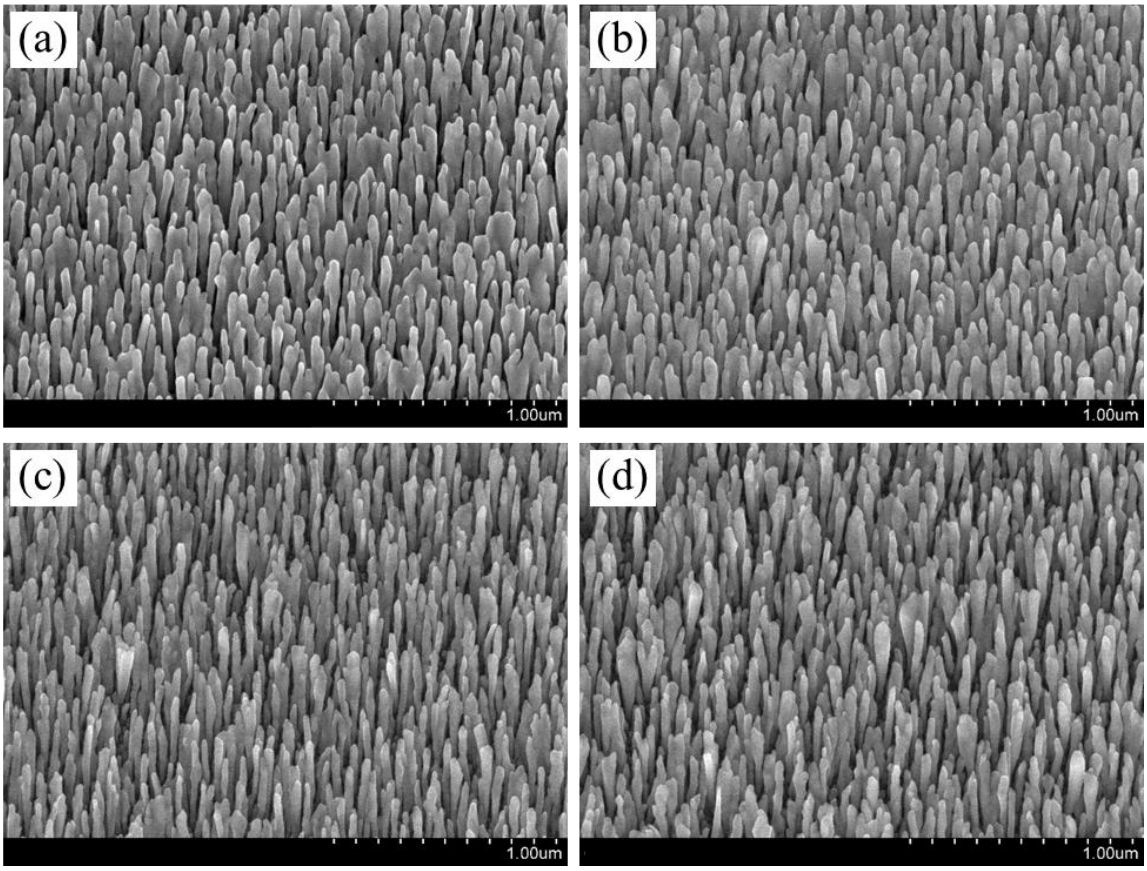

Figure 45. SEM images of Cu nanorods without vacuum break between Ga and Cu deposition. Ga amounts are (a) 0nm, (b) 1nm, (c) 5nm, (d) 10nm.

Gallium quickly forms an oxide shell when exposed to gaseous oxygen even at low levels. This and gallium oxide has a similar surface energy to that of silicon oxide which exists on silicon wafers. When Cu is deposited in the break case where the gallium has had a chance to form the oxide it shows very similar morphology to that of the flat silicon oxide surface, but when the copper is deposited on pure gallium in the no break case the morphology changes.

III.2 Core-Shell Nanorods

Here, we demonstrate coating Ag nanorods with a high-melting temperature metal oxide material. This provides a protective shell on the nanorod that improves its thermal stability and longevity. We also demonstrate capping of Cu nanorods with low melting temperature metals. These form a thin coating and can be used to produce eutectic alloys between nanorods.

Enhanced thermal stability of Ag nanorods through capping

Nanorods of Ag are first produced by EBPVD. These are approximately 500 nm long, and are deposited at 86 degrees from substrate normal at a rate of 1.0 nm/s. The nanorods are then coated with a shell of the high melting temperature titanium dioxide (TiO_2) or silicon dioxide (SiO_2). Figure 46 shows the resulting morphology change of uncoated Ag nanorods after being heated to various temperatures for 10 min. The as-grown uncapped Ag nanorods are well separated and have high aspect ratios as seen in Figure 46 (a). After annealing at 50 °C for 10 minutes, the uncapped Ag nanorods coarsen and merge with one another; Figure 46 (b). When heated to 75 °C for 10 minutes the nanorods completely collapse creating a film on the substrate with large voids; Figure 46 (c). If heated to 100 °C for 10 minutes the grain size increases and the voids become larger. These changes show the instability of the Ag nanorods at raised temperatures.

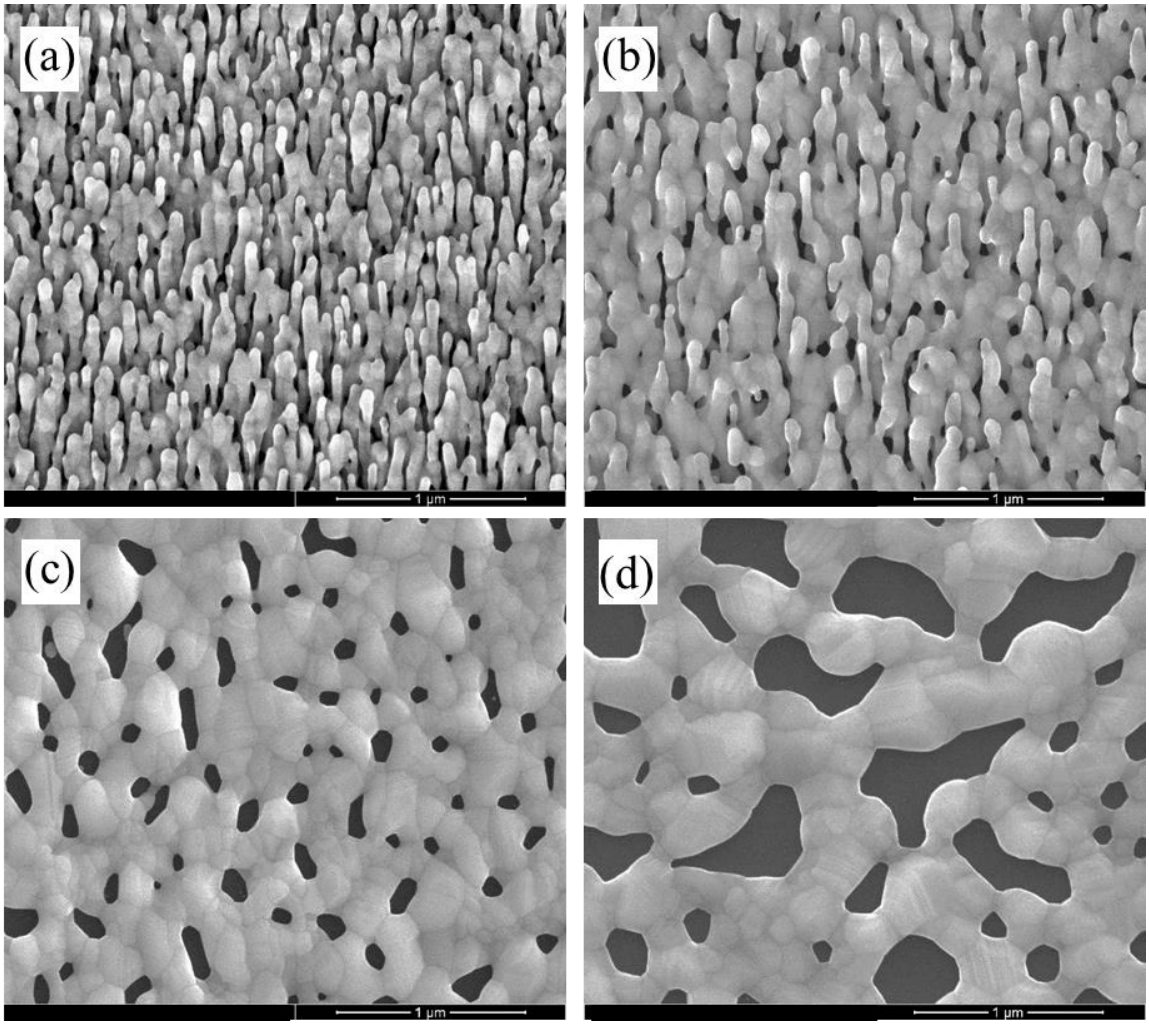

Figure 46. SEM images of Ag nanorods (a) as fabricated; after annealing for 10 minutes at (b) 50 °C, (b) 75 °C, and (d) 100 °C.

To reduce the changes in morphology, the Ag nanorods are capped with different materials. The first material shown is SiO_2. This is deposited on top of the Ag nanorods at a very slow rate of 0.01 nm/s. When these are heated to 100 ^oC there is some coarsening of the nanorods apparent, Figure 47 (b), but they retain their shape significantly better than when no coating is present, Figure 46 (d). Even at 400 ^oC the nanorod morphology is still largely apparent; Figure 47 (c).

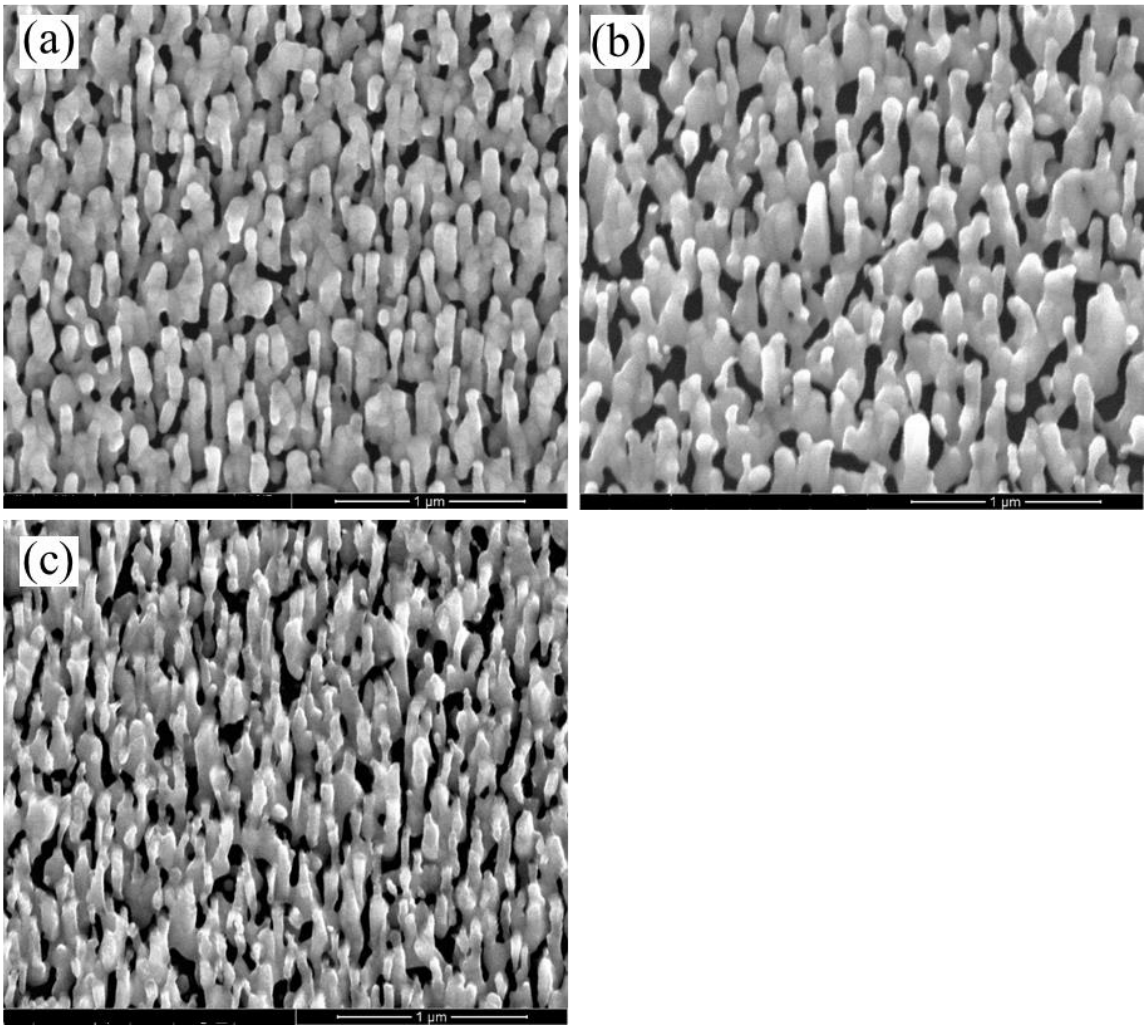

Figure 47. (a) SEM image of capped Ag nanorods as grown, and (b) Ag nanorod with SiO_2 coating 100 ^oC 10min (c) 400 ^oC 10 min.

To more clearly show the shell of SiO2, TEM images are taken of the control Ag, Figure 48 (a), and nanorods with a shell, Figure 48 (b). The coated nanorods show a greater thickness of the shell on one side as compared to the other. The thicker coating side receives more deposition via line-of-sight. A coating on the opposite side can be seen, and indicates that there is likely some movement of the shell material on the nanorod. The very slow deposition rate of the shell material maximizes this process. As shell material lands on nanorod material it has a higher probability of sticking due to a higher free surface energy, so shell material that lands on shell material may end up moving off to move evenly coat the nanorod.

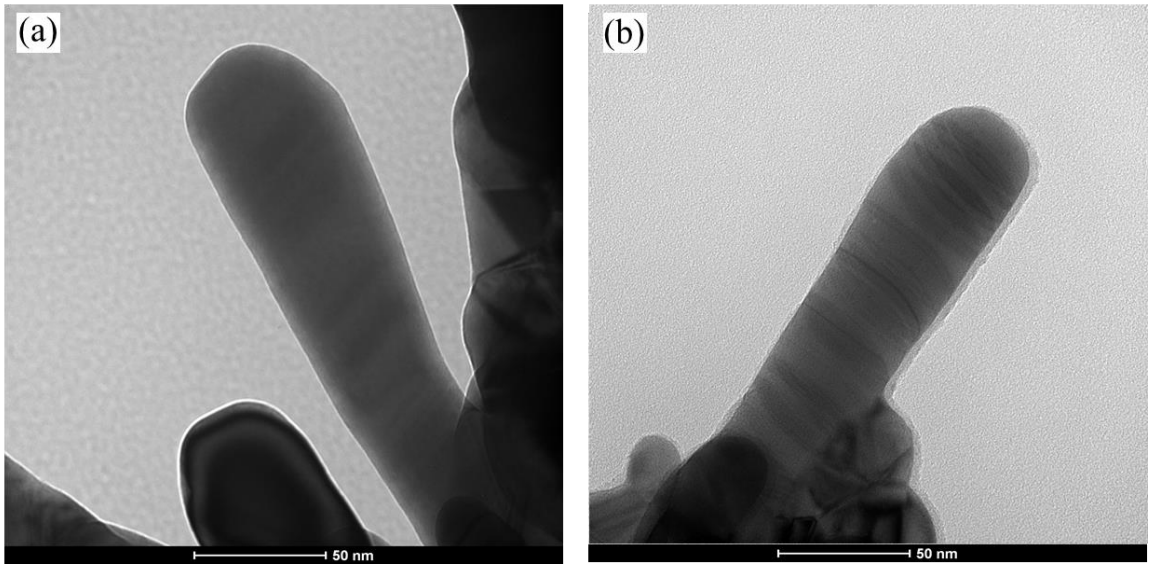

Figure 48. (a) TEM image of uncoated Ag nanorod as grown, and (b) Ag nanorod with 5nm SiO_2 coating.

Similarly, TiO_2 is also used to coat Ag nanorods; Figure 49 (a). The capped Ag nanorods closely resemble the uncapped nanorods in Figure 47 (a). After heating the nanorods to 100 ºC and 200 ºC, Figure 49 (a) and (b) respectively, similar slight degradation of the nanorod morphology can be seen in both cases. In contrast, for the uncapped Ag nanorods, annealing at 100 °C for 10 minutes leads to complete collapse; and even annealing at 50 °C for 10 minutes leads to substantial coarsening, as shown in Figure 32. After heating to 400 ºC, Figure 49 (d), the nanorods are largely gone, but there is still a fair amount of height variation, as compared to the uncoated case at 100 ºC.

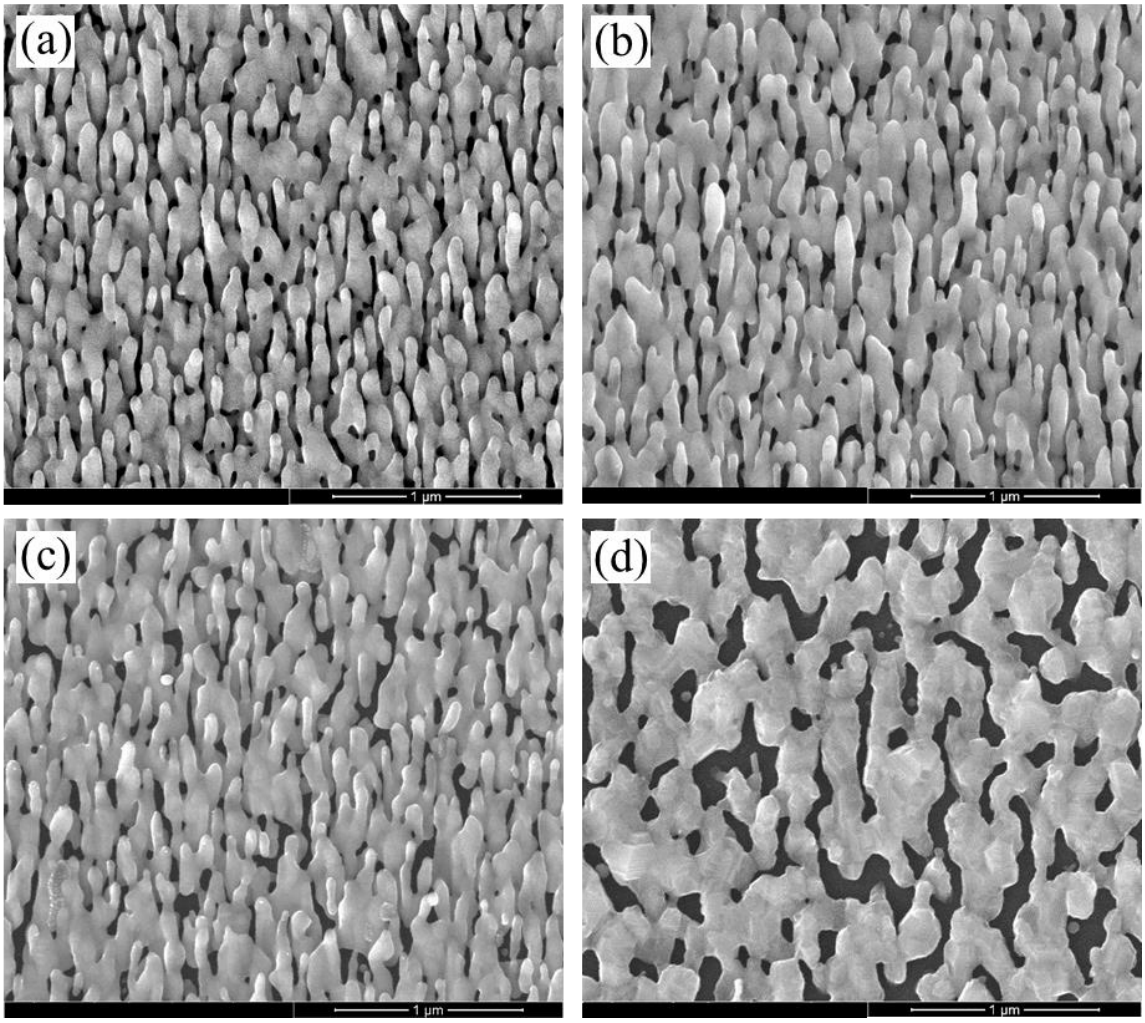

Figure 49. Scanning electron micrographs of Ag nanorods with TiO_2 coating after annealing for 10 minutes at (a) control, (b) 100 °C, (c) 200 °C, and (d) 400 °C.

By examining closer using a TEM the TiO_2 cap on the nanorods can be seen; Figure 50 (a). Figure 50 (b) shows a coated nanorod after it has been annealed at 100 ºC for 10 min. The nanorod morphology is clearly evident and largely unchanged. The cap, similarly remains very consistent.

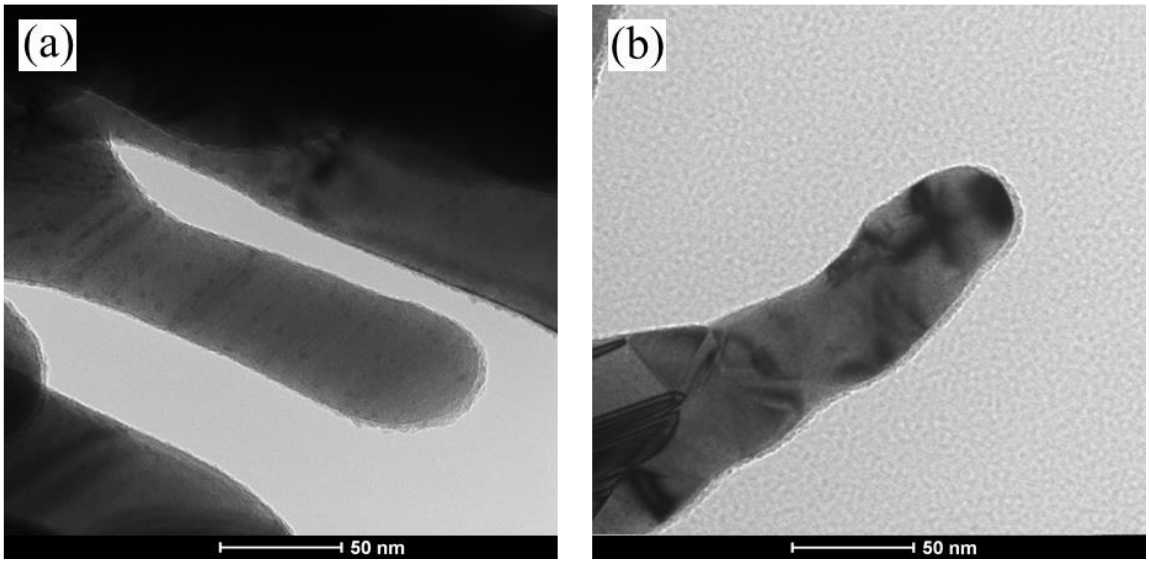

Figure 50. (a) TEM image of Ag nanorod coated with 5 nm TiO_2 as grown, and (b) TiO_2 coated Ag nanorod after 10 min at 100 ^oC.

To understand the mechanism of enhanced stability, we use TEM to characterize the TiO_2 capped Ag nanorods after annealing at 100 °C and 200 °C. After annealing at 100 °C for 10 minutes, the TiO_2 remains on the top of the Ag nanorods, although more crystalline regions are present, as the diffraction pattern and micrograph show; Figure 51 (a). After annealing at 200 °C for 10 minutes, the TiO_2 disappears from the top of the Ag nanorod; Figure 51 (b). From this analysis, as long as TiO_2 remains as the cap, it is effective to slow down the Ag mass transport regardless of whether the TiO_2 is amorphous or crystalline. As soon as the TiO_2 is no longer there as a cap, coarsening occurs. We note that the coarsening of capped Ag nanorods at 200 °C is still slower than that of uncapped Ag nanorods at 50 °C; this slow coarsening may be the result of Ag oxide formation, but such an oxidation process is beyond the scope of this work.

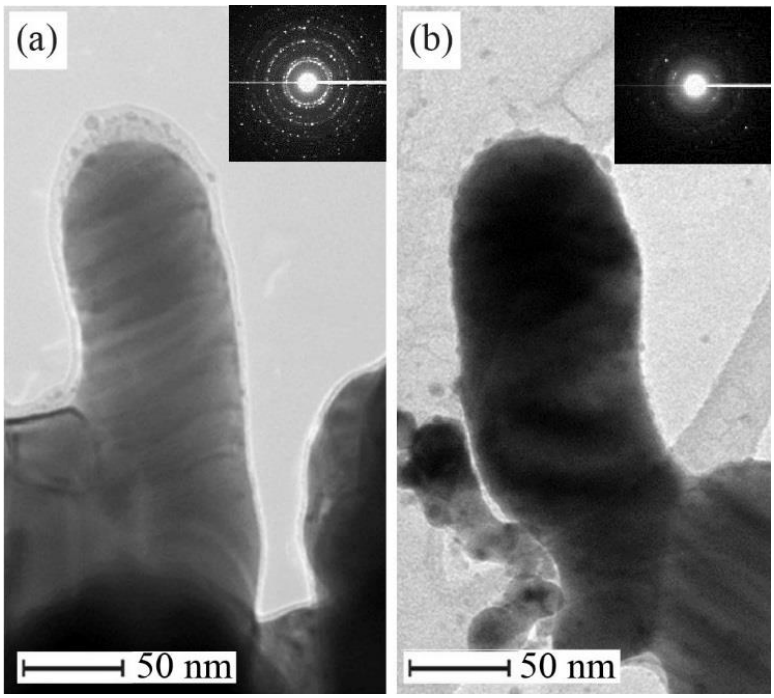

Figure 51. Transmission electron micrographs, with accompanying electron diffraction patterns as insets, of TiO2 capped Ag nanorods after annealing at (a) 100 °C for 10 minutes and (b) 200 °C for 10 minutes.

Having established the effectiveness of TiO_2 capping in stabilizing the morphology of Ag nanorods, we next characterize the effectiveness in maintaining the SERS sensitivity. Figure 52 (a) shows the SERS spectrum of as grown Ag nanorods, with and without TiO_2 capping. The capping does not substantially perturb the spectrum, before annealing for 10 minutes. The peak at 1540.18 1/cm is of particular relevance in sensing, because it is the most dominating N719 peak, and the dominance of this peak is consistent for all substrates and annealing levels tested here, and in the works of Qiu et al. and Lee et al [127, 128]. For annealed nanorods, we measure the intensity at this Raman shift using normalized intensity of uncapped Ag nanorods as fabricated at 1540.18 1/cm. The relative intensity of the annealed Ag nanorods (relative to that of the uncapped as-grown Ag nanorods) changes as a function of annealing temperature; Figure 52 (b). Without capping, the relative intensity precipitously decreases to 2% after annealing at 100 °C; corresponding to the morphological change in Figure 46. With TiO_2 capping, the relative intensity decreases

slowly with annealing temperature, in correspondence to enhanced morphological stability shown in Figure 49.

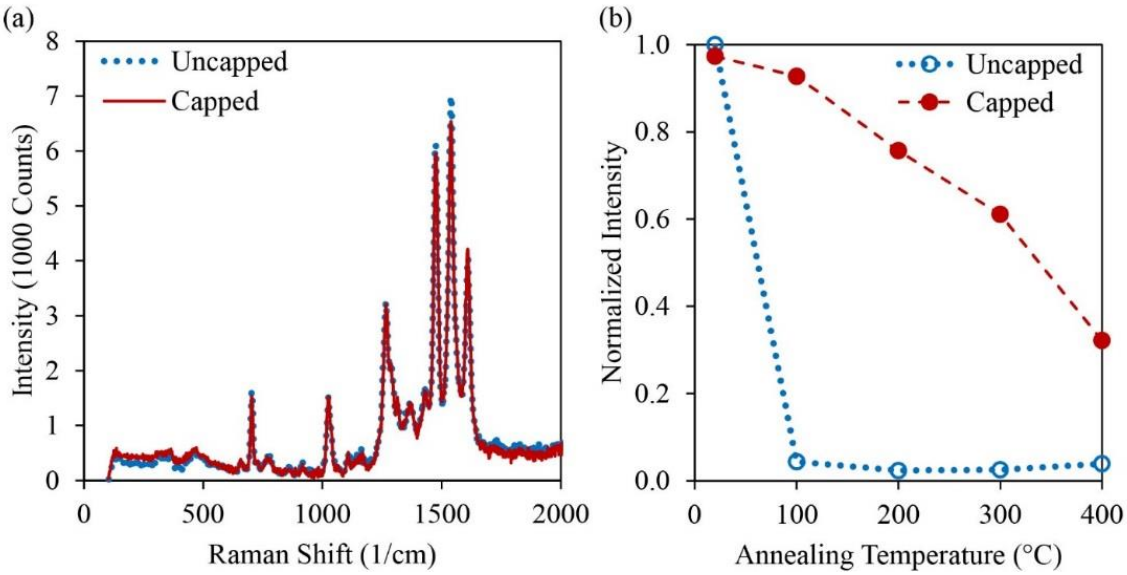

Figure 52. (a) Raman spectra of N719 dye on Ag nanorod arrays as fabricated, and (b) Raman intensity with respect to annealing temperature of uncapped and capped Ag nanorods, normalized to that of uncapped Ag nanorods as fabricated.

Eutectic Coating

While metal oxide coatings can be used on nanorods to provide durable coatings, metal coatings can also be used with various benefits. These can include resistance to surface changes for more reactive materials that tend to form oxidizes or carbides due to interaction with oxygen, organics, water vapor, or carbon dioxide. Other coatings can be used to provide materials that can be combined by placing them in physical contact to form metal alloys. This process will be discussed further in the next section.

Cu nanorods are first produced on a Si substrate, Figure 53 (a). These are then coated with a film of either In, Figure 53 (b), or Ga, Figure 53 (c). With the addition of the metal shell, a slight change in morphology can be observed in the nanorod structure. They become a bit larger in diameter and the sides

are less smooth. With the addition of the same amounts of In and Ga (200 nm) the resulting morphologies are similar.

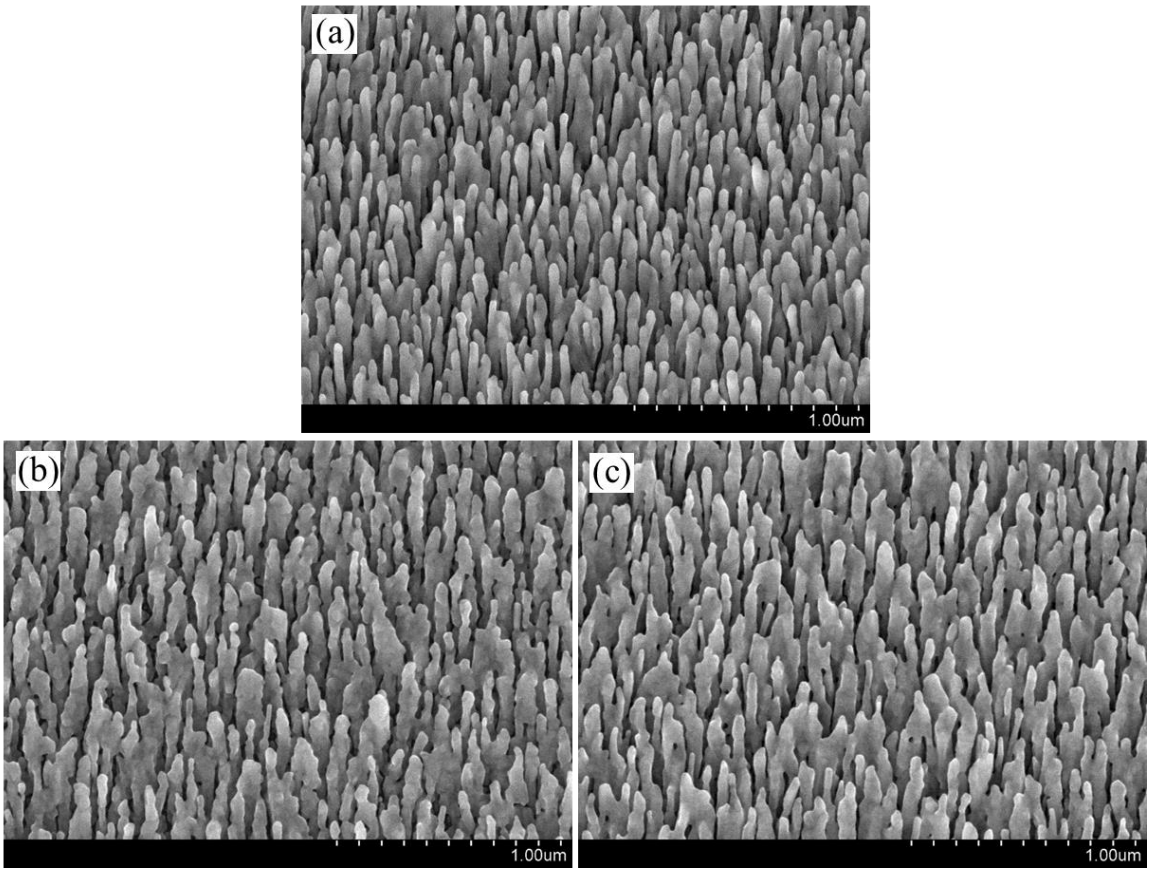

Figure 53. (a) Cu nanorods coated with a shell of (b) In, or (c) Ga.

By using TEM we look closer at the shell on the nanorods. In Figure 54 the Ga shell on both Cu nanorod in the image can be seen. The right image corresponds to the black box in the left image. The shell is consistent over the nanorod and is approximately 2.5nm is thickness. This consistent shell is a bit different than what was observed earlier with the metal oxide shell, which tended to be thicker on one side than the other.

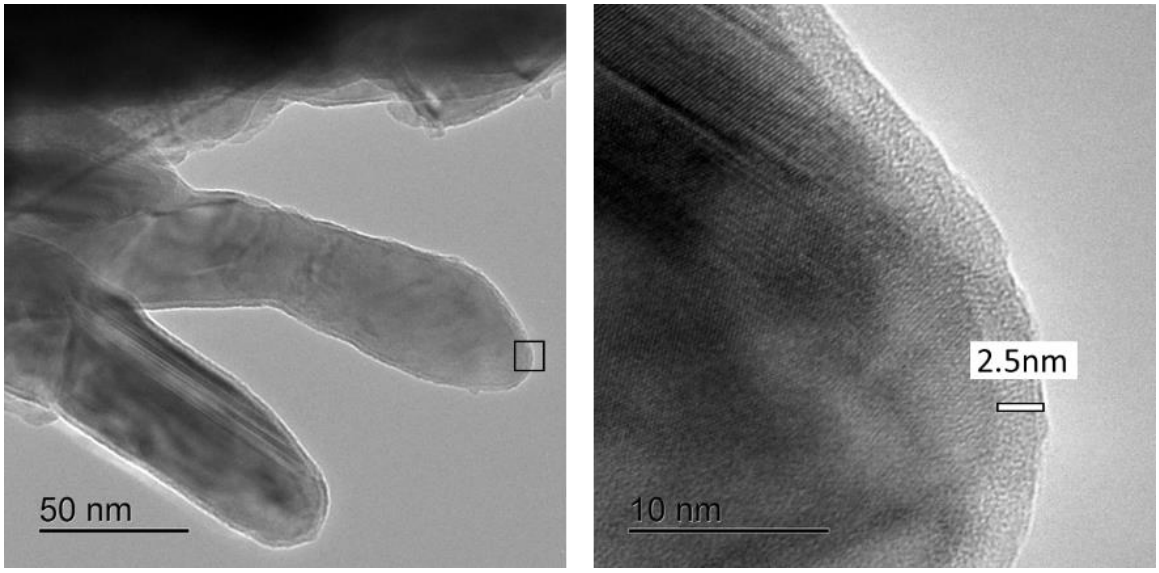

Figure 54. TEM image of Cu nanorods with a Ga shell.

Shown in Figure 55 is a Cu nanorod with an In shell. The right image is zoomed in to approximately the black box in the left image. The indium coating of approximately 3nm is apparent.

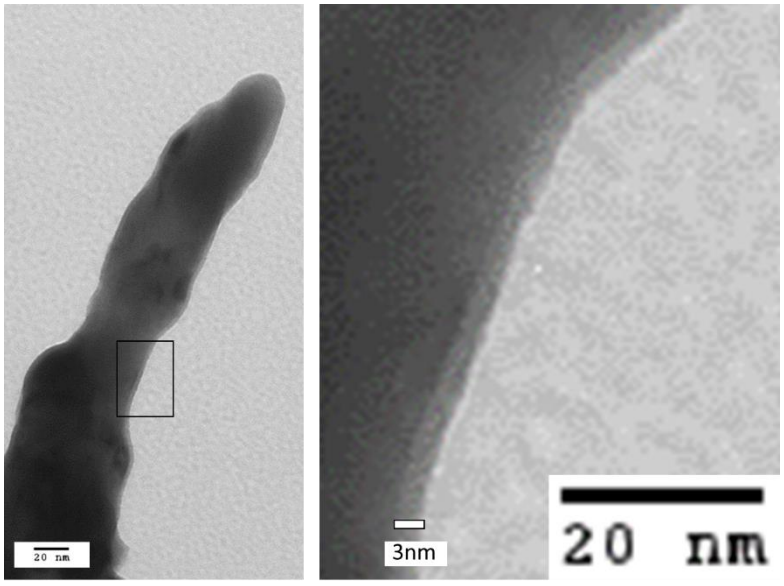

Figure 55. TEM image of Cu nanorods with In shell.

III.3 Metallic Glue (Vacuum Process)

In a previous study, Cu nanorods were used to bond wafers together [54]. This required high temperatures under pressure in a reducing environment. Meeting these requirements for processing method are not possible in many cases. By using coatings on the Cu nanorods, the bonding temperature can be reduced and the reducing environment can be eliminated.

Here is demonstrated the bonding two surfaces together with copper, at room temperature using low pressure and no reducing environment. Two surface with Cu nanorods were both coated with a thin film of a second metal. On one side Ga was used and on the other In. These structures were proposed in the introduction as a schematic in Figure 23. These are pressed together for 10 minutes using a pressure of 10MPa.

Shown in Figure 56 is a bonded region where the Ga and In coated nanorods meet. The SEM image is taken 45 degrees from normal to the substrate. Roughly the top half of the image is the back side of the In coated Cu rods where they attached to the substrate. The Si substrate has been removed to allow for imaging of the area. The darker region in the middle is a cross section of where the bonding begins. The region above, showing the backside of the In coated rods, is bonded to the Ga coated rods beneath them. In roughly the bottom half of the image the Ga coated Cu nanorods can be seen.

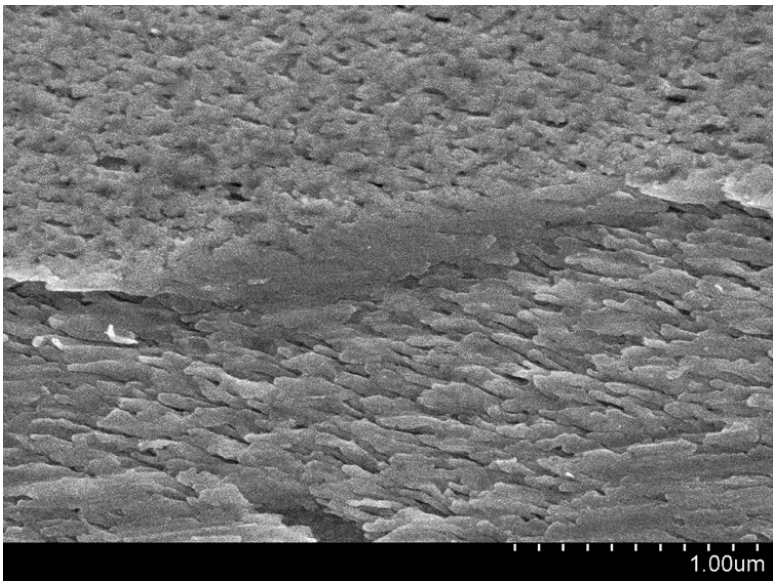

Figure 56. SEM image of eutectic nanorod bond with In nanorods in top and Ga nanorods on bottom. The darker section in the center is the start of the bonded area. Image is taken 45 degrees off substrate normal.

While there is attachment of the layers two sides together the mechanical properties achieved are poor. Only small areas of the surface are observed to bond together. It is speculated that this is due to not enough Ga and In material to form a eutectic. Without enough Ga and In, then the spaces between nanorods will not be well filled, and there will not be enough liquid alloy to interact with the Cu nanorods to form higher order alloys.

Layer Coated Rods

In attempt to overcome the problem observed using the core-shell structure of Cu nanorods with In or Ga coatings, where there is not enough Ga and In to form a strong bond, larger amounts of In and Ga deposited. In these cases the coating material is deposed normal to the substrate as opposed to at the same angle of the nanorods as in the core-shell case. Depositing normal to the structure allows for less material waste. Additionally, a vacuum break is used to increase the oxide shell thickness on the Cu rods

before the In or Ga is deposited, which acts as a diffusion barrier, leaving more pure In and Ga free to combine to form an alloy when they are later pressed together.

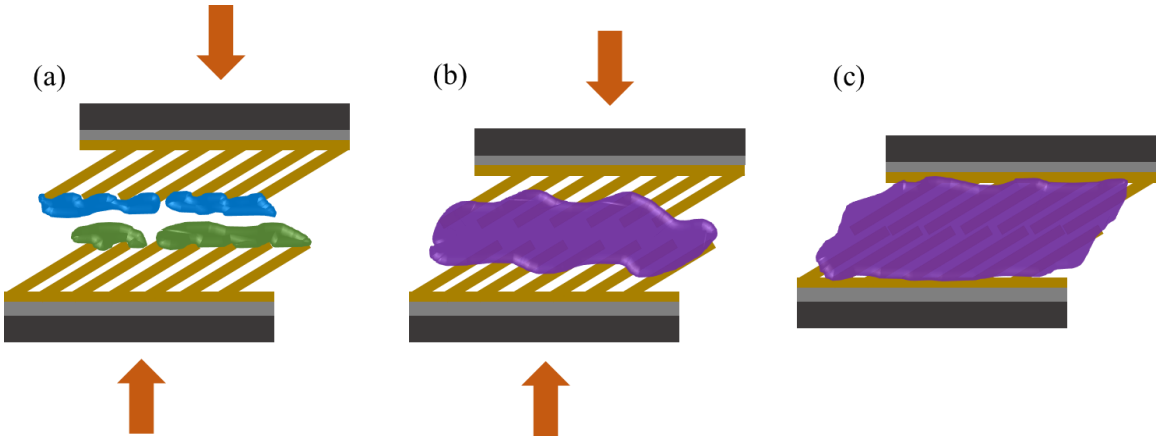

Figure 57. Schematic of Cu nanorods with In layer (blue) and Ga layer (green) being pressed together (a). A eutectic alloy forms when In and Ga combine (purple) (b) which fills the space between rods as the surfaces are pressed together (c).

Three different amounts of In and Ga were used to test the bonding ability of the layer coating. These were all in the ratio of approximately 75.5:24.5 for Ga:In. This ratio corresponds to the eutectic point for the mixture with a melting temperature of 16 oC. In each case the In and Ga film forms blobs of various sizes on top of the Cu nanorods instead of a thin film due to the complex morphology and the wetting condition. When the two sides are pressed together for bonding a pressure of 10 MPa at 100 oC for 30 minutes is used.

The first test has values of 25nm for In and 95nm for Ga. In this case, there was no attachment, and results are not shown. The second test had values of 50nm for In and 190nm for Ga. This resulted in decent bonding between the two surfaces and some force had to be used to separate the sides. It is apparent from the SEM images that bonding occurred in small areas over the entire surface. It appears that eutectic alloy did form in certain areas and that the attachment was sufficient to break off a large portion of nanorods from one side. However, it does not appear that the eutectic penetrated deeply

between the nanorods and thus was not able to interact with the sides of the nanorods. Additionally, the nanorods were not able to interpenetrate.

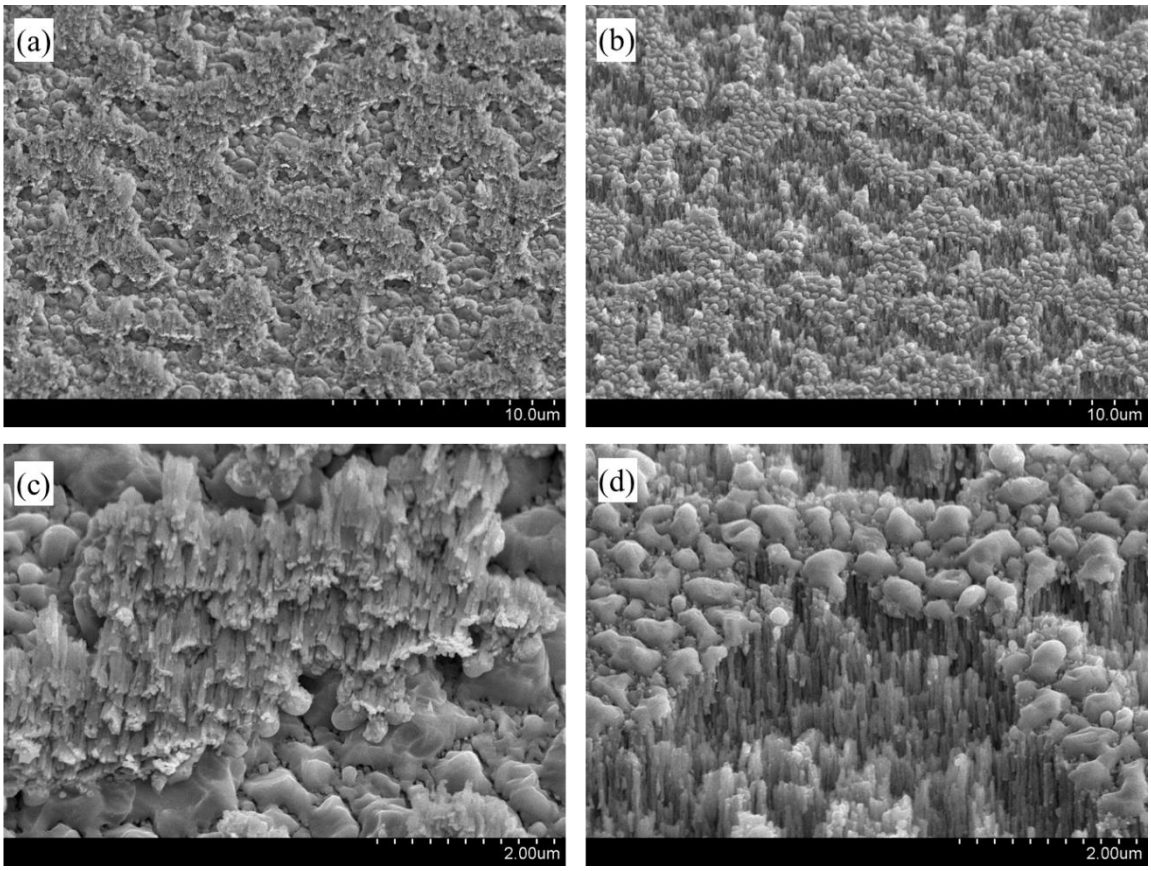

Figure 58. SEM images of interface after bonding and separating in the In 50 nm Ga 190 nm case. In (a) and (c) the underside of patches of broken off Cu nanorods are seen attached to the Ga layer. At different magnifications. Images (b) and (d) show the opposing side with patches of missing Cu nanorods surrounded by whole rods with In layer.

The final amounts used were 100 nm for In and 380 nm for Ga. In this case the overall adhesion was similar to that of the 50 nm of In case. The results appear very similar to the In 50 nm case with patches of Cu nanorods being ripped off of one side and adhering to the other. It seems that the crushing force on the nanorods are pressing them together which keeps the eutectic from penetrating deeply. This limits the strength of the bond of the two sides to the strength of the weakest part of the nanorod, which seem to break off fairly easily near the substrate.

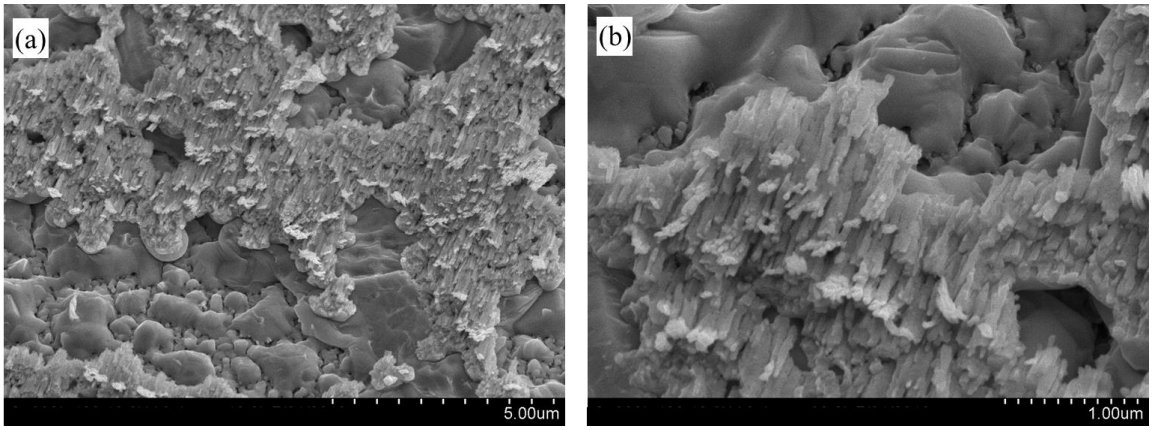

Figure 59. SEM images of interface after bonding and separating in the In 100 nm Ga 380 nm case. Image (a) and (b) show the underside of patches of broken off Cu nanorods attached to the Ga layer of the opposing side at different magnifications.

Mechanical Properties of Metallic Glue

Tests were conducted to determine the shear and pull off strength of the bond while using Si as the substrate. The details of these tests are described in section II.2. Various test conditions were used to determine the effect of the adhesion layer material, the angle of deposition, and the temperature, pressure, and time of pressing.

Tests began with a comparison of the adhesion layer materials Cr, Ti, and Ta. The material Ti showed the highest strength with the failure occurring between the nanorod layers. A Teflon pad was used in some cases between the sample and the heated press to see if this would improve the evenness of the applied force and thus improve the final strength. The results with the Teflon pad used were similar or worse than without, so its use was discontinued.

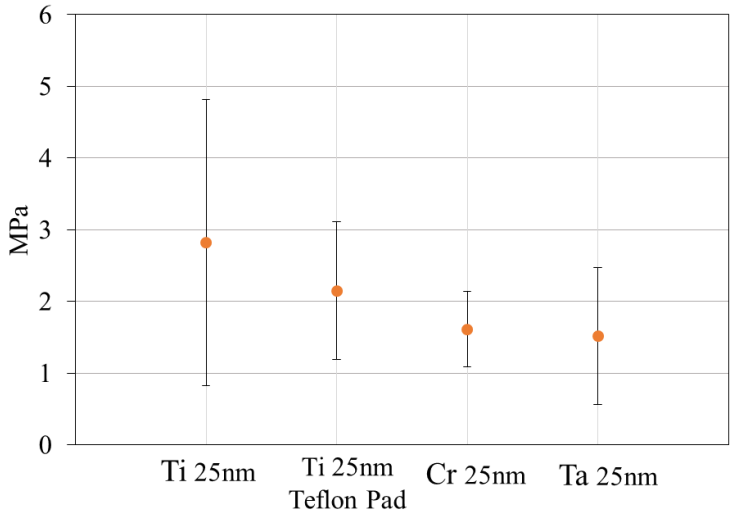

Figure 60. Chart showing pull off strength test of different adhesion layer materials.

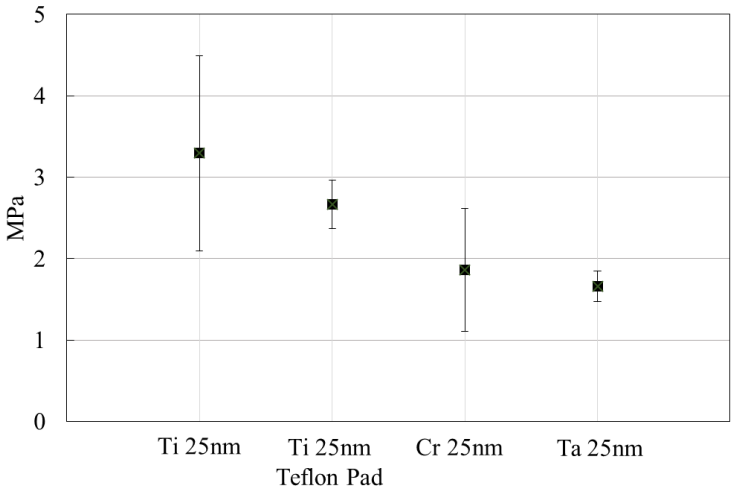

Figure 61. Chart showing shear strength test of different adhesion layer materials

Unless specified, the remainder of the tests used only Ti as the adhesion material. The thickness of the Ti layer was 25nm. One test compared the deposition angle of the nanorods. The values tested were 85, 88, 89 degrees. The increase in angle causes the nanorods to become thinner in diameter and have a larger spacing. The angle of 88 deg was found to produce the strongest bonds.

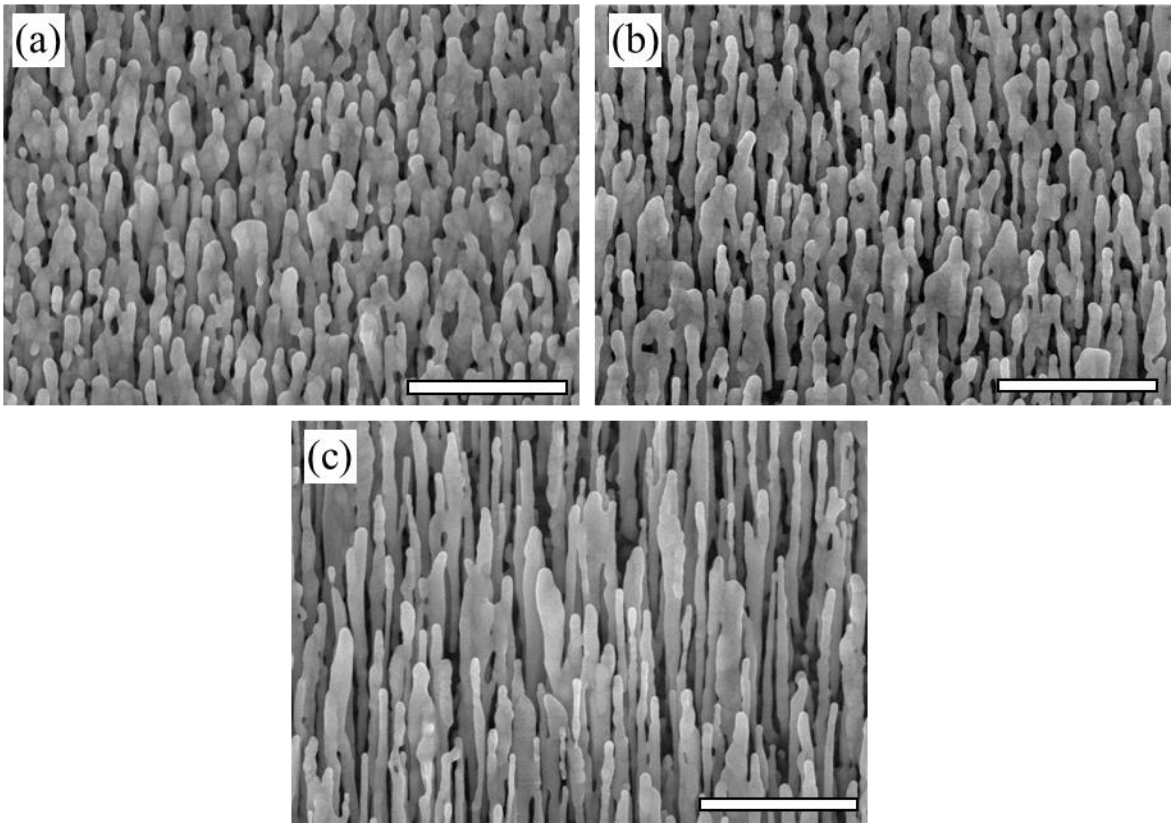

Figure 62. Images of Ag nanorods deposited at the deposition angles of (a) 85deg, (b) 88deg, and (c) 89deg. Scale bars represent 1um.

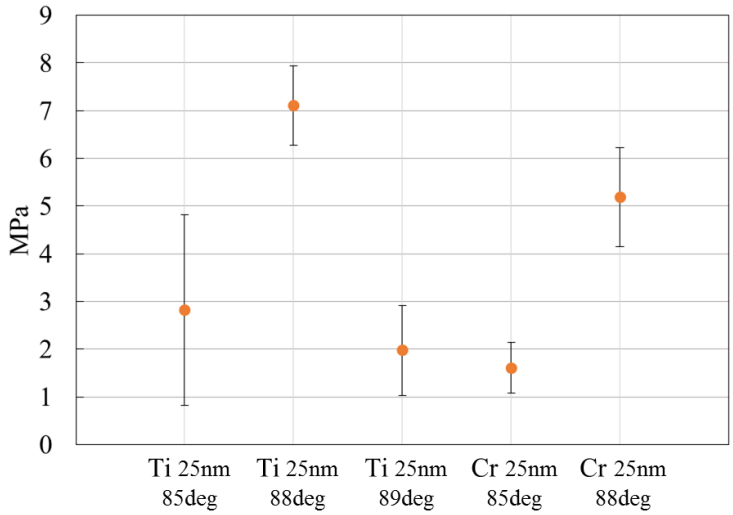

Figure 63. Chart showing pull off strength of depositions performed at different incidence angles.

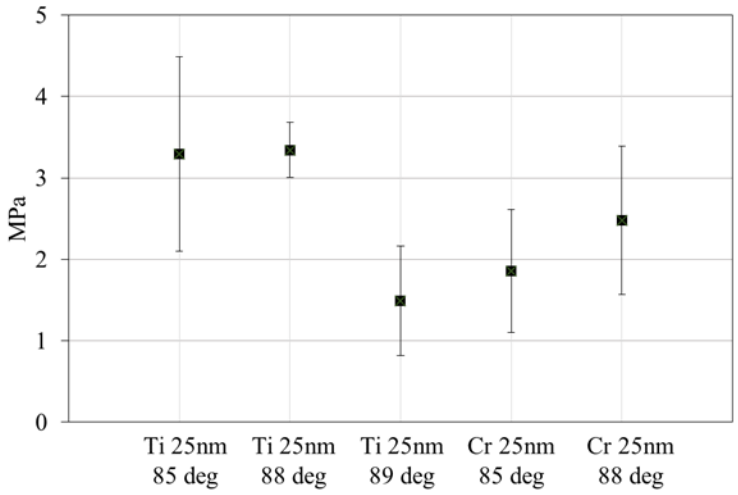

Figure 64. Chart showing shear strength of depositions performed at different incidence angles.

When comparing the temperature, pressure, and time of pressing, the higher values showed marginal improvement over the lower. For example, at the same conditions, when pressed for 60 min the average shear strength was 4.21 MPa, but when reduced to 30 min the shear dropped to 3.34 MPa. In the case of pull off testing, the change in time made no difference in the final bond. Tests conducted while pressing at 1Mpa failed completely and it was seen that at 5 MPa suitable bonding occurred. The best bonds were formed while pressing at 7.5 MPa at 200 ºC for 30 min. This is, somewhat better than the strength observed when bonding at 100 ºC, 5.27 MPa vs 3.34 MPa shear and 7.45 MPa vs 7.11 MPa in Pull Off.

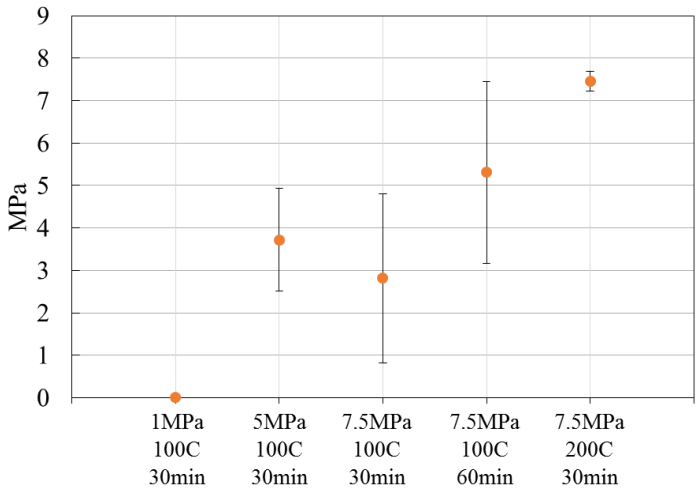

Figure 65. Chart showing pull off strength where different bonding conditions are used.

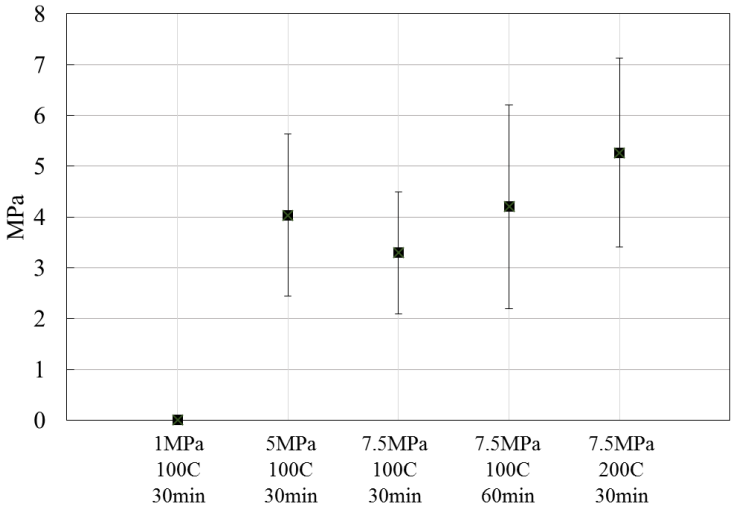

Figure 66. Chart showing shear strength of depositions performed at different incidence angles.

Indium seeds were used to control the morphology of the nanorod structures to determine the effectiveness that this had on the bonding. When small In seeds of 10 nm deposition were used, which corresponds to the smallest nanorods with best spacing, an improvement in the shear strength was observed. Pull off testing showed a reduction in strength. When other amounts of In was used, a reduction in strength was observed for both shear and pull off.

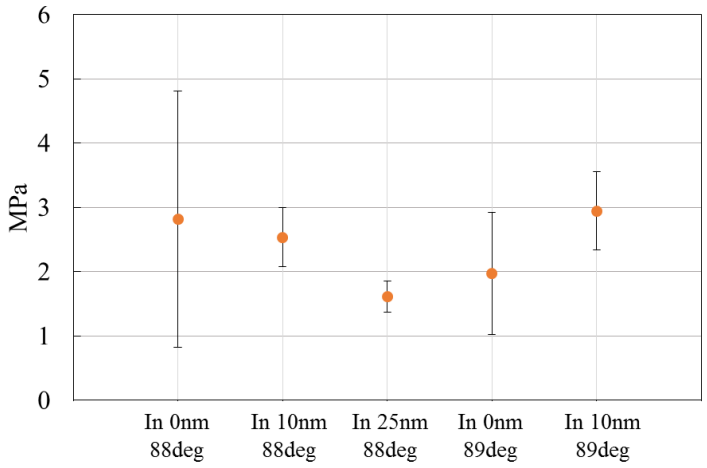

Figure 67. Chart showing pull off strength when different amounts of In are used at incidence angle of 88 and 89 degrees.

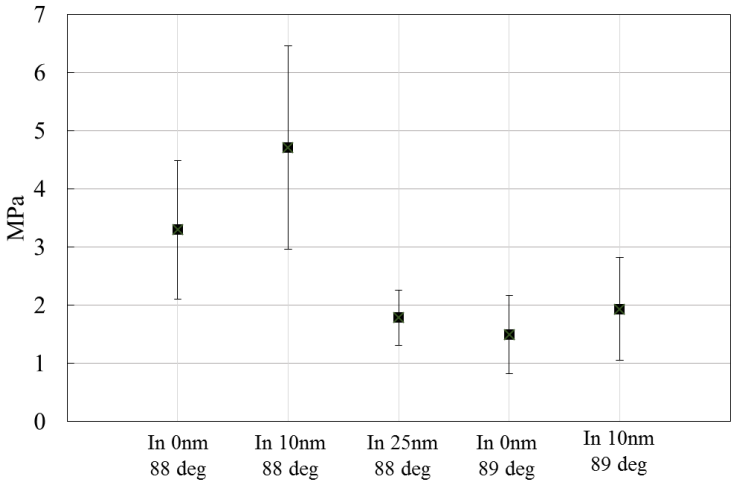

Figure 68. Chart showing shear strength when different amounts of In are used at incidence angle of 88 and 89 degrees.

The failure of most of the bonds occurred at the interface between the nanorods. Above around 5 Mpa in shear and 6 Mpa in pull-off the glue holding the samples to the Al holders began to fail before the bond. Recorded valued above these levels in tests indicate that the bond is actually stronger than this value. For further maturation of the technology an improved method of testing must be devised.

Thermal Conductivity of Metallic Glue

Thermal conductivity measurements were taken of metallic glue between two Cu disks that are bonded together. The copper disks are 1.33in in diameter and around 0.12in thick. The actual thicknesses are measured more accurately using a micrometer. These tests were conducted on an AnalysisTech TIM 1400. The adhesion layer materials of Cr and Ti were both tested to explore any differences in thermal conductivity.

First, to determine the contact resistance between the tester and the disk, a single disk is tested. By dividing the thickness of the disk by the thermal conductivity of the material, the thermal resistance of the disk is calculated.

$$\boldsymbol{RA_{CuDisk}} = \frac{\boldsymbol{X_{CuDisk}}}{\boldsymbol{388\ W/mK}} \quad \textbf{(2)}$$

The thermal resistance of the disk is then subtracted from the total measured resistance to determine the contact resistance.

$$\boldsymbol{RA_{Contact}} = \boldsymbol{RA_{Total}} - \boldsymbol{RA_{CuDisk}} \quad \textbf{(3)}$$

To determine the resistance of the metallic glue the resistance of the disk and the contact resistances are subtracted from the total resistance of the sample.

$$\boldsymbol{RA_{Metal\ Glue}} = \boldsymbol{RA_{Total}} - (\boldsymbol{2 * RA_{CuDisk}} + \boldsymbol{RA_{Contact}}) \quad \textbf{(4)}$$

The thickness of the metallic glue layer is determined by subtracting the total thickness by the measured thicknesses of the individual disks that were taken before bonding occurred.

$$X_{Metal\ Glue} = X_{Total} - (X_{CuDisk1} + X_{CuDisk2}) \quad \textbf{(5)}$$

The thermal conductivity of the metallic glue layer is then calculated by dividing the thickness of the metal glue layer by the resistance of this layer.

$$K = X_{Metal\ Glue}/RA_{Metal\ Glue} \quad \textbf{(6)}$$

The first round of testing consisted of two samples, one with Ti adhesion layer and one with Cr, each of 100 nm. The calculated conductivity using Ti was 0.28 W/m-k and the conductivity using Cr was 0.13 W/m-k. This is significantly less than the value for bulk silver at 406.0 W/m-k. While the disks were machined to have very flat and parallel sides, and were also polished, it seemed possible that airgaps between the disks at the interface were causing the poor thermal conductivity.

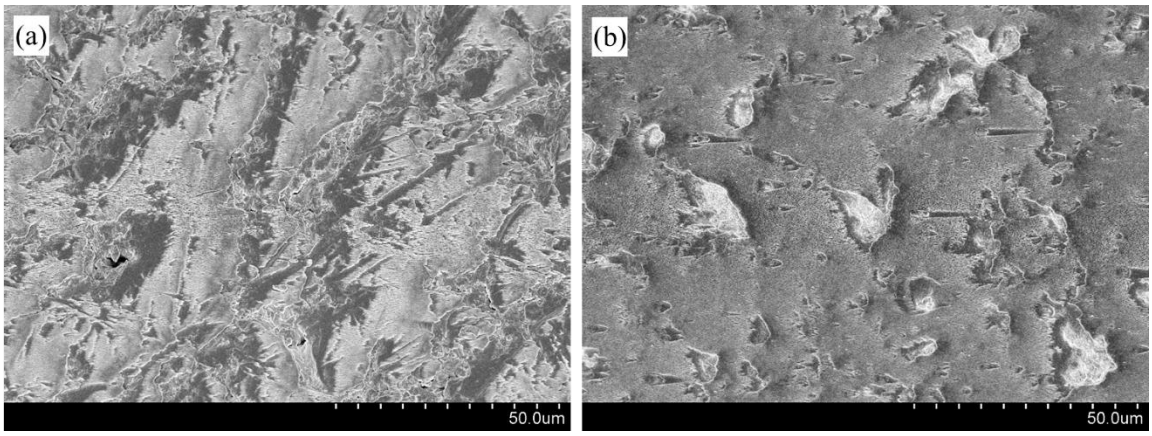

Figure 69. SEM images of Cu thermal tester disks with nanorods grown on surface. Surfaces are (a) as received and (b) with additional polishing.

To examine the influence of surface flatness disks were further polished using 1um media. Adhesion layers of Ti and Cr were again used with Ag nanorods being deposited on these layers. Figure 69 (b) shows more uniformity in the nanorod layer after polishing as compared to (a) though there is still significant areas sufficiently rough to develop no nanorods. The measured value for conductivity for Ti

was 2.4 W/m-k with the value for Cr being 1.6 W/m-k. This is roughly an order of magnitude improvement.

Sample	Thermal Conductivity (W/m-k)
Ti (Unpolished)	0.28
Cr (Unpolished)	0.13
Ti (Polished)	2.4
Cr (Polished)	1.6

Figure 70. Thermal conductivity values for different adhesion layers with and without additional polishing.

These results highlight how crucial the flatness and smoothness of the surfaces is, and how challenging this is to achieve. A small increase in roughness results in an order of magnitude lower value for thermal conductivity. While it is relatively straightforward to deposit large areas of very consistent nanorods onto Si wafers, this becomes more challenge on other materials, such as metals and especially Cu which tends to pit during polishing. The small variations in surface height appear to have a significant impact in reducing thermal conductivity by introducing gaps between the surfaces.

III.4 Metallic Glue (Non-Vacuum Process)

One method to produce a more cost effective way of bonding over using nanorods directly deposited on a surface is to remove the vacuum chamber as part of the process. This reduces the upfront equipment cost and reduces the processing time, as pumping down of a vacuum chamber or load lock in not required. Here two methods are described to accomplish the goal of room temperature metal bonding without using a vacuum chamber. The first method, referred to as the Glue Gun method uses a liquid eutectic mixture of metals combined with nanoparticles which solidifies at room temperature. The second, the Spray Gun method, utilizes a liquid eutectic and nanoparticles sprayed onto a surface, which then combine and solidify. Each method has specific advantages and disadvantages, and are better in different scenarios.

The Glue Gun Method

With the Glue Gun Method, the user holds a device, much like a polymer hot glue gun, or caulking gun, presses a trigger and liquid metal glue is dispensed. Here, there is a device that prepares and dispenses a liquid consisting of a liquid metal component mixed with a powdered metal component which then solidifies. The powdered metal component can be mixed with other substances such as a solvent to allow for easier dispensing or a flux which may aid in wetting of surfaces to be coated or bonded or reduce oxidation. The liquid metal component can be stored in the device in different forms such as a liquid, or as powder, pellets, wire, or cylinder which is melted. The liquid metal and the metal powder are combined in a mixing chamber. The materials can be stored in containers on the device and moved to the mixing chamber by various means, such as a piston, screw, or pump. The mixing chamber can be a disposable attachment which mixes the combination as it passes through various baffles in the chamber. This chamber can also function as a nozzle with the mixed liquid being dispensed from the tip. The tip allows for the placement of the liquid onto small specific locations, such as solder pads for electronics or

between heatsinks and computer chips. The component gallium tends to wet other metals and ceramics making it possible to bond similar and dissimilar materials together, but flux can also be added to improve wetting of surfaces for improved bonding. Flux can be combined with the powder or liquid components or it can be added to the mixing chamber by a separate opening or may be applied to the substrate directly.

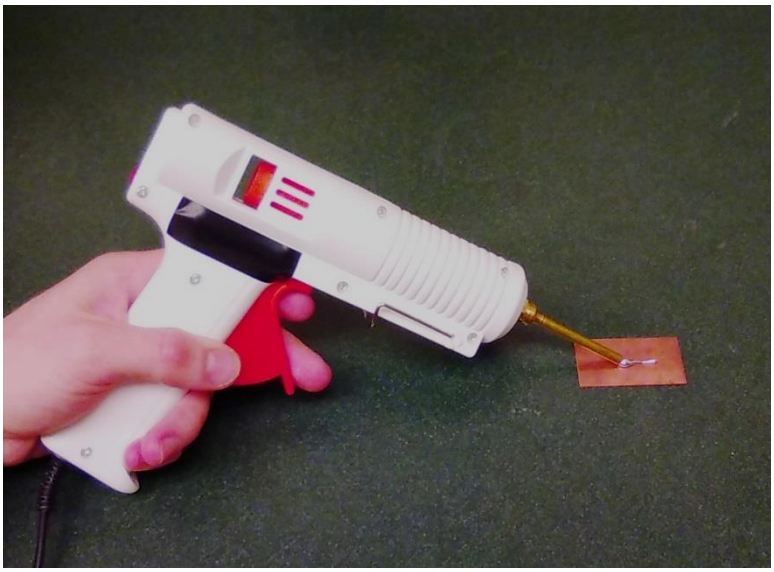

Figure 71. A photograph of a prototype device dispensing a liquid metal.

In one prototype device the liquid metal component and the powder metal component are housed in two separate disposable containers. These may be attached and may have a double plunger type device at one end that is able to apply pressure on the components. At the opposite end to the plunger device there is an opening where the components would be dispensed. These openings may lead to a mixing chamber which may be attached to the disposable container and may also be disposable. The mixing chamber would contain an orifice or nozzle where the mixed components would exit the device.

Figure 72, shows a cross sectional schematic of a metal glue dispenser. This utilizes a disposable container containing the raw materials that is placed into the device. The disposable container may be made of an inexpensive material such as plastic with a relatively high melting temperature or metal. The container material must have a sufficiently high melting temperature that it does not melt or weaken

during the operation of the device. The disposable container contains two sections. The first section contains the liquid metal component. This can be in the form of a liquid, or solid pellets, powder, larger pieces, or one piece. The disposable container contains a second section that contains the powder component. This can be in powder form, or can be mixed with a substance to make it a gel or liquid. Such mixing materials might include a solvent such as ethanol or a flux. The double plunger, when pressed, forces the liquid component and the powder component to the front end of the two sections and out the two openings. The two openings lead to the mixing nozzle, where the two components are combined and mixed. These are then forced out the front of the nozzle through a hole.

The double plunger is pressed by the pressing piece, causing it to move into the disposable container. The pressing piece is driven by the actuator, which is activated when the trigger is pressed by the user. The actuator may be electrically controlled or may work by mechanical force provided by the user when the trigger is pressed.

A heating element is used to heat the liquid component in some cases where a higher temperature alloy is used. This converts the alloy from a solid phase to a liquid as it reaches the front of the device. This heating element may extend to heat part of the powder component section. The heating element may also extend forward to surround and heat the mixing nozzle. Heating the powder component may also be used to remove a protective layer, such as a polymer, or aid in the removal of a solvent by evaporation.

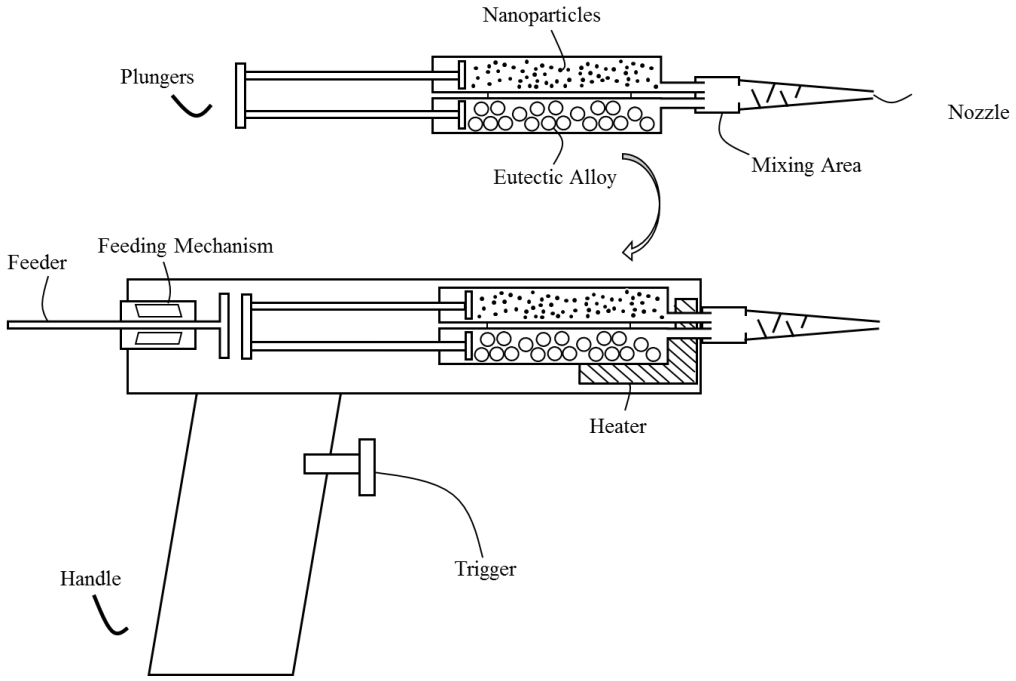

Figure 72. A cross-sectional schematic of the mixing and dispensing device.

The metal powder is made of micro or nanoparticles of particular metals, alloys, oxides, or ceramics and can include Ag, Cu, Al, and Ni, among others. The liquid component consists of a single element or an alloy of metals such as Ga, In, Sn, Sb, Zn. The reaction between the liquid metal component and the powder metal component causes the hardening of the liquid as various higher order alloys are formed. The speed of this reaction can be increased by decreasing the size of the metal powder particles and by increasing the temperature after the components are mixed. The mixture, once applied, can be cured at a raised temperature for decreased cure time.

The dispenser of the mixture contains a heating element which allows for the use of metals or alloys that form a liquid above room temperature. A heating element may also be used to heat the metal powder which may remove a protective coating.

In one case the powder component is coated with a protective layer and then is mixed with the liquid component. This can be done at raised temperature if the liquid component is solid at room temperature. The mixture can then be cooled causing it to solidify, or the mixture can be added to the

apparatus as a liquid. The protective coating keeps the liquid component from reacting with the powder component until the coating is removed. Once removed, alloys are formed by a combining of the components. The protective coating may be removed by heat or by other methods such as a solvent. In the case of heat, the protective coating should be stable at the melting temperature of the liquid component so the powder and liquid components can be mixed together without them reacting. During use, the temperature applied is above the stable temperature of the protective coating, causing the removal of the coating and resulting in the reaction between the powder and liquid components.

The advantages in this form is primarily ease of use. The user merely pulls a trigger to dispense the metal mixture which then hardens within minutes. Various surfaces that are being bonded may require various methods of pretreatment to improve adhesion of the metal bond, such as sanding, chemical etching, or plasma cleaning.

Mechanical Testing Data

Tests to measure the shear strength of the metallic glue are conducted. The substrate was Cu with the glue being spread on a 0.5 x 0.5 in area. Various glue formulas and bonding conditions were tested. Figure 73 shows and image of samples after they are tested.

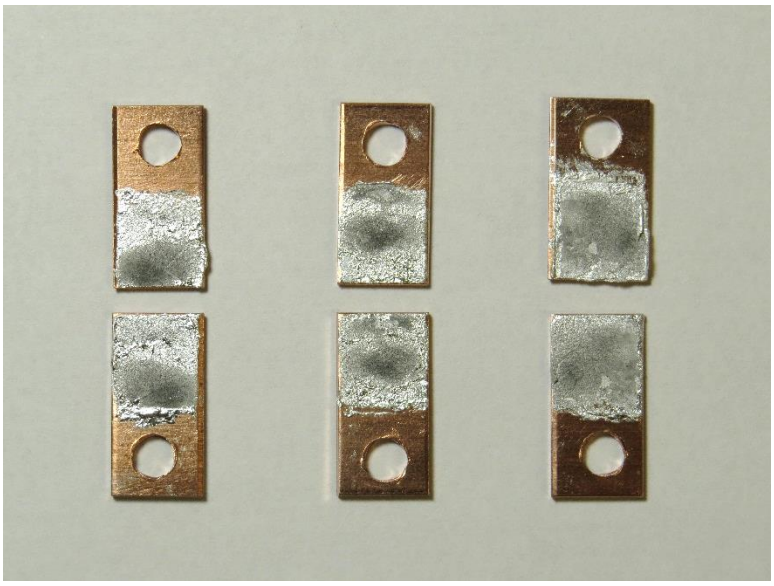

Figure 73. Cu shear test samples with metallic glue after being separated though testing.

The shear strengths of one formula bonded using various conditions is described in Figure 74. In sample (a) the metal glue was applied as a small bead in the center of the bonding area. The two copper pieces were then pressed together under low pressure for 12 hr. In (b) the glue was spread evenly across the surface and a high pressure was used for 12 hr. In (c) the glue was spread evenly and a low pressure was used for 12 hr. This showed significant improvements over the high pressure case, resulting in an average shear strength of 1.09 MPa instead of 0.32 MPa. The surface of the Cu was sanded in (d) with the same conditions, showing a similar average strength, but a decrease in the variability. In (e) the bond was left to cure for 24 hr, with a resulting increase of average shear strength measured at 1.49 MPa.

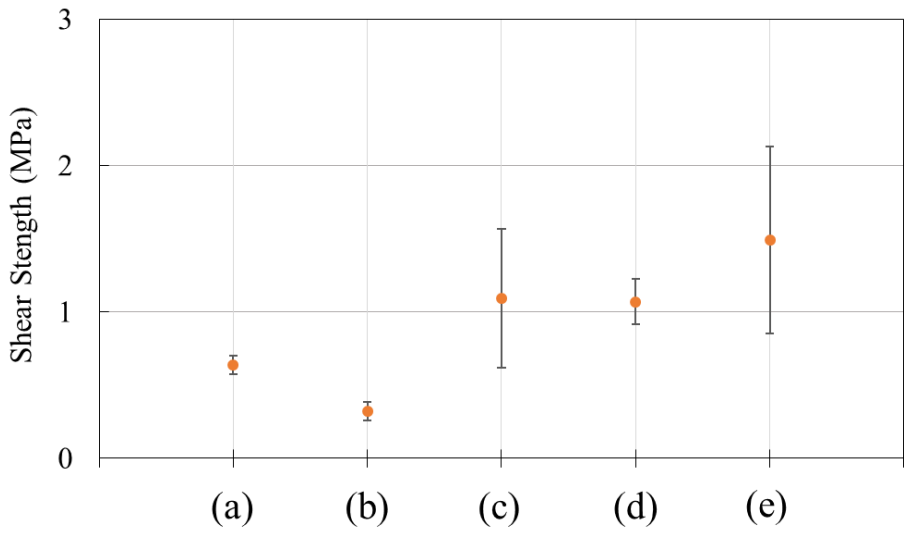

Figure 74. Shear strength test data for various bonding conditions of one metallic glue formula on Cu. (a) Low bonding pressure, glue applied as bead. (b) High bonding pressure, 12 hr cure, even spread. (c) Low pressure, 12 hr cure, even spread. (d) Low pressure, 12 hr cure, even spread, surface sanded. (e) Low pressure, 24 hr cure, even spread, surface sanded.

The Spray Gun Method

The Spray Gun Method operates somewhat like an airbrush that is used for painting or like a powder coating gun which is also used to apply coatings such as paint. One objective of this method is to provide a way of producing a metal coating by using liquid metal and fine metal particles by spraying them onto a surface at a low velocity and low temperature. This is in contrast to Cold Spray or Thermal Spray which uses high velocity and/or high temperatures to produce metal coatings. Coatings with the Spray Gun Method can be very thin or thick depending on the spraying conditions. Another objective of this invention is to bond materials together with a liquid metal that solidifies, as a type of spray adhesive.

Figure 75 shows a particular version of a dual spray device. This is an external isometric view. In this particular case, the spray device has liquid component reservoir which contains the liquid component. This is fed into liquid component spray gun and then is sprayed out of one nozzle. This device also

contains powder component reservoir which feeds powder into the powder component spray gun which is then sprayed out of a second nozzle. The handle allows for the device to be held in one hand and when pressed, the trigger activates the spraying of both powder and liquid components. The cable attachment allows for various connections to the device such as to provide electricity, compressed gas, or raw materials.

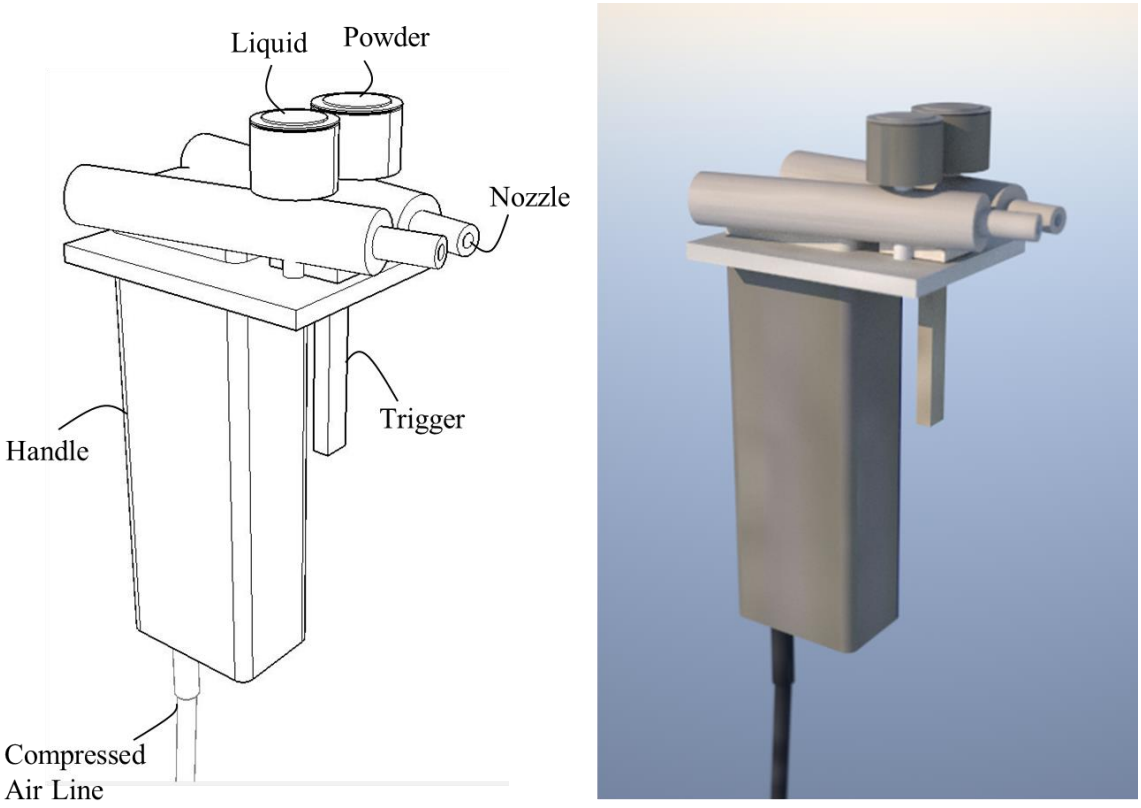

Figure 75. A model of the Spray Gun Device as a line drawing with labels (left) and as a rendering (right).

The device contains two separate spray nozzles that when activated simultaneously spray two components that mix as they travel or once they strike a surface. One component is primarily a metal powder and the second is primarily a liquid metal. The powder may be mixed with other materials, such as a fluid, resin, or solvent to make a slurry, and the liquid metal may be mixed with other materials to enhance the interaction with the powder, substrate, or improve bonding.

Figure 76 shows a process diagram for the dual spray device. The spray device has liquid spray nozzle and a powder spray nozzle. The liquid spray nozzle contains an orifice for the insertion of liquid and an orifice for the insertion of pressurized gas. The liquid can be forced in by an optional liquid feeder, which might take the form of a pump, a rotatable screw, or a plunger. A liquid reservoir contains the liquid component for the process. The liquid component can be added to the reservoir as a liquid, or as a solid in the form of pellets, powder, or wire, among others. These solid forms can be heated by optional heater to form a liquid before moving to the liquid spray nozzle when high temperature alloys are used.

The powder spray nozzle contains an orifice for the insertion of a powder component and an orifice for the insertion of pressurized gas. The powder component is added to powder reservoir and can consist of a powder in the form of micro or nanoparticles as well as a mixture of powder with various compounds such as a solvent or a flux to form a liquid or paste. The optional powder feeder can be used to move the powder component by various methods such as with a rotating screw or with a plunger. The powder component may pass through optional heater which may raise the temperature of the powder component. Particles may be coated with a protective layer such as a polymer or citrate that may be removed with the heater just before spraying. These may be a dry powder or may be mixed with various substances such as a solvent like ethanol or methanol or with a flux paste. An optional electric charge can be applied to liquid spray nozzle and an optional electrical charge can be applied to powder spray nozzle.

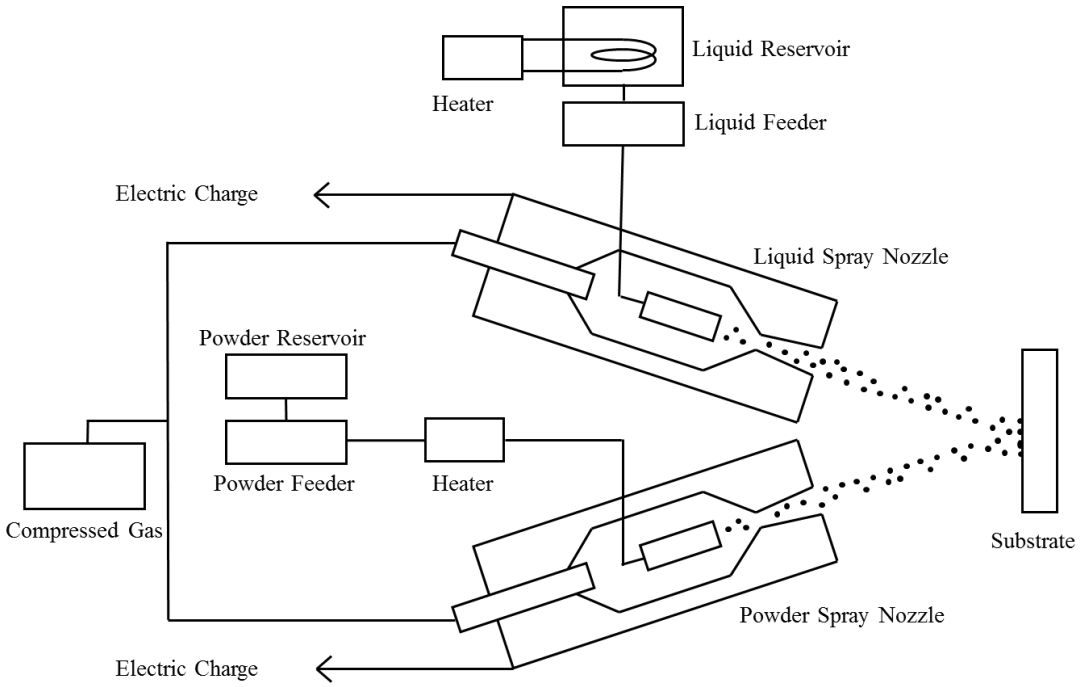

Figure 76. A process diagram of a two nozzle spray method.

Figure 77 is a side view cross section of a particular design where the dispensers for both a liquid and a powder component are combined into a single spray nozzle. The powder reservoir contains the powder component for use in the device. This is injected into the air steam by particle injection orifice. The air stream is provided by the pressurized gas which is provided through the pressurized gas path. The liquid reservoir contains the liquid component. The needle can be adjusted left and right in the device to control the amount of liquid component that is injected into the air stream by way of liquid injection orifice. The liquid component and then the powder component are injected into the pressurized air path and then exit the front of the device through the front exit orifice.

In this device the pressurized air path may form a ring as it travels past the liquid reservoir toward the front exit orifice. The rate of particles injected into the stream can be controlled by a flap or needle in particle injection orifice, similar to the needle used for this purpose with the liquid component. The liquid injection orifice and the particle injection orifice can be after each other in the air stream, as shown, or side by side.

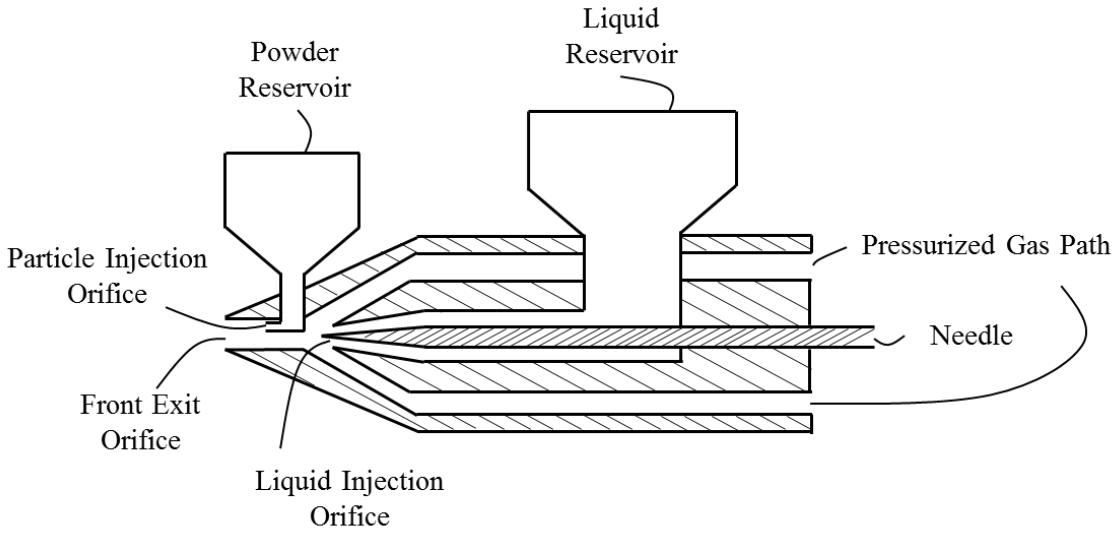

Figure 77. A Cross-sectional schematic of a nozzle where the powder and liquid components are injected into the same airstream.

The two components are forced out of the two nozzle spray device with compressed gas that may be compressed air or other gas such as nitrogen, carbon dioxide, or helium, typically operating in the range of 10-100 psi. The liquid or powder components are entrained in the gas as it flows through the spray device and out the front nozzle. This forms small droplets in the case of a liquid or disperses the particles in the case of a powder. Liquid and powder components are contained in reservoirs on the spray device or provided through tubes to the device. Heaters may be used with the reservoirs to maintain a liquid, or may be used to prepare the materials in some way, such as by removing a protective coating. Heaters may also be used in other areas of the spray device to prepare the components. In one embodiment two separate spray guns can be used instead of one with two nozzles, with the liquid component being sprayed first and then then powder component being sprayed, or they can be applied in alternating layers.

After being sprayed the liquid component strikes a surface and adheres. The powder then adheres to the liquid forming a composite as the surface being sprayed is quickly completely covered with a thin

layer. Additional material can be sprayed to form a thicker coating. The particles now in the liquid react and combine to form higher order alloys. These alloys continue to form until most or all of the liquid is affected, causing the melting temperature of the liquid to increase, thus causing it solidify. Cooling of the liquid metal may also help in the solidification.

The liquid metal may be made of a metal or metal alloy that is liquid at room temperature, such as In-Ga. This may also be a metal or metal alloy that is liquid at above room temperature that is melted before use in the spraying device. Preferential materials that may be used for the liquid metal may include; In, Ga, Sn, Bi, Sb, Zn among others.

The powder may consist of micro or nanoparticles. Preferably these are materials that are resistant to oxidation and have very thin or no oxide shells. Materials used for powder may include: Au, Ag, Pt, Cu, Ni, Al, among others. The powder may have a thin shell that may aid in keeping the powder from clumping or the particles from coarsening together. This shell may be removed by heat or another method. The powder may be combined with a carrier fluid that may be removed by heat, such as solvent like ethanol.

An optional electric charge can be applied to one or both the liquid component spray nozzle and the powder component spray nozzle to apply charge to the liquid and powder components as they leave the nozzles. The charge may be positive or negative to encourage the attachment of the sprayed components to the substrate, which may be neutral or oppositely charged. Additionally, the powder component may be oppositely charged to the liquid component to encourage their attachment to each other before adhering to the substrate.

One advantage of this method is the ability to cover large areas with a metal coating. Another is the ability to produce small droplets of liquid eutectic which improves the consistency of the mix and the reaction rate between the liquid and solid components. However, a significant disadvantage is the aerosolization of the nanoparticles and small droplets of liquid. These constitute a potential health hazard and must be contained or the user must wear appropriate protection.

Coatings on Glass

Coatings were produced on glass using the Spray Gun method. Here liquid eutectic alloy particles and nanoparticles were sprayed together onto a substrate. Figure 78 shows a photograph of an uncoated pieces of glass next to a coated piece. The droplets of liquid alloy are quite large and create an uneven, textured surface. The drop size needs to be reduced for more uniform coverage of the substrate and better mixing between the liquid and solid parts.

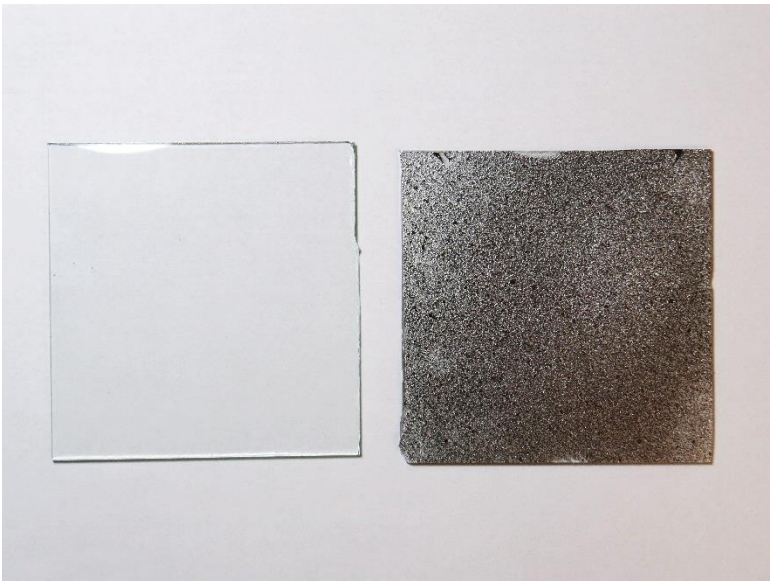

Figure 78. Image of metal spray coating on glass next to an uncoated glass piece.

IV. Discussion and Conclusions

Nanorod Diameter and Spacing Control

From our review of literature we saw a need to improve the control of nanorod structures. In work done by Stagon et al., it is postulated that it is the spacing of nanorods which makes the first realization of low temperature metallic seals a reality [4]. Sufficient spacing allows nanorods to interpenetrate when they are pressed together allowing contact over high surface area. Fast surface diffusion then causes the bond to be formed. It is generally not sufficient to merely get something that works to produce a viable technology. To reach a necessary level of maturity, many areas of the system must be controllable and tunable to allow for optimization.

In this case it is ideal to precisely control the spacing of nanorods so that they interpenetrate in the best possible way. When the spacing is too small, the nanorods may not be able to slide past each other. This would block the ability to form bonds at low temperature as is seen in the wafer bonding work with Cu performed by Wang et al. [54]. Here the nanorods are very tightly packed and form more of a rough porous film. Similarly, spacing that is too large is likely to perform poorly as well. If nanorods were highly spaced then they may not come in contact at all leaving them to crush on the surface. If they do come in to contact with very high spacing, there may not be enough contact for the fast surface diffusion to effectively work, or enough pressure of one nanorod acting on another to effectively fuse them together.

From another area of literature we see that when nanorods are grown on a particular surface, they develop a certain nanorod spacing and nanorod diameter based on deposition conditions and intrinsic properties of the substrate. The rate of deposition for example can affect the spacing distance as higher rates allow adatoms on a substrate less time to move before they are trapped in a group. This causes more, smaller clusters to form, causing the resulting nanorods to be closer together. In the case of substrates,

those with higher surface energies, such as metal as compared to plastic, will develop nanorods spaced closer together as adatoms will similarly be less mobile on the surface and the initial clusters of atoms will be closer together. These conclusions are based on fundamental research in the field of nanorod growth. Without this foundation to build upon, we would not be able to move forward with better control. At the same time the current state of understanding is not sufficient and needs to progress.

The first method we use to move forward with our nanorod control is In seeds produced on a substrate before nanorods are formed. At the initial stage, In is deposited onto a Si substrate and forms islands instead of a continuous film due to the non-wetting interaction. Subsequently, Ag is deposited and Ag atoms preferentially bind to the In islands. This method of using seeds occurs entirely in the vacuum chamber and can be performed just prior to the deposition for the growth of the nanorods, without a vacuum break, in minutes. When certain materials are deposited on to the substrate clusters of various sizes form. By controlling various parameters like the deposition amount and substrate angle the size of these clusters can be controlled. These clusters then act as nucleation sites for the deposition of nanorods, thus controlling the nanorod spacing (Ls). A few requirements exist for the material that serves as the patterning material. It must be (1) non-wetting on the substrate, it must (2) bond well with the metal to be deposited later, and (3) will preferably help nanorod growth (surfactant).

In the specific case of Cu nanorods a vacuum break was used in some cases to form an oxide layer on seeds. The nanorods grown on seeds with no vacuum break showed changes in morphology whereas the seeds with a vacuum break did not. The changes in morphology indicate that the higher surface energy of the Ga seeds in the non-vacuum break case, as compared to the Ga oxide in the break case, likely acts as traps for the Cu atoms with the Cu tending to stick on Ga seeds. This trapping acts as nucleation sites that the Cu nanorods then grow off of. This supports the position that it is not merely the morphology of the seeds that causes the nanorod diameter changes but also the surface energy of the material being contacted.

Here we have demonstrated improved control of nanorod size and spacing. The seed material has been shown to work with a few different materials; with In, Sn and Ga all being effective methods of

control. Additionally, both Ag and Cu nanorods are used to show control of nanorods made of these materials. This improvement in control advances our understanding of the technology and ability to make structures as we wish. This benefits directly the technologies of SERS as well as low temperature metallic glue as described in the next sections.

Core-Shell Nanorods and Eutectic Combinations

Nanorods have also been produced with a core-shell configuration. This arrangement can add value to the nanorod by combining beneficial properties of different materials into one structure. In this study we use a shell for two primary functions. (1) To provide longevity and durability to the nanorod, and (2) to add a material that will interact with other materials later to form a desirable alloy.

In the first case we have demonstrated the enhancement of the thermal stability of Ag nanorods through SiO2 and TiO2 capping, and experimentally demonstrated the feasibility of this proposal. The morphology of capped Ag nanorods is stable up to at least 100 °C; in contrast, the morphology of uncapped Ag nanorods becomes unstable at 50 °C. The capped Ag nanorods remain separate at 300 °C; in contrast, the uncapped Ag nanorods completely collapse at 100 °C. When used as a SERS substrate, the sensitivity of capped Ag nanorods decreases by only 10% at 100 °C; in contrast, that of uncapped Ag nanorods decreases by 95%. Based on the morphology and SERS sensitivity, capping is effective in stabilizing Ag nanorods.

For the second shell function we coat Cu nanorods with the materials of In and Ga. The In and Ga when brought into contact later form a liquid alloy at room temperature. This is also extended to the area of layer coated rods. This provides a similar function to the shell, but allows for more of the shell material to be present. In this case, a shell still likely forms on the nanorods due to the diffusion of atoms along the sides of the nanorods, but most of the material sits in a layer on the tips of the rods.

Metallic Glue

The current state of metallic attachment of two surfaces shows a great deal of room for improvement. The most readily available processes are welding, brazing, and soldering. These are able to form very strong bonds with other properties that are valuable in some cases, such as a highly electrically and thermally conductive interface. They can also form seals with very good resistance to leaks which can be important where a high pressure differential exists over the bond, or where sensitive materials are on one side, and air or water that can damage them are on the other. These processes can work well in many cases and are relatively inexpensive. A significant disadvantage, however, is the high temperatures that must be used to form the metal bond in this manner. Another important difficulty is using metals to attach materials together with very different coefficients of thermal expansion. This difference often causes the bond to separate as the materials cool after the bond is formed. By creating the bonds at low temperature some of these problems can be overcome. This will allow temperature sensitive components to be attached together without damage. It will also allow the materials with different CTE to be attached at low temperature, so that delamination and bond separation is not an issue.

Work has been done to accomplish these goals already. Cold welding has been shown to weld metals together at low temperatures. However, very high pressures must be used, and this is not practical in cases where delicate electronics need to be attached or where brittle glasses are being attached to metals. The work of Wang et al. attempts to bond Cu together at low temperature and fairly low pressure [54]. It is significant that they are able to achieve bonding well below the melting temperature of Cu, but the temperatures required are still too high to be able to be used widely or to compete with other soldering methods that are already available.

Silver particles are used by Alarifi et al. to form a lower temperature bond [44]. These have the challenge of an oxide shell that must be removed in a high temperature step. The most recent step is the work done by Stagon et al. where Ag nanorods are used to produce bonds at low temperature and low pressure [4]. This is an important step in the process, but we desire to take this further to produce a

technology that is safe to use on all integrated circuit devices. We also want this to be able to be used outside of the lab in people's homes, to really take the next step of making nanotechnology useful to people. This requires reducing the temperature required for the bond further still, down to room temperature. It also requires reducing the pressure to set the bond down to a common household clamp, or ideally, pressure than can be applied with a fingertip. To do this we have developed the eutectic core-shell nanorod technology.

Looking forward, we expect the core-shell nanorod glue to have significant advantages over the current single element nanorod method for low temperature bonding. First, the use of eutectic alloys through the core-shell nanorods should reduce or completely eliminate the voids. As a result, the leak resistance will further increase, and the heat conduction will become even more effective. Second, the presence of liquid alloys instead of solids will likely reduce the processing pressure from a few megapascals to a fraction of a megapascal, or finger-tip pressure.

Low temperature metallic seals can be used as a thermal interface material to improve the heat transfer out of high power density circuit components. The metal seal, once set, provides a solid metal connection between any two flat surfaces, such as a device to a heat sink. This solid metal connection provides a high thermal conductivity pathway for high heat transfer that would allow heat generating devices to operate at a lower temperature, or at a higher power using the same heat sink hardware. The target metals of Ag and Cu have thermal conductivities roughly 5-20x higher than typical solders and 50-100x better than typical thermal greases [15, 10, 11]. The higher conductivities and ability to use a thin interface give metal glue a significant advantage in improving heat transfer out of a device.

For bonding processes we have demonstrated that a certain size and spacing of nanorods produces the best bonds. This was primarily controlled by changing the substrate angle. Seeds of other materials on the surface can be used to further fine tune this control. When seeds of In were used to produce Ag nanorods with smaller diameter and larger spacing, a higher shear strength was recorded. However, the normal adhesion of In to Ag must also be considered. It is observed that the strength of the bond in the normal

direction was poorer when using In seeds in the 88 deg case. This is understandable as Ag nanorods are likely to attach more strongly to the Ag film layer used in this study, than to an In mound. This work may be extended in the future by examining the use of seeds that may bond more strongly to the film underlayer.

To take the next step we extend the understanding gained in the vacuum process to possible solutions in areas where vacuum is not required. These make the use of liquid metal alloys and micro and nanoparticles, produced by non-vacuum methods. The purity in these systems is lower than in the vacuum process, but the reductions in cost and ease of use can make this a more desirable solution in many cases. While these technologies have a long way to go to become mature we have demonstrated two methods to produce a metal glue without vacuum.

The first method is called the Glue Gun Method. This method is easy to use and provides a liquid metal combination that hardens in minutes. We have demonstrated this method on Cu substrates and have observed a maximum shear strength of 2 MPa. This technology shows great promise and will continue to be investigated.

The second method is the Spray Gun Method. This combines liquid metal droplets and micro and nanoparticles in an airstream and as they land on a substrate to provide good mixing and easy coverage of large surfaces. As a spray method, this is better to coat bigger areas, or to coat multiple areas at once with the rest of the surface having been masked off such as solder pads on a PCB. This method experiences the additional challenge of aerosolized particles which must be contained. In this technology we have successfully demonstrated the coating of glass surfaces. Further development will investigate decreasing the droplet size of the liquid metal for better mixing and a more uniform surface coating.

Further Applications

This work lays a foundation for understanding how our metallic glue bonds perform thermally and mechanically. Future research will investigate optimizing bonding between a wide variety of different

materials for high mechanical strength and high thermal conductivity. In addition, future work will also investigate the production of seals with high electrical conductivity for applications such as solder replacement in electronics. Research will also pursue the attachment of materials with much different coefficients of thermal expansion. This will impact glass-to-metal attached components, such as light bulbs, laser optics, and high temperature coatings for projectiles and aerospace, as well as viewports for inspection in vacuum chambers and other industrial processes.

An initial application area for low temperature bonding is GaN and semiconductor devices, especially high power density chips for power electronics and high brightness LEDs that require improved cooling. Military applications of these devices include radars, such as active electronically scanned arrays, communications, and electronic warfare such as IED jammers. A forecast of the GaN microelectronics predicts the market will be $335 million in 2017, with aerospace and defense making up slightly more than 50% [129].

The closely related market of the attachment of silicon ICs to heat sinks such as those used for computer CPUs would also benefit. The thermal interface market here is estimated to be around $962 mil [130]. The currently used thermal grease has low thermal conductivity and is a bottleneck for fast, more power dense devices. Our improved heat transfer capability would be of interest first in high end, gaming type, computer systems. Following good results, the technology has the potential to be phased into use on most systems.

In the longer term, low temperature metallic bonds can be useful in electronic manufacturing services as a solder replacement to attach electronics to circuit boards. It will be possible to attach surface mount components during the pick and place step, where electrical components are picked up and placed in the correct location by a robotic arm, thus eliminating the required reflow heating process. This removes the necessity for a costly oven with different heat zones requiring careful monitoring that processes circuit boards slowly.

An additional benefit is a solution that contains none of the element lead and which produces no whiskers. This is beneficial in that lead is known to be toxic to humans and its use in electronics is banned in Europe. Use of lead is still accepted in the US, but it is being phased out. Our metallic glue also does not produce whiskers, thus eliminating the threat of shorts and failures.

This work has progressed the field of low temperature metallic sealing by building on previous work to improve the control of nanorods and mature the technology. We have improved the ability to control the size and spacing of nanorods on a surface, as well as demonstrated producing shells on nanorods with PVD to make them more temperature stable and give them coatings for low melting temperature alloy creation. This opens the door to a number of applications where high thermal and electrical conductivity is important, and where attaching materials with a mismatch of CTE is challenging.

Conclusions

This study has set out to explore the control of the growth of nanorod structure using EBPVD. The first way this was done was with seeds to control nanorod spacing and size. The second was producing shells on nanorods. These areas are based on many years of related research in our group and now is approaching the point where basic science research will begin to provide a real benefit to humanity. This is not an easy process. Nanotechnology has so far taken a very slow road to being incorporated into our daily lives through products. It gets a lot of buzz in the press but has been slow to live up to the hype. Lots of excitement can be generated, for example, from a nanostructured surface that never needs to be cleaned, that might be used on pans, clothing, or boat hulls, but solutions that will work economically in the long term are few. To move toward this goal of durable, affordable nanotechnology a deeper understanding must be reached. This understanding comes slowly and is based on years of experience.

The integrated circuit industry is an excellent example of a mature nanotechnology field that is providing real world benefits. In fact, we use these devices every day, almost constantly, in the form of computers and smartphones and even the circuitry for fluorescent light bulbs. Starting arguably in 1954 with the first silicon transistor from Texas Instruments [*131*], the huge amount of man-hours that has poured into this field has allowed it to reach the incredible and effective 14nm technology in computer CPUs today. Many other fields haven't had the chance to catch up. Nanotechnology is creeping its way into everyday life. It will get there, but it will take time, just as the computer industry took ~25 years to begin after the transistor.

In our work to mature the field of nanotechnology to make low temperature metal bonds a reality, we have accomplished two tasks. The first has improved control the diameter and spacing of nanorods by using seeds on a substrate. The second was to control surface properties of nanorods by creating shells of different materials on the outside. Both methods were successfully tested, leading to improvements in SERS substrates and with improvements in low temperature metallic sealing.

To demonstrate nanorod control in the growth of Ag nanorods using physical vapor deposition In was used as a seed material. When no In is used, Ag forms nanorods of ~100 nm in diameter when deposited at an oblique angle of 86 degrees and a deposition rate of 1 nm/s onto silicon substrates. By controlling the conditions of incidence angle and surface kinetics, through substrate temperature and deposition rate, only a small range of nanorod diameters and spacings are possible, being limited by the interplay between the spacing of nanorod nuclei, Ls, and the minimum diameter, Lmin. When In is deposited onto the substrate first, it forms non-wetting clusters and acts as preferential nucleation sites for Ag, which wets the In clusters. By varying the incidence angle and amount of In pre-deposited onto the substrate the diameter and spacing of In clusters, and the resulting Ag nanorods, can be controlled from ~7nm to over 250 nm. The In seeds of 5 nm in nominal thickness give rise to the largest separation and the smallest diameter of Ag nanorods. In addition, the substitution of In with Sn indicates that the proposed mechanism is generic. Other substrate materials are also used, onto which seeds are demonstrated. Further, seed materials are used to control the

growth of Cu nanorods. This new mechanism and the control over nanorod morphology that it enables may positively impact emerging technologies such as SERS and hermetic sealing.

Secondly, we have explored the coating of nanorods by further deposition of a second material after the nanorod growth is completed. By using shell materials of metal oxides we have enhanced the thermal stability of Ag nanorods. The morphology of capped Ag nanorods is stable well beyond 100 °C; in contrast, the morphology of uncapped Ag nanorods becomes unstable at 50 °C. The capped Ag nanorods remain separate at 300 °C; in contrast, the uncapped Ag nanorods completely collapse at 100 °C. When using these nanorods for SERS, the sensitivity of capped Ag nanorods decreases by only 10% at 100 °C; in contrast, that of uncapped Ag nanorods decreases by 95%. Based on the morphology and SERS sensitivity, capping is effective in stabilizing Ag nanorods.

Coatings of metals also provide benefits to nanorods. We have demonstrated the coating of Cu nanorods with low melting temperature metals of In and Ga. Bonds using these nanorod structures have also been demonstrated. Bonding based on this idea has the potential to have a significant impact in a wide area of metal joining solutions. This may include room temperature solder replacement, high thermal conductivity thermal interface materials, and joining of materials with different coefficients of thermal expansion.

To improve the bonding of the eutectic core shell nanorods a few areas should be first approached. Important information could be gained from an in situ TEM study of bonding of nanorods. Observing an In coated Cu nanorod coming into contact with a Ga coated Cu nanorod would be very insightful to confirming that our understanding of what is occurring is indeed going on. This could be similar to the work done by Lu et al. with Au nanorods [35]. A high resolution TEM image of a thin slice out of a bonded area would be very useful as well. This would allow us a better understanding of what happens to the thin oxide shell on the Ag nanorods after bonding, especially if the bonding process could be observed in situ. Better understanding of the oxide in the bonded layer would lead to better understanding of the heat and electricity transfer properties through the layers. The thicknesses of the eutectic coating layers on the

outsides of the nanorods should be studied. Perfecting these amounts will allow the area in-between nanorods to fill completely with liquid alloy, while using as little material as possible to keep the percentage of Cu high for best thermal conductivity.

Another area of interest may be using rods oriented normal to the substrate to perform bonding. Currently the nanorods come off of the surface at a high angle relative to surface normal. This requires substrates to be oriented correctly so the nanorods interpenetrate during bonding. If the rods were normal to the substrate, the need for this alignment could be avoided and the two surfaces to be bonded together could be at any orientation as long as the surfaces were parallel. This can be accomplished by rotating the substrate during deposition, however Ag and Cu tend to form complex ropelike or balloon like shapes when using this method, which are not ideal for bonding. Also, different materials can be explored for single element nanorod bonding such as Au, and Pt, and different core and shell materials can be investigated for the core-shell nanorods, such as Al for the core and Bi, and Sn as shell.

Finally, we have also begun to explore the area of using non-vacuum processes to produce metallic bonds. This stems directly from the understanding gained through our vacuum work and is a logical next step to reduce the cost and complexity of the process. Promising results have been observed in the areas of a liquid glue solution and a spray glue solution, but there is much work to be done in this area.

While just a few more pieces in the puzzle, this work gets us to the brink of a feasible room temperature metallic glue. This concept has been demonstrated here by using Ag nanorods with In seeds, by using Cu nanorods with eutectic coatings, and by using lower cost nanoparticle methods that could be more accessible and affordable. The underlying science is strengthened, and there are many areas that will benefit from the improvement of this technology. Control of nanorods and core-shell nanorod structures will benefit SERS technology and are likely to lead to advances in other unthought-of of areas. This piece of the puzzle is laid, and we move forward to address the many new challenges we now face to getting our technology to a maturity where it can truly be useful, to bring science and engineering together, to produce a unique solution that can have real world impacts.

References

1. Kalpakjian, S. & Schmid, S. *Manufacturing Engineering and Technology*, 7th Ed., Pearson, Upper Saddle River, NJ, (2014).

2. Lewis, J. Material challenge for flexible organic devices, *Mater. Today*, Vol. 9, p 38–45, (2006).

3. Harshorn, S. R. *Structural Adhesives: Chemistry and Technology*, Plenum Press, New York, NY, (1986).

4. Stagon, S. P. & Huang, H. C. Airtight metallic sealing at room temperature under small mechanical pressure. *Sci. Rep.* 3, 3066 (2013).

5. Stagon, S., Knapp, A., Elliott, P., & Huang, H. Metallic Glue for Ambient Environments Making Strides. *Adv. Mater. Processes.* 174, 22 (2016).

6. Markoff, J. "Intel's Big Shift After Hitting Technical Wall," New York Times, May 17, (2004).

7. Yovanovich, M.M. Marotta, E.E. Thermal spreading and contact resistances, in: A. Bejan, A.D. Kraus (Eds.), Heat Transfer Handbook, Wiley, Hoboken, New Jersey, pp. 261e395 (2003).

8. Due, J. & Robinson, A. J. Reliability of thermal interface materials: A review. *Applied Thermal Engineering* 50, 455–463 (2013).

9. Lee, G.-W., Park, M., Kim, J., Lee, J. & Yoon, H. Enhanced thermal conductivity of polymer composites filled with hybrid filler. *Composites Part A: Applied science and manufacturing* 37, 727–734 (2006).

10. Young, H.D. *University Physics*, 7th Ed., Addison Wesley, Reading, MA, 1992.

11. Gwinn, J.P. & Webb, R.L. Performance and testing of thermal interface materials, *Microelectr. J.*, (2003).

12. Lasance, C. J. M. “Problems with Thermal Interface Material Measurements: Suggestions for Improvement,” Electronics Cooling, November (2003).

13. Viswanath, R. Wakharkar, V. Watwe, A. & Lebonheur, V. Thermal Performance Challenges from Silicon to Systems, *Intel Technol. J.*, Vol. 4, No. 3, p 1-16, (2000).

14. Fair, R. B. Challenges to manufacturing submicron, ultra-large scale integrated circuits, *Proceedings of the IEEE*, Vol. 78, p 1687–1705, (1990).

15. King, J.A. *Material Handbook for Hybrid Microelectronics*, Artech House, Norwood, MA, (1988).

16. Henshall, G. Bath, J. & Handwerker, C.A. *Lead-Free Solder Process Development*, Wiley, Hoboken, NJ, (2011).

17. DerMarderosian, A. & Gionet, V. The Effects of Entrapped Bubbles in Solder Used for the Attachment of Leadless Ceramic Chip Carriers, *Reliability Physics Symposium*, p 235-241, (1983).

18. Sarvar, F., Whalley, D.C. & Conway, P.P. Thermal interface materials-A review of the state of the art. *Proceedings of the 1st Electronics System Integration Technology Conference, IEEE, Vol. 2, pp 1292-1302*, (2006).

19. Macris, C. G., Sanderson, T. R., Ebel, R. G. & Leyerle, C. B. Performance, Reliability, and Approaches Using a Low Melt Alloy as a Thermal Interface Material. Enerdyne Solutions Internal Document. IMAPS 2004, 37th Int. Symp. On Microelectronics. (2004).

20. Macris, C. & Ebel, R. Liquid metal thermal interface material system. Patent number US7755184 B2. (2010).

21. Webb, R.L. & Gwinn, J.P. Low melting point thermal interface material. Inter Society Conf. on Thermal Phenomena, Itherm, May 30-June 01, pp. 671-676 (2002).

22. Wei, J. Challenges in Cooling Design of CPU Packages for High-Performance Servers, Heat Transfer Engineering, 29:2, 178-187 (2008).

23. Ma, H. & Suhling, J. C. A review of mechanical properties of lead-free solders for electronic packaging. *J. Mater. Sci.* 44, 1141-1158 (2009).

24. Chin, H.S., Cheong, K.Y. & Ismail, A.B. A review on die attach materials for SiC-based high-temperature power devices. Metallurgical and Materials Transactions B, Vol. 41B (2010).

25. Abtew, M. & Selvaduray, G. Lead-free solders in microelectronics. *Mat. Sci. Eng., R* 27 95-141 (2000).

26. Lei, T., Calata, J., Lu, G.-Q., Chen, X. & Luo, S. Low-temperature sintering of nanoscale silver paste for attaching large-area chips. Components and Packaging Technologies, IEEE Transactions on 33, 98–104 (2010).

27. ASM International, Electronic Material Handbook, Vol. 1, Materials Park, OH, pp. 1161-1162. (1989).

28. Bunyan, D., Ashworth, M.A. & Wilcox, G.D. Tin whisker growth from electroplated finishes–a review. *Transactions of the IMF, 91:5,* 249-259 (2013).

29. Akande, W. O., Cao, Y., Yao, N. & Soboyejo, W. Adhesion and the cold welding of gold-silver thin films. *J. Appl. Phys.* 107, 043519 (2010).

30. N. Bay, Cold pressure welding-the mechanisms governing bonding. J. Eng. Ind. 101, 121 (1979).

31. NEPP NASA, http://nepp.nasa.gov/Whisker/photos/index.html

32. Wang, Z. L. Petroski, J. M. Green, T. C. and El-Sayed, Shape Transformation and Surface Melting of Cubic and Tetrahedral Platinum Nanocrystals. M. A. J. Phys. Chem. B 102, 6145 (1998).

33. Wang, B. Wang, G. Chen, X. & Zhao, J. Melting behavior of ultrathin titanium nanowires. Phys. Rev. B 67, 193403, (2003).

34. Wang, X. Chen, G. Wang, B. Wang, W. Lu, and J. Zhao, Melting behavior in ultrathin metallic nanowires. Phys. Rev. B 66, 085408 (2002).

35. Lu, Y., Huang, J. Y., Wang, C., Sun, S. & Lou, J. Cold welding of ultrathin gold nanowires. Nat. Nanotechnol. 5, 218–224 (2010).

36. Goldstein, A.N., Echer, C.M. & Alivisatos. A.P. Melting in Semiconductor Nanocrystals. *Science 256*, 1425–1427 (1992).

37. Kato, M., Sawamoto, H., Kumazawa, M. & Wada, N. Synthesis of coesite from ultra fine particles. Japanese Journal of Applied Physics 14, 181 (1975).

38. Iwama, S. & Sahashi, T. Sintering of Ultrafine Metal Powders. I. Coalescence Growth Stage of Au and Ag. Japanese Journal of Applied Physics 1039–1044 (1980).

39. Iwama, S & Hayakawa, K. Sintering of ultrafine metal powders. II. Neck growth stage of Au, Ag, Al and Cu. Japanese Journal of Applied Physics (1981).

40. Takagi, M. Electron-diffraction study of liquid-solid transition of thin metal films. *J. Phys. Soc. Jpn. 9, pp. 359-363* (1954).

41. Jiang, Q., Zhang S. & Zhao, M. Size-dependent melting point of noble metals. *Mater Chem Phys* 82, 225–227 (2003).

42. Siow, K. S. Are sintered silver joints ready for use as interconnect material in microelectronic packaging? Journal of electronic materials 43, 947–961 (2014).

43. Ide, E. *et al*. Metal–metal bonding process using Ag metallo-organic nanoparticles. *Acta Materialia 53*, 2385-2393 (2005).

44. Alarifi, H., Hu, A., Yavuz, M. & Zhou, Y. N. Silver nanoparticle paste for low- temperature bonding of copper. J. Electron Mater. 40, 1394–1402 (2011).

45. Henkel, Low temperature sintering die attach for Power Electronics, http://www.henkel-adhesives.com/fullproductlist-electronics.htm (2014).

46. Wakuda, D., Hatamura, M. & Suganuma, K. Novel method for room temperature sintering of Ag nanoparticle paste in air. Chem Phys Lett 441, 305–308 (2007).

47. Wakuda, D., Kim, K. & Suganuma K. Room temperature sintering of Ag nanoparticles by drying solvent. *Scr Mater*. 59(6):649-652 (2008).

48. Magdassi, S., Grouchko, M., Berezin, O. & Kamyshny, A. Triggering the sintering of silver nanoparticles at room temperature. ACS Nano 4, 1943–1948 (2010).

49. Grouchko, M., Kamyshny, A., Mihailescu, C.F. & Anghel, D.F. Conductive inks with a 'built-in' mechanism that enables sintering at room temperature. ACS Nano, Vol. 5, No.4 3354-3359 (2011).

50. Kahler, J., Heuck, N., Stranz, A., Waag, A. & Peiner, E. Pick-and-Place Silver Sintering Die Attach of Small-Area Chips. *Ieee Transactions Components Package Manufacturing Technology* 2, 199–207 (2012).

51. Schwarzbauer, H. Method and apparatus for fastening semiconductor components to substrates. US Patent 4903886 A (1990).

52. Karabacak, T. et al. Low temperature melting of copper nanorod arrays. J Appl Phys 99, 064304 (2006).

53. Lisiecki, I., Sack-Kongehl, H., Weiss, W., Urban, J. & Pileni, M.-P. Langmuir 16, 8807, (2000).

54. Wang, P.-I. et al. Low Temperature Wafer Bonding by Copper Nanorod Array. Electrochem Solid-state Lett 12, H138 (2009).

55. Bajwa, A. & Wilde, J. Reliability modeling of Sn–Ag transient liquid phase die-bonds for high-power SiC devices. Microelectron Reliab 60, 116–125 (2016).

56. Cook, G.O. & Sorensen, C.D. Overview of transient liquid phase and partial transient liquid phase bonding, J. Mater. Sci. 46, 5305–5323 (2011).

57. Masson, A., Buttay, C., Morel, H., Raynaud, C., Hascoet, S. & Gremillard, L. High temperature die-attaches for SiC power devices, Proc. 14th Eur. Conf. Power Electron. Appl. pp. 1–10 (2011).

58. Wilde, J. Pchalek, N. Kontaktierung von solarzellen durch isotherme erstarrung, Verbindungstechnik Elektronik 5, 172–179 (1993).

59. Czarnetzki, A. & Ehrhardt S. Re-dating the Chinese amalgam-filling of teeth in Europe. *International Journal of Anthropology*. 5 (4): 325–332 (1990).

60. Herø, H., Okabe, T. & Wie, H. Corrosion of gallium alloys in vivo. *Journal of Materials Science: Materials in Medicine, 8, 357-360,* (1997).

61. Cruickshanks-Boyd, D. W. Physical metallurgy of dental amalgams 1. Particle-size analysis and phase content of amalgam alloys. J Dent 10, 207–216 (1982).

62. Beech, D. R. High copper alloys for dental amalgam. International dental journal 32, 240–251 (1982).

63. Bernhoft, R. A. Mercury toxicity and treatment: a review of the literature. Journal of Environmental and Public Health. Volume 2012, Article ID 460508 (2011).

64. Zahir, F., Rizwi, S., Haq, S. & Khan, R. Low dose mercury toxicity and human health. Environ Toxicol Phar 20, 351–360 (2005).

65. McComb, D. J. Gallium restorative materials. Can Dent Assoc 64:645-4 (1998).

66. Navarro, M., Franco, E.B. & Bastos, P. Clinical evaluation of gallium alloy as a posterior restorative material. Quintessence 27 (5), 315-20. (1996).

67. Hawkeye, M. M. & Brett, M. J. Glancing angle deposition: Fabrication, properties, and applications of micro- and nanostructured thin films. J. Vac. Sci. Technol. A 25, 1317-1335 (2007).

68. Usui, H. Preparation of polymer thin films by physical vapor deposition. Functional Polymer Films Wiley-VCH Verlag GmbH & Co. KGaA (2011).

69. Schulz, U., Saruhan, B., Fritscher, K. & Leyens, C. Review on Advanced EB-PVD Ceramic Topcoats for TBC Applications. Int J Appl Ceram Tec 1, 302–315 (2004).

70. Holleck, H. & Schier, V. Multilayer PVD coatings for wear protection. Surface and Coatings Technology 76, 328–336 (1995).

71. Selvakumar, N. & Barshilia, H. C. Review of physical vapor deposited (PVD) spectrally selective coatings for mid- and high-temperature solar thermal applications. Sol Energ Mat Sol C 98, 1–23 (2012).

72. May, C. & Strümpfel, J. ITO coating by reactive magnetron sputtering–comparison of properties from DC and MF processing. Thin Solid Films 351, 48–52 (1999).

73. Hanlon, J. Handbook of Package Engineering, 1st ed. Lancaster, PA, Technomic Publishing: ISBN 0-87762-924-2. Chapter 4 Coatings and Laminations. (1992).

74. Rigney, D.V., Viguie, R. & Wortman, D.J. PVD thermal barrier coating applications and process development for aircraft engines. Journal of thermal spray Technology, 6: 167 (1997).

75. Solovyev, A. A. et al. Application of PVD methods to solid oxide fuel cells. Appl Surf Sci 310, 272–277 (2014).

76. Kossel W. Zur Theorie des Kristallwachstums. Nach. Ges. Wiss. Göttingen, Math.-Phys. Kl., 135–143 (1927).

77. Stranski I.N. Zur Theorie der Kristallwachstums. Z. Phys. Chem. 136, 259–278 (1928).

78. Robbie K. & Brett M. Sculptured thin films and glancing angle deposition: Growth mechanics and applications. *Journal of Vacuum Science & Technology A: Vacuum, Surfaces, and Films* 15(3):1460-1465. (1997).

79. Mattox, D. M. *Handbook of Physical Vapor Deposition (PVD) Processing: Film Formation, Adhesion, Surface Preparation and Contamination Control.* Westwood, N.J.: Noyes Publications, (2010).

80. Stagon, S. P. & Huang, H. Controllable growth of aluminum nanorods using physical vapor deposition. *Nanoscale Res Lett* 9, 400 (2014).

81. Smith, D. L. *Thin-film deposition: principles and practice*. (McGraw-Hill, 1995).

82. Fisher, J.C. Calculation of Diffusion Penetration Curves for Surface and Grain Boundary Diffusion. J Appl Phys 22, 74–77 (1951).

83. Burton, W.-K., Cabrera, N. & Frank, F. The growth of crystals and the equilibrium structure of their surfaces. *Philosophical Transactions of the Royal Society of London. Series A, Mathematical and Physical Sciences* 299–358 (1951).

84. Lagally, M. & Zhang, Z. Thin-film cliffhanger. *Nature* 417, 907–10 (2002).

85. Liu, S. J., Huang, H. C. & Woo, C. H. Schwoebel-Ehrlich barrier: from two to three dimensions. Appl. Phys. Lett. 80, 3295–3297 (2002).

86. Ehrlich, G. & Hudda, F. Atomic View of Surface Self Diffusion: Tungsten on Tungsten. *The Journal of Chemical Physics* 44, 1039–1049 (1966).

87. Schwoebel, R. L. & Shipsey, E. J. Step motion on crystal surfaces. *Journal of Applied Physics* 37, 3682–3686 (2004).

88. Liu, S. J., Wang, E. G., Woo, C. H. & Huang, H. Three-dimensional Schwoebel–Ehrlich barrier. *Journal of Computer-Aided Materials Design* 7, (2000).

89. Zhang, R. & Huang, H. Another kinetic mechanism of stabilizing multiple-layer surface steps. *Applied Physics Letters* 98, (2011).

90. Zhou, L. & Huang, H. Characteristic length scale of nanorod diameter during growth. *Physical review letters* 101, 266102 (2008).

91. Niu, X., Stagon, S., Huang, H., Baldwin, J. & Misra, A. Smallest metallic nanorods using physical vapor deposition. *Physical review letters* 110, 136102 (2013).

92. Stagon, S. P., Huang, H. C., Baldwin, J. K. & Misra, A. Anomaly of film porosity dependence on deposition rate. *Appl. Phys. Lett.* 100, 061601 (2012).

93. Choi et al. Synthesis of silicon nanowires and nanofin arrays using interference lithography and catalytic etching. Nano Lett 8, 3799–802 (2008).

94. Fu, Y. & Bryan, N. Fabrication and characterization of slanted nanopillars array. J Vac Sci Technology B Microelectron Nanometer Struct 23, 984 (2005).

95. Wang, X., Summers, C. & Wang, Z. Large-Scale Hexagonal-Patterned Growth of Aligned ZnO Nanorods for Nano-optoelectronics and Nanosensor Arrays. Nano Letters 4, 423–426 (2004).

96. Lee, J., Mubeen, S., Ji, X., Stucky, G. & Moskovits, M. Plasmonic Photoanodes for Solar Water Splitting with Visible Light. Nano Lett 12, 5014–5019 (2012).

97. Zhou, C. & Gall, D. Two-Component Nanorod Arrays by Glancing-Angle Deposition. Small 4, 1351–1354 (2008).

98. Li, Y., Duan, G., Liu, G. & Cai, W. Physical processes-aided periodic micro/nanostructured arrays by colloidal template technique: fabrication and applications. Chemical Society Reviews 42, 3614–3627 (2013).

99. Jensen, M. O. & Brett, M. J. Periodically Structured Glancing Angle Deposition Thin Films. IEEE Transactions On Nanotechnology 4, 269–277 (2005).

100. Kumar, S. et al. Growth specificity of vertical ZnO nanorods on patterned seeded substrates through integrated chemical process. Mater Chem Phys 133, 126–134 (2012).

101. Xiang, S. K. & Huang, H. C. Binding of In and Pb surfactants on Cu{1 1 1} surfaces. Surf. Sci. 604, 868-871 (2010).

102. Goh, C., Coakley, K. & McGehee, M. Nanostructuring Titania by Embossing with Polymer Molds Made from Anodic Alumina Templates. Nano Lett 5, 1545–1549 (2005).

103. Nishi, Y. & Doering, R. Handbook of semiconductor manufacturing technology. 395-413 (2000).

104. Elliott, P. R. Stagon, S. P. & Huang, H. Control of Separation and Diameter of Ag Nanorods through Self-organized Seeds. *Sci. Rep.* 5, 16826 (2015).

105. Zhou, L. G. & Huang, H. C. Smallest separation of nanorods from physical vapor deposition. *Appl. Phys. Lett.* 100, 141605 (2012).

106. Chaney, S. B., Shanmukh, S., Dluhy, R. A. & Zhao, Y.-P. Aligned silver nanorod arrays produce high sensitivity surface-enhanced Raman spectroscopy substrates. *Appl. Phys. Lett.* 87, 031908 (2005).

107. Sun, X., Stagon, S. P., Huang, H. C., Chen, J. & Lei, Y. Functionalized aligned silver nanorod arrays for glucose sensing through surface enhanced Raman scattering. *RCS Adv.* 4, 23382-23388 (2014).

108. Vo-Dinh, T. Surface-enhanced Raman spectroscopy using metallic nanostructures. *Trends Anal. Chem*. 17, 557-582 (1998).

109. Vitos, L., Ruban, A. V., Skriver, H. L. & Kollár, J. The surface energy of metals. Surf. Sci. 411, 186-202 (1998).

110. Brunauer, S., Kantro, D. L. & Weise, C. H. The surface energies of amorphous silica and hydrous amorphous silica. Can. J. Chem. 34, 1483-1496 (1956).

111. M. E. Toimil-Molares, A. G. Balogh, T. W. Cornelius, R. Neumann and C. Trautmann, Applied Physics Letters 85, 5337 (2004).

112. S. Karim, M. E. Toimil-Molares, A. G. Balogh, W. Ensinger, T. W. Cornelius, E. U. Khan and R. Neumann, Nanotechnology 17, 5954 (2006).

113. Zweben, C. Thermal Materials Solve Power Electronics Challenges, Power Electronics Technology. Vol. 32 Issue 2, p40 (2006).

114. Hartung, Roman, The Truth about CPU Soldering, http://overclocking.guide/the-truth-about-cpu-soldering/, (2015).

115. Abbe, E. Beiträge zur Theorie des Mikroskops und der mikroskopischen Wahrnehmung. *Archiv für mikroskopische Anatomie Volume 9, Issue 1, pp 413–418* (1873).

116. Heilemann, M. *et al.* Subdiffraction resolution fluorescence imaging with conventional fluorescent probes.*Angewandte Chemie International Edition* 47, 6172–6176 (2008).

117. Humpston, G., & Jacobson, D. M. *Principles of soldering*. Materials Park, OH: ASM International. (2004).

118. A. Margomenos, et al. Novel packaging, cooling and interconnection method for GaN high performance power amplifiers and GaN based RF front-ends, 615–618 (2012).

119. Roehr, B. Mounting Considerations for Power Semiconductors, 1-20 (1993).

120. Catalog #87–HS–9, page 8, Thermalloy, Inc. (1987).

121. "Navy Power Supply Reliability – Design and Manufacturing Guidelines" NAVMAT P4855–1, NAVPUBFORCEN, Dec. (1982).

122. Blazej, D. Thermal Interface Materials, Electronics Cooling, Vol. 9, No. 4, pp. 14-20, (2003).

123. Becker, G. et al., Thermal Conductivity in Advanced Chips, Emerging Generation of Thermal Greases Offers Advantages, Advanced Packaging, July (2005).

124. De Broglie L. Waves and quanta. *Nature*. 112 (2815):540-540 (1923).

125. McMullan, D. Scanning electron microscopy 1928–1965. *Scanning.* Vol. 17 (3): 175–185. (1995).

126. Williams D.B. & Carter C>B. The transmission electron microscope. In: *Transmission electron microscopy.* Springer; 3-22. (2009).

127. Qiu, Z. et al. Raman Spectroscopic Investigation on TiO2–N719 Dye Interfaces Using Ag@TiO2 Nanoparticles and Potential Correlation Strategies. Chemphyschem 14, 2217–2224 (2013).

128. Lee, K., Gomez, M., Elouatik, S. & Demopoulos, G. Further Understanding of the Adsorption Mechanism of N719 Sensitizer on Anatase TiO2 Films for DSSC Applications Using Vibrational Spectroscopy and Confocal Raman Imaging. Langmuir 26, 9575–9583 (2010).

129. E. Highman, Commercial RF GaN Market Finally Arrives, Strategy Analytics. (2015).

130. Thermal Interface Material Market by Type (Greases & Adhesives, Tapes & Films, Gap Fillers, Metallic TIMs, and PCM), by Application (Computers, Telecom, Medical Devices, Industrial Machinery, Consumer Durables, and Automotive Electronics), by Region - Trends & Forecasts, Marketsandmarkets. (2015).

131. Morris, P. R. A history of the world semiconductor industry. IEE History of technology series 12. Institution of Electrical Engineers. pp. 171 (1990).